Degradation of H3PO4/PBI High Temperature Polymer Electrolyte Membrane Fuel Cell under Stressed Operating Conditions

Effect of Start/Stop Cycling, Impurities Poisoning and H2 Starvation

Zhou, Fan

Publication date:
2015

Document Version
Publisher's PDF, also known as Version of record

DEGRADATION OF H3PO4/PBI HIGH TEMPERATURE POLYMER ELECTROLYTE MEMBRANE FUEL CELL UNDER STRESSED OPERATING CONDITIONS

EFFECT OF START/STOP CYCLING, IMPURITIES POISONING AND H_2 STARVATION

by

Fan Zhou

AALBORG UNIVERSITY
DENMARK

Dissertation submitted to the Faculty of Engineering and Science in partial fulfilment of the requirements for the degree of

Philosophiae Doctor (Ph.D.)

Aalborg University

Department of Energy Technology

Aalborg, Denmark

Thesis submitted: August 5, 2015
PhD supervisor: Prof. SØREN KNUDSEN KÆR,
Aalborg University
Assistant PhD supervisor: Associate Prof. SØREN JUHL ANDREASEN,
Aalborg University
PhD committee: Professor Thomas J. Schmidt,
ETH Zürich & Paul Scherrer Institute
Professor Qingfeng Li,
Technical University of Denmark
Associate Professor Henrik Sørensen,
Aalborg University

PhD Series: Faculty of Engineering and Science, Aalborg University

ISSN: xxxx- xxxx
ISBN: xxx-xx-xxxx-xxx-x

Published by:
Department of Energy Technology
Pontoppidanstræde 101
DK – 9220 Aalborg Ø

Printed in Denmark by UniPrint, 2015

Title: Degradation of H_3PO_4/PBI High Temperature Polymer Electrolyte Membrane Fuel Cell under Stressed Operating Conditions: Effect of Start/Stop Cycling, Impurities Poisoning and H_2 Starvation

Ph.D. Student: Fan Zhou

Supervisor: Søren Knudsen Kær

Co-supervisor: Søren Juhl Andreasen

List of publications:

Paper 1: Zhou F, Araya SS, Grigoras IF, Andreasen SJ, Kær SK. Performance Degradation Tests of Phosphoric Acid Doped Polybenzimidazole Membrane Based High Temperature Polymer Electrolyte Membrane Fuel Cells. Journal of Fuel Cell Science and Technology. 2015;12:021002(1)-(9).

Paper 2: Zhou F, Andreasen SJ, Kær SK, Yu D. Analysis of accelerated degradation of a HT-PEM fuel cell caused by cell reversal in fuel starvation condition. International Journal of Hydrogen Energy. 2015;40:2833-9.

Paper 3: Zhou F, Andreasen SJ, Kær SK. Experimental study of cell reversal of a high temperature polymer electrolyte membrane fuel cell caused by H_2 starvation. International Journal of Hydrogen Energy. 2015;40:6672-80.

Paper 4: Zhou F, Andreasen SJ, Kær SK, Park JO. Experimental investigation of carbon monoxide poisoning effect on a PBI/H_3PO_4 high temperature polymer electrolyte membrane fuel cell: influence of anode humidification and carbon dioxide. International Journal of Hydrogen Energy. 2015;40:14932-41.

Paper 5: Simon Araya S, Grigoras IF, Zhou F, Andreasen SJ, Kær SK. Performance and endurance of a high temperature PEM fuel cell operated on methanol reformate. International Journal of Hydrogen Energy. 2014;39:18343-50.

This present report combined with the above listed scientific papers has been submitted for assessment in partial fulfilment of the PhD degree. The scientific papers are not included in this version due to copyright issues. Detailed publication information is provided above and the interested reader is referred to the original published papers. As part of the assessment, co-author statements have been made available to the assessment committee and are also available at the Faculty of Engineering and Science, Aalborg University.

ABSTRACT

The Polymer electrolyte membrane (PEM) fuel cells are promising fuel cell technology which can convert the chemical energy in for example hydrogen into electricity efficiently and environmentally friendly. It has attracted considerable attention because it helps to mitigate issues related to greenhouse gas emission and environmental pollution. The most widely studied PEM fuel cell is the low temperature (LT) PEM fuel cell. However, the catalyst of LT-PEM fuel cells can be poisoned by small trace amounts of CO in the fuel. Due to the high impurity tolerance, along with other advantages such as simplified water management and easy heat removal, the H_3PO_4/PBI membrane based high temperature (HT) PEM fuel cell is thought to be very promising.

In this work, some degradation issues of the HT-PEM fuel cell are experimentally investigated. Given the current challenges for production and storage of the H_2, it is more practical to use a liquid fuel such as methanol as the energy carrier. However, the reformate gas produced from methanol contains impurities such as CO, CO_2 and unconverted methanol. For stationary applications, especially for HT-PEM fuel cell based micro-CHP units for households, the daily startup/shutdown operation is necessary. Moreover, the faults in the H_2 supply system or in controlling the reformer can cause the H_2 starvation of the HT-PEM fuel cell. The effects of these operating conditions to the degradation of the HT-PEM fuel cell are studied in the current work. Both in-situ and ex-situ characterization techniques are conducted to gain insight into the degradation mechanisms of the HT-PEM fuel cell under these operating conditions.

The experimental results in this work suggest that the presence of methanol results in the degradation in cell performance of the HT-PEM fuel cell by increasing the charge transfer resistance and mass transfer resistance. The CO with volume fraction of 1% – 3% can cause significant performance loss to the HT-PEM fuel cell at the operating temperature of 150 ^oC. The cell performance loss caused by CO poisoning can be alleviated by the presence of water vapor. The CO oxidation via the water gas shift reaction is the main reason for the mitigated CO poisoning with the presence of water vapor. Meanwhile, the CO poisoning can deteriorate with the presence of CO_2, although the CO_2 alone does not affect the cell performance. H_2 starvation results in reversal in the cell polarity. The carbon corrosion and water electrolysis reactions occur in the anode under H_2 starvation conditions as confirmed by the presence of CO_2 and O_2 in the anode exhaust. The current density distribution becomes uneven under H_2 starvation conditions, with high current density values in upstream regions and low current density values in downstream regions. The cell reversal and uneven current density distribution become more severe under lower H_2 stoichiometry and higher current load conditions. The rapid

decay in cell performance during a H_2 starvation degradation test reveals that the H_2 starvation can cause severe damage to the HT-PEM fuel cell. The degradation under H_2 starvation conditions occur in the catalyst layer, mainly in the anode, while the membrane is not affected. The carbon corrosion in the anode and consequently the decrease in ECSA is the main reason for the degradation under H_2 starvation conditions.

The results obtained in this work help to understand and mitigate the degradation of HT-PEM fuel cell.

DANSK RESUME

Polymer elektrolyt membran (PEM) brændselsceller udgør en lovende brændselscelleteknologi. De kan konvertere den kemiske energi i for eksempel hydrogen til elektricitet, effektivt og miljøvenligt. Dette har særligt tiltrukket sig opmærksomhed, da det hjælper med at mitigere problematikkerne relateret til drivhusgasemissioner og den miljømæssige forurening. De mest udbredte studier af PEM-brændselsceller, er lavtemperatur (LT) PEM-brændselsceller. LT-PEM-brændselsceller besidder dog en katalyst der kan forurenes ved selv små mængder af CO i det benyttede brændstof. På grund af de høje tolerancer over for forurening, samt andre fordele, såsom forsimplet water management og nemmere køling, anses H_3PO_4/PBI-membranbaserede højtemperatur (HT) PEM-brændselsceller for en lovende teknologi.

I dette arbejde undersøges, for HT-PEM-brændselsceller, forskellige degraderings problematikker eksperimentelt. Givet de nuværende udfordringer for produktion og lagring af H_2, er det mere praktisk at benytte et flydende brændstof, som for eksempel metanol, som energibærer. Dog indeholder det reformatgas der producers fra metanol forurenende elementer af bl.a. CO, CO_2 og ukonverteret metanol. For stationære applikationer, særligt HT-PEM-brændselsceller baserede mikro-kraftvarme enheder til almindelige husholdninger, er daglig start/stop drift nødvendig. Ydermere kan fejl i H_2 forsyningssystemet eller regulering af reformeren forårsage H_2-sultning af HT-PEM-brændselscellen. Effekterne af disse driftsbetingelser på degraderingen af HT-PEM-brændselscellerne bliver studerent it dette arbejde. Både in-situ og ex-situ karakteriseringsteknikker foretages for at få indsigt i degraderingsmekanismerne i HT-PEM-brændselsceller i netop disse driftssituationer.

De eksperimentelle resultater i dette arbejde foreslår at tilstedeværelsen af metanol resulterer i degradering af HT-PEM-brændselscelle performance, ved forhøjet charge transfer resistance og mass transfer resistance. CO med volumenfraktioner på 1 % – 3 % kan forårsage signifikant performancetab for HT-PEM-brændselsceller ved driftstemperaturer på 150 ^oC. Celleperformancetab forårsaget af CO-forgiftning kan afhjælpes ved tilstedeværelsen af vanddamp. CO-oxidationen via water-gas-shift-reaktionen er hovedårsagen til den forbedrede CO-forgiftningssituation ved tilstedeværelsen af vanddamp. I mellemtiden kan CO-forgiftningen forværres ved tilstedeværelsen af CO_2, på trods af at CO_2 alene ikke påvirker celleperformance. H_2-sultning resulterer i reversering af cellepolariteten. Carbon corrosion og vandelektrolysereaktioner sker på anodesiden under H2-sultningsbetingelser, hvilket bekræftes af tilstedeværelsen af CO_2 og O_2 i anodeudstødningen. Strømdensitetsdistributionen bliver ujævn under H_2-sultningsbetingelser med høje strømdensiteter i upstream-regionerne og lave

strømdensiteter i downstream-regionerne. Cellereversering og ujævn strømdensitetsdistribution bliver værre under lavere H_2-støkiometrier og højere strømbelastningstilstande. Den hurtige forringelse af celleperformance under H_2-sultnings-degradering, viser ved tests, at H_2-sultning kan forårsage alvorlig skade på HT-PEM-brændselscellen. Degraderingen under H_2-sultning sker i katalystlaget, primært på anodesiden, mens membranen ikke bliver påvirket. Carbon corrosion på anoden formindsker konsekvent ECSA og er hovedårsagen til degraderingen under H_2-sultningsbetingelser.

De opnåede resultater I dette arbejde hjælper med forståelsen og forbedringen af degradering af HT-PEM-brændselsceller.

ACKNOWLEDGEMENTS

Finally, I can see the completion of my thesis. Looking back on the last three years of studying in Department of Energy Technology, Aalborg University, I had lots of good memories and gained a lot, both in academic and in other aspects of my life. This three-year journey has become the most wonderful and valuable experience in my life, and will be the helpful wealth for my future life. I would like to show my gratitude to many people, without whom I cannot finish my PhD study for sure.

First and foremost, I would like to say thank you to my supervisors: Søren Knudsen Kær and Søren Juhl Andreasen. Their professional guidance and suggestions guide me forward when doing my PhD project. Søren Kær is always concerned about my progress in research. His valuable and timely guidance helps me to prevent taking detours in this journey. Søren Juhl's experience in doing the experiments in the lab really helps me a lot when I get in troubles when fighting with the experimental instruments. Except for the guidance, their courage and the relaxing atmosphere they build are also the key points which support me all the way through the journey.

I would also thank the colleagues in the Fuel Cell and Battery group: Xin Gao, Xiaoti Cui, Christian Jeppesen, Simon Lennart Sahlin, Kristian Kjær Justesen, Jakob Rabjerg Vang, Vincenzo Liso, Anders Christian Olesen and other people in this group which I cannot list here for the consideration of the length of this part, for their valuable discussion and kindly help. I really enjoy working with you guys. A special thank you is sent to Samuel Simon Araya who helped me a lot in the beginning of my PhD study and gave me many valuable suggestions in the past three years.

Further, special thanks are sent to all my friends and all the secretaries and all the employees in the Department of Energy Technology. Thank you for your support all through my PhD period. I will always remember the comfort from my friend when I am upset.

Last but not least, I would like to express the deeply appreciation to my beloved parents, for their unconditionally love and support to me over the last twenty eight years. I will always love you!

A special thank you is sent to China Scholarship Council (CSC) for the financial support for my studying in Denmark.

TABLE OF CONTENTS

LIST OF FIGURES

LIST OF TABLES

NOMENCLATURE

Acronyms	
AC	Alternating Current
APU	Auxiliary Power Unit
CHP	Combined Heat and Power
CL	Catalyst Layer
CV	Cyclic Voltammetry
DC	Direct Current
DMAc	N,N-dimethylacetamide
DMFC	Direct Methanol Fuel Cell
DOE	Department of Energy
EC	Equivalent Circuit
ECSA	Electrochemical Surface Area
EIS	Electrochemical Impedance Spectroscopy
GDL	Gas Diffusion Layer
HOR	Hydrogen Oxidation Reaction
HT	High Temperature
ICE	Internal Combustion Engine
LT	Low Temperature
MCFC	Molten Carbonate Fuel Cell
MEA	Membrane Electrode Assembly
OCV	Open Circuit Voltage
ORR	Oxygen Reduction Reaction
PA	Phosphoric Acid
PAFC	Phosphoric Acid Fuel Cell
PBI	Polybenzimidazole
PEM	Polymer Electrolyte Membrane
PEMFC	Polymer Electrolyte Membrane Fuel Cell
PPA	Polyphosphoric Acid
ppm	Parts per Million
PSA	Perfluorinated Sulfonic Acid
RHE	Reference Hydrogen Electrode
SEM	Scanning Electron Microscopy

SOFC	Solid Oxide Fuel Cell
TFA	Trifluoroacetic Acid
TGA	Thermogravimetric Analysis
UPS	Uninterrupted Power Supplies
XRD	X-ray Diffraction

CHAPTER 1. INTRODUCTION

This section gives a brief overview of the global energy consumption and the importance of the development of the fuel cell technology. It then introduces the classification of fuel cells and the operational principle of the PEM fuel cell, which is of interest in this project. Lastly, the state-of-art of the PEM fuel cell and its application are outlined.

1.1. THE IMPORTANCE OF FUEL CELLS

Despite the recent global economic recession, the global energy consumption has been increasing over the last several decades and is expected to increase over the next 20 years. The global energy demand is expected to rise by 37% from 2013 to 2035 [1]. Fossil fuels, which take up more than 70% of the total energy production, are the main sources of the CO_2 emission. The IPCC predicts that the global temperature will be increased by 4 ^oC by the end of the 21st century, if the global CO_2 emission continues increasing [2]. Therefore governments all over the world have reached a consensus that the CO_2 emission has to be reduced as soon as possible, although there are still heated debates on the exact CO_2 emission target between developed countries and developing countries. Denmark, which is rather ambitious on CO_2 emission reduction, aims to reduce 40% of CO_2 emission by 2020 compared with 1990 and become complete carbon neutral by 2050 [3]. With the more and more severe conflictions between increasing energy demand and urgency in CO_2 emission reduction, the renewable energy supply should rise more rapidly and take up higher percentage in the total energy consumption.

A fuel cell is an electrochemical device which can directly convert the chemical energy into electric energy. Its efficiency is not limited by the Carnot Cycle because there is no working medium cycled between high temperature and low temperature heat sources in the fuel cell. Therefore its efficiency can be higher than the traditional thermal engines. Moreover, if hydrogen is adopted as the fuel, water is the only product of the operation, which makes the fuel cell very environmentally friendly provided the hydrogen is produced from renewables [4]. The high efficiency and low emission of the fuel cell make it a very promising solution to the global energy crisis and environmental pollution issues.

1.2. FUEL CELL TYPES

The fuel cells can be classified according to the materials of the electrolyte used. In Table 1.1 several common types of fuel cells are listed.

Table 1.1 – The classifications of different fuel cell types

Fuel cell type	Abbreviation	Electrolyte material	Operating temperature (^oC)	Conductive ions
Polymer electrolyte membrane fuel cell	PEMFC	Proton exchange membrane	60 – 80	H^+
High temperature polymer electrolyte fuel cell	HT-PEMFC	Phosphoric acid doped proton exchange membrane	120 – 200	H^+
Direct methanol fuel cell	DMFC	Proton exchange membrane	60 – 80	H^+
Phosphoric acid fuel cell	PAFC	Immobilized phosphoric acid	150 – 200	H^+
Molten carbonate fuel cell	MCFC	Immobilized liquid molten carbonate	620 – 660	CO_3^{2-}
Solid oxide fuel cell	SOFC	Ceramic	800 – 1000	O^{2-}
Alkaline fuel cell	AFC	Aqueous alkaline solution	23 – 250	OH^-

1.3. PEM FUEL CELLS

Fig. 1 illustrates the typical structure of a PEM fuel cell. In both anode and cathode, there are catalyst layer (CL), gas diffusion layer (GDL) and bipolar plate with flow channels. The PEM fuel cell (also known as proton exchange membrane fuel cell) uses a solid polymer membrane as the electrolyte which is capable of conducting protons (H^+). This polymer membrane also separates the air in cathode and H_2 in anode. Currently the most commonly used membrane material for PEM fuel cell is perfluorinated sulfonic acid (PSA), i.e. Nafion [5]. The sulfonic groups in Nafion

provide sites for proton transfer under fully hydrated conditions. Therefore the reactant gas usually needs to be humidified prior to entering the fuel cell to provide sufficient water vapor to maintain the high conductivity of the membrane [6].

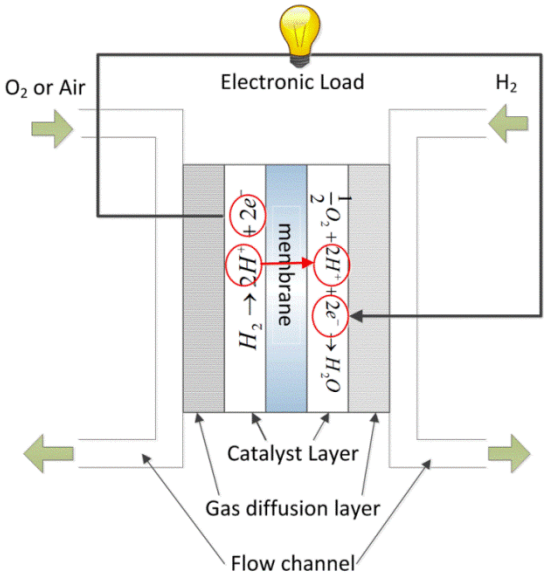

Fig.1.1 – The structure and the operational principle of the PEM fuel cell

The catalyst layer is where the electrode reactions take place. It consists of porous carbon material with nanometer-sized catalyst particles attached on the surface and ionomer to create the required triple-phase boundary required for the electrochemical reaction. In the cathode the pure platinum particles are usually adopted as the catalyst, while in the anode either platinum or platinum-ruthenium alloy can be used. The oxidation reaction and the reduction reaction taking place on anode and cathode follow Eq. (1.1) and (1.2), respectively.

$$H_2 \rightarrow 2H^+ + 2e^- \tag{1.1}$$

$$\frac{1}{2}O_2 + 2H^+ + 2e^- \rightarrow H_2O \tag{1.2}$$

The GDL is constructed from carbon fiber or carbon cloth with porous media structure. It provides the path for reactant gas and electron transfer. Additives such as Teflon are usually used to provide the hydrophobic property of the GDL, to avoid the pores being blocked by liquid water.

The membrane, catalyst layer and gas diffusion layer are usually assembled by hot pressuring into the so-called membrane electrode assembly (MEA). The MEA is usually sandwiched between two bipolar plates with flow channels which can distribute the reaction gas evenly on the electrode plane.

1.4. PEM FUEL CELL APPLICATIONS

The application of PEM fuel cells focus on the following three aspects: transportation, stationary and portable power generation. Due to the excellent dynamic characteristics and fast startup of the PEM fuel cell, compared with other types of fuel cell, most transportation applications of fuel cell are related to the PEM fuel cell [7]. The output power of PEM fuel cell for transportation application ranges from 20 kW to 200 kW. The stationary and portable generation applications of PEM fuel cells are also very successful because of the high power density, high energy efficiency and good output power flexibility. For portable power application, the typical power range of the PEM fuel cell is 5 – 50 W. For stationary application, the output power of the PEM fuel cell can either be in the low range of 100 – 1000 W, for example for backup power of the remote telecommunication station, or in the high range of 100 kW – 1 MW, for example for distributed power generation.

1.4.1. TRANSPORTATION APPLICATIONS

Most of the conventional engines for transportation applications, such as internal combustion engines (ICEs), rely on the fossil fuels, which give rise to many environmental and energy issues such as global warming, air pollution and crude oil crisis. The PEM fuel cell has the potential to solve these issues by replacing the ICEs in the future. As reported by McNicol et al. [8], the fuel cell vehicles equipped with carbon containing fuel processor can be superior to the conventional ICE vehicles in all aspects except for initial cost.

Many automotive manufacturers have launched their fuel cell cars in the last decade, for example Honda FCX Clarity [9], Toyota Mirai [10], Mercedes-Benz F-CELL Electrical Car [11], Chevrolet Equinox [12] and Hyundai ix35 FCEV [13]. The fuel cell cars can either be powered only by the fuel cell stacks or by the fuel cell stacks and batteries in a hybrid system. The production of automobiles powered by fuel cells has been increasing in recent years. Besides the automotive companies, the governments in some countries also contribute to the development of fuel cell vehicles. The US DOE initiated the “Controlled Hydrogen Fleet and Infrastructure Demonstration and Validation” Project in 2004 [14], aiming to demonstrate the performance of fuel cell vehicles and the support refueling infrastructure in parallel, under real-life conditions. The target of this project for the range of fuel cell vehicles is above 300 miles. They have employed 152 fuel cell vehicles and 24

hydrogen-refueling stations. Japan initiated the “Japan Hydrogen Fuel Cell (JHFC)” Project in 2002 which involved the activities related to fuel cell vehicles [15].

Fuel cell buses are another successful application of fuel cells in transportation. There have been several government funded fuel cell bus project announced in the past decade, such as US National Fuel Cell Bus project [16], European CUTE (Clean Urban Transport for Europe) [17] and Australian STEP (Sustainable Transport Energy Project) programs. All around the world, fuel cell buses are demonstrated, including in Whistler Canada, San Francisco USA, Hamburg Germany, Shanghai and Beijing China, London England, São Paulo Brazil as well as several others [4].

Other applications of fuel cells in transportation can be found in the literature, such as fuel cell bicycles [18], fuel cell scooters [19], fuel cell forklifts [20].

1.4.2. STATIONARY APPLICATIONS

Distributed power generation has shown many advantages over the centralized power generation, including utilizing the waste heat through cogenerating heat and power for local usage. The PEM fuel cell has been applied for small-scale decentralized stationary power generation. The application of PEM fuel cell in stationary power generation mainly focuses on small scale combined heat and power (CHP) system, uninterrupted power supplies (UPS) and auxiliary power units (APU) [21]. The GenSys Blue developed by Plug Power to be compatible with existing home heating systems such as forced air or hot water [22]. In 2009 Plug Power received an award from the New York State Energy Research and Development Authority (NYSERDA) for installing and operating the CHP GenSys fuel cell systems in New York State homes [23]. The Ballard Power System developed the FCgen-1030 V3 stacks which can be incorporated into the residential CHP system [24]. Ballard also works with Dantherm Power A/S of Denmark to provide back-up power solutions to telecommunications providers. The application of PEM fuel cell in stationary power generation faces competitions from other types of fuel cell, mainly from SOFC and MCFC. To enhance the competitiveness of PEM fuel cell in stationary power generation, research work aiming to improve the durability and fuel flexibility of the PEM fuel cell should be conducted.

1.4.3. PORTABLE APPLICATIONS

Due to the unsatisfying battery technology in terms of low power density and long charging time, there is a growing demand for portable PEM fuel cells for portable electronic devices. The world production of portable fuel cell has been increasing continuously [25]. The portable PEM fuel cell can be used for laptops, mobile phones, remote control (RC) toys and emergency lights [26]. In addition, the portable PEM fuel cell also receives attention for the military application to power

portable electronic devices such as radios. There are several negative opinions of PEM fuel cell in portable application. One is related to the safety of hydrogen, and another one is about the lower volumetric energy density of hydrogen. However the PEM fuel cell shows some advantages and potential in this field. The PEM fuel cell fueled with liquid methanol, namely direct methanol fuel cell (DMFC), is thought to be a promising candidate for the portable power source.

1.5. SUMMARY

In this chapter the important role which the fuel cell will play in the future of energy supply and environment protection has been introduced. As a very highly-efficient and environment-friendly power source, the fuel cell is expected to play a more and more important role in the future world, to promote the efficiency of energy conversion and to utilize the H_2 energy more efficiently. The classification of fuel cells has been listed. And the components and the operational principle of the PEM fuel cell are summarized. Many successful applications of the PEM fuel cell in different aspects have been seen. However the durability and the lifetime is still a barrier on its way to successful commercialization, which motivate the current research work conducted in this thesis.

CHAPTER 2. DEGRADATION ON HIGH TEMPERATURE PEM FUEL CELL

This section introduces a specific type of PEM fuel cell, phosphoric acid doped PBI membrane based high temperature PEM fuel cell, which is investigated in this project. After introducing the advantages, disadvantages and applications of this type of PEM fuel cell, the working principle and components of the HT-PEM fuel cell is described. Then the degradation mechanisms of each component under steady state and some stressed operating conditions are introduced, to elicit the motivation and the main objects for this project.

2.1. OVERVIEW OF HT-PEM FUEL CELLS

The Nafion membrane based PEM fuel cell with operating temperature in the range of 60 – 80 ^{o}C is recognized as a very successful type of fuel cell due to its high energy efficiency, fast startup and high power density. However it faces many technical challenges associated with the low operating temperature. Firstly, proper water management is needed for the Nafion based PEM fuel cell [6]. The water content in the Nafion based PEM fuel cell should not be neither too high to avoid the blockage of the pores in GDL and CL by liquid water nor too low to maintain sufficient proton conductivity of the membrane. Normally humidifiers are installed in the fuel cell system to prevent the dry-out of the polymer membrane, which increases the complexity of the system. Although a lot of work has been conducted to develop the fuel cell system without humidifiers, these systems still need further improvement for better reliability and performance [27]. Another challenge for Nafion based PEM fuel cells are that the catalyst can be easily contaminated by impurities in the fuel stream. For example the CO with concentration of several ppm can cause significant cell performance drop [28].The intolerance to impurities makes a reactor for eliminating CO in the fuel stream necessary in the fuel cell system fueled by reformate gas, which increases the complexity of the fuel cell system. Moreover, the low operating temperature brings about the difficulties in expelling and utilizing the waste heat generated by electrochemical reactions, since the temperature gradient between the fuel cell and the environment is relatively low [29].

It is recognized that elevating the operating temperature above 100 ^{o}C can effectively solve these temperature related problems. However the Nafion membrane only shows good chemical and mechanical properties in the temperature range of 60 – 80 ^{o}C. Thus many researchers have devoted themselves to new materials for polymer membranes which have good chemical and mechanical stability and sufficient proton conductivity at higher temperature [30-35]. Among

different new materials, phosphoric acid (PA or H_3PO_4) doped polybenzimidazole (PBI) which shows promising properties for PEM fuel cell application. The PEM fuel cell which is based on the PA doped PBI membrane can be operated in the temperature range of 120 – 200 ^oC, and therefore is normally referred to as high temperature (HT) PEM fuel cell. And the traditional Nafion based PEM fuel cell is often referred as low temperature (LT) PEM fuel cell. The first PBI/H_3PO_4 HT-PEM fuel cell was proposed by Wainright et al [36]. Since then, many research works on the manufacturing and characterization of the HT-PEM fuel cell have been reported.

The proton conductivity of the H_3PO_4/PBI membrane does not rely on liquid water, which makes the non-humidification operation of the fuel cell possible [37]. And there is no liquid water in the HT-PEM fuel cell during operation because the operational temperature is above water boiling temperature, which makes the water management very easy. Moreover, higher operating temperature enables better utilization of the heat in the exhaust gas of the HT-PEM fuel cell. Jensen et al. [38] proposed a HT-PEM fuel cell system using the excess heat from the fuel cell to vaporize the water and methanol for a fuel processor. Gao et al. [39] proposed a method installing the thermoelectric devices in the HT-PEM fuel cell system to utilize the exhaust heat and improve the electric efficiency of the fuel cell system. Last but most importantly, the tolerance of the HT-PEM fuel cell to the impurities in the fuel stream is largely enhanced by the high operating temperature. It is reported that the performance of a HT-PEM fuel cell shows no significant loss under an operating temperature of 180 ^oC with CO concentrations of 5% in the anode stream [40]. Therefore the HT-PEM fuel cell can be easily integrated with a reformer to utilize the traditional fossil fuels such as methanol, methane and natural gas [41, 42]. The fuel flexibility is largely increased by integrating the reformer to the HT-PEM fuel cell. In addition the H_2 storage issues can be solved because of the high energy density of the fossil fuels.

The first H_3PO_4/PBI based HT-PEM fuel cell system integrated with a fuel reformer was developed by Holladay et al [41]. Pan et al. [43] managed to integrate a HT-PEM fuel cell with a methanol reformer without any CO removal devices. Efficiency of the system was improved by utilizing the water and heat from the exhaust gas of the fuel cell. A methanol reformer for HT-PEM fuel cell was also presented by Andreasen et al [44]. And it was managed to be integrated into a HT-PEM fuel cell system as shown in Fig. 2.1 [44]. Karstedt et al. [45] presented a system consisting of a methane fuel processor and a HT-PEM fuel cell unit with an electrical output of 4.5 kW. With the system model they optimized the operating parameters such as gas stoichiometries and steam/carbon ratio to achieve maximum system efficiency. The HT-PEM fuel cell integrated with a glycerol reformer was reported by Authayanun et al [46]. The optimal system parameters were found to be dependent on the current density and operating temperature of the fuel cell.

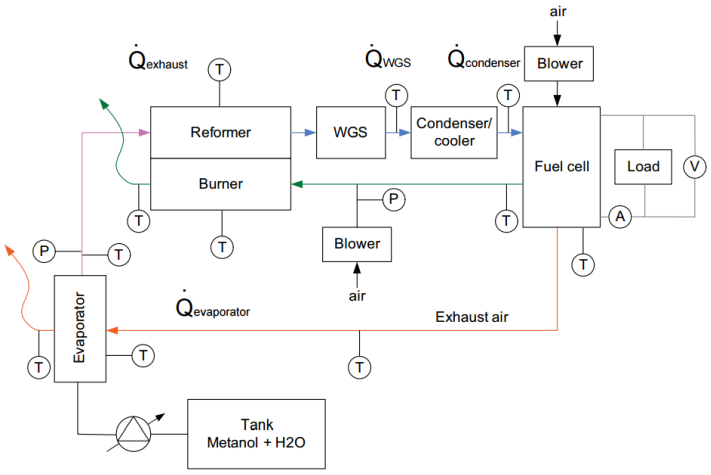

Fig. 2.1 – Diagram of a HT-PEM power system integrated with a methanol reformer (reproduced from [44])

Another method to utilize the methanol for HT-PEM fuel cell is to integrate the methanol reforming catalyst into the anode of the fuel cell, namely internal reforming [47]. The same temperature range for methanol reforming and for HT-PEM fuel cell operation makes this technology feasible. Avgouropoulos et al. [48] proposed and developed an internal reforming methanol fuel cell. The methanol is directly fed into the anode and then reformed at the operating temperature of 200 ^{o}C. This fuel cell showed promising performance and no significant performance degradation. Meanwhile the system volume and weight was minimized at a large extent.

The high temperature exhaust gas makes the HT-PEM fuel cell very suitable for stationary applications such as combined heat and power (CHP) and co-generation [49]. A residential energy system based on PBI HT-PEM fuel cell for single household was proposed by Arsalis et al. [50], as well as some operational strategies. The energy efficiency of the HT-PEM fuel cell based micro-CHP system was found to be higher than that of traditional thermal engine based micro-CHP system. The automotive application of the HT-PEM fuel cell is impeded by some factors such as the time and energy required during the startup period. However, improving the operation strategy can help to minimize this drawback. Andreasen et al. [51] presented an electric vehicle powered by the HT-PEM fuel cell stacks and the Li-ion battery packs. The fuel cell stacks are connected parallel to the battery packs, which can charge the battery and extend the driving range.

Although there are many advantages and successful applications, the further commercialization of HT-PEM fuel cell still face many obstacles and challenges.

The using of platinum as a noble metal catalyst brings about high cost of the HT-PEM fuel cell, although many works have been conducted to decrease the platinum loading in the catalyst layer and figure out alternative non-noble metal catalyst [52]. Moreover, the performance and energy density of the HT-PEM fuel cell is generally lower than that of the LT-PEM fuel cell because the catalyst is partly covered by the PA and the oxygen diffusion coefficient is pretty low in the PA and the ionomer [37]. These drawbacks can be compensated by the enhanced impurity tolerance and the simplified water management of the HT-PEM fuel cell. Nowadays, the relatively short lifetime and high performance degradation rate is the most important barrier which needs to be solved.

2.2. COMPONENTS OF THE HT-PEM FUEL CELLS

A typical single cell setup of H_3PO_4/PBI membrane based HT-PEM fuel cell usually consists of the MEA, bipolar plates with flow channels, end plates and gaskets. All the components are illustrated in Fig. 2.2.

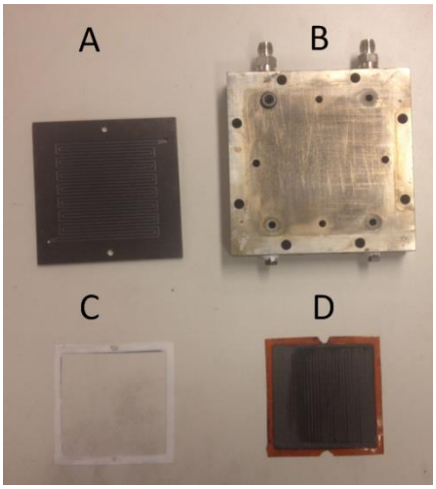

Fig. 2.2 – The components of single cell setup of the HT-PEM fuel cell (A: bipolar plate, B: endplate, C: gasket, D: MEA)

The PBI, as a thermoplastic polymer, provides the polymer electrolyte membrane high enough thermal and mechanical stability and sufficient chemical resistance. However, the pristine PBI polymer shows weak proton conductivity, thus it has to be doped with PA to obtain high conductivity [53]. The PA is a typical type of amphoteric acid which has both proton donors and proton acceptors. The proton can be easily transferred in the hydrogen bond network in the PA by the formation and the breakage of the hydrogen bond. In the H_3PO_4/PBI system, the proton is migrated according to the Grotthus mechanism with the assistant of counter anion

[54]. In addition, the good thermal stability of the PA makes its application on the HT-PEM fuel cell feasible. Typically the H_3PO_4/PBI membrane is fabricated by solution casting. There are two typical cast methods: direct casting and indirect casting [37]. For direct casting, the acid doped PBI membrane is casted from the PBI solution in polyphosphoric acid (PPA) or in mixture of PA and trifluoroacetic acid (TFA). For indirect casting, the membrane is first casted from organic solution, most commonly the *N*,*N*-dimethylacetamide (DMAc), then immersing the membrane in the PA solution to make it proton conductive. The proton conductivity of the PA doped PBI membrane is related to the acid doping level which is defined by the number of acid molecules per repeating PBI unit. It is found that when the acid doping level is higher than 2 the free acid can be observed, which contributes to most of the proton conductivity [55]. Therefore the PA content in the membrane should be maintained at the sufficient level to avoid the decrease in proton conductivity. Additionally, since the proton transfer in the H_3PO_4/PBI membrane does not rely on water, the electro-osmotic drag coefficient of water is almost zero.

The catalyst layer and the gas diffusion layer of the H_3PO_4/PBI based HT-PEM fuel cell are similar to those of the LT-PEM fuel cell and PAFC. Noble metal catalyst such as platinum particles is attached on the high surface area carbon material to create enough active sites for electrochemical reactions. The ionomer such as PA doped PBI is used as the binder in the catalyst layer to provide the hydrophobic property and the proton transfer path. The ionomer loading in the catalyst layer should be optimized to obtain both high levels in proton conductivity and catalyst activity [56]. Hot pressing is the most common method to fabricate the MEA of the HT-PEM fuel cell [30]. It is important to ensure good contact between different components of the MEA and maintain the structure integrity.

2.3. DEGRADATION AND DURABILITY ISSUES OF THE HT-PEM FUEL CELLS

The limited lifetime is one of the obstacles which hinder the HT-PEM fuel cell to be successfully commercialized. Several organizations have set the durability targets for the HT-PEM fuel cell for both stationary and automotive applications. According to the Fuel Cell Technologies Program Multi-Year Research, Development, and Demonstration Plan (MYRD&D Plan) released by US DOE [57], the lifetime of a HT-PEM fuel cell should be above 5000 hours for automotive application and 60000 hours for stationary application by the year of 2018. Many research works about the degradation test and investigation of degradation mechanisms have been conducted to improve the durability of the HT-PEM fuel cell and reduce the cell performance degradation rate. In this section, degradation mechanisms of different components of the HT-PEM fuel cell and several stressed degradation modes are reviewed.

2.3.1. DEGRADATION OF THE MEMBRANES

The most typical membrane for HT-PEM fuel cell is based on polybenzimidazole doped with phosphoric acid. Excellent thermal stability and high proton conductivity of the PA in the temperature range of 120 – 200 ^{o}C ensure that the PA doped PBI membrane is suitable for HT-PEM fuel cell application. The degradation mode of the PA doped PBI membrane include the chemical oxidative degradation, mechanical degradation and thermal stressed degradation. Loss of PA in the membrane can result in the decrease in the proton conductivity of the membrane and consequently the degradation in the membrane. This section will focus on the degradation in structure of the PBI membrane. The loss of PA will be introduced in the Section 2.2.4.

The attack of C-H bond in the polymer by hydrogen peroxide (H_2O_2) and its radical (-OH or -OOH), which could be generated by oxygen reduction reaction in cathode and by reaction of hydrogen and oxygen in anode, is believed to be The general chemical degradation mechanism of polymer membranes under typical operating conditions of the PEM fuel cell [58]. LaConti et al. [59] proposed a possible mechanism for the formation of H_2O_2. The O_2 molecules permeating through the membrane from the cathode side are reduced at the catalyst layer of the anode, forming H_2O_2 as following equations:

$$H_2 + 2Pt \rightarrow 2Pt - H \tag{2.1}$$

$$Pt - H + O_2 \rightarrow -OOH \tag{2.2}$$

$$-OOH + Pt - H \rightarrow H_2O_2 \tag{2.3}$$

Most of the works about the chemical degradation of PBI membrane are conducted through the so-called Fenton test in which the PBI membrane is exposed to ferrous ions (Fe^{2+}/Fe^{3+}) containing H_2O_2 solutions [60]. The ferrous ions (Fe^{2+}/Fe^{3+}) play the role of catalyst for H_2O_2 decomposition in the Fenton solution. It was reported that the weight of the PBI membrane decreased with the increase in exposure time on the Fenton reagent at the temperature of 68 ^{o}C [61]. After 20 hours of exposure to the 3% H_2O_2, the weight loss of the PBI membrane in the range of 10% and 40% can be observed. Liao et al. [62] studied the chemical degradation of PBI membrane under higher temperature condition. They proposed a chemical oxidative degradation mechanism of the PBI membrane based on the FTIR spectrum obtained in the experiment. The H-containing end-groups, e.g. N-H bond in the imidazole ring can be attacked by the peroxide radicals, which can lead to the opening of imidazole ring and scission of the macromolecular chain. They investigated the chemical degradation of the PBI membrane in acid environment in a later work [63]. The PA was found can relieve the membrane degradation by suppressing the

decomposition of H_2O_2. The effect of PA to the degradation of PBI membrane was also reported in the literatures [64] and [65].

Some physical factors such as compressing and swelling can lead to the membrane degradation. When the fuel cell is assembled, the membrane is under compressive force from the bipolar plates. Membrane creep and microcrack fracture can be observed after long-term deformation of the membrane caused by the compressive stress, which can result in the increase in gas crossover through the membrane and consequently more severe chemical degradation of membrane [59]. In addition, mechanical stress of the membrane can be caused by the swelling and shrinking of the PBI membrane under load cycling or relative humidity cycling operating conditions. Improving mechanical strength of the membrane helps to reduce the mechanical degradation [66]. The pristine PBI membrane shows very good mechanical strength, with tensile strength of 60 – 70 MPa under dry condition and 100 – 160 MPa under saturated condition [31]. However, the mechanical strength of the PA doped PBI membrane is much weaker because the backbones of the polymer are separated by the free acid especially at high temperature [55]. From proton conductivity point of view, the acid doping level should be high. However, the doping level of the membrane cannot be too high because of the decreasing mechanical strength of the membrane with increasing doping level. The chemical stability and mechanical strength of the PBI membrane can be improved by membrane modification such as cross-linking. However, the cross-linked PBI membrane showed poorer thermal stability because the high temperature can break the cross link.

The polymer in the PBI membrane would not experience significant thermal degradation in the typical operating temperature range of the HT-PEM fuel cell. No significant weight loss of the PBI membrane is observed in the temperature range of 150 – 500 ^{o}C in the thermogravimetric analysis (TGA) experiment [67]. However, the phosphoric acid doped in the membrane can experience the evaporation and the dehydration, resulting in a continuous decrease in proton conductivity of the membrane under typical operating temperature of the HT-PEM fuel cell. The evaporation and dehydration of PA in the PBI membrane was confirmed by the weight loss peak in the temperature range of 150 – 175 ^{o}C in the TGA experiment of the PBI membrane [68]. In the HT-PEM fuel cell, the dehydration of PA can be alleviated by the protection of the GDL and the water vapor generated through ORR in the cathode. However, the dehydration of PA can influence the durability of the HT-PEM fuel cell in a long-term operation, especially at the end of the lifetime. Modestov et al. [69] observed that the hydrogen crossover rate increased by a factor of 14 at the end of the lifetime test of a HT-PEM fuel cell, which can be ascribed to the local thinning or even pinhole formation of the membrane.

2.3.2. DEGRADATION OF THE CATALYST

The material and structure of the catalyst layer of the HT-PEM fuel cell are similar to that of the LT-PEM fuel cell and the PAFC. The platinum particles or its alloys, such as Pt/Ru, Pt/Co and Pt/Cr, are attached on the surface of carbon support with high specific surface area [70]. Therefore the degradation mechanisms of the catalyst layer of the HT-PEM fuel cell are similar that of the LT-PEM fuel cell and PAFC.

Under the harsh operating conditions of the PEM fuel cell, especially at high electrode potential, the platinum particles can be dissolved gradually into platinum ions, followed by redeposition on existing platinum surface forming particles with larger diameter or migration to other parts of the MEA where is not accessible to reactant gas [71]. The increase in platinum particle size caused by dissolution, migration and reprecipitation of the platinum particles is known as the Ostwald ripening [72]. In addition, the collisions between platinum particles which are close to each other also result in the increase in platinum particle size. This process is called the platinum agglomeration, which mainly occurs when the particle size is small and the Gibbs free energy is high [73]. The electrochemical catalyst surface area (ECSA) can be reduced by the continuous increase in platinum particle size, which results the degradation in the performance of PEM fuel cell. Except for the increase of platinum particle size, the migration of platinum ions to other parts of the fuel cell such as membrane and GDL also contributes the reduction of ECSA. Ferreira et al. [74] reported that Ostwald ripening and dissolution of the platinum particles contribute equally to the overall loss of the ECSA. The increase in platinum particle size and the migration of platinum particle can be accelerated by the corrosion of carbon support during the operation of PEM fuel cell. The mechanisms of carbon corrosion will be discussed in Section 2.2.3.

With higher operating temperature and more acidic environment, the degradation in the catalyst layer of the HT-PEM fuel cell is more severe than that of the LT-PEM fuel cell. Many works have been conducted to investigate the stability and degradation of platinum catalyst in the catalyst layer of the HT-PEM fuel cell under both steady-state conditions [69, 75-85] and under dynamic conditions [79, 80, 86-89].

The increase in average platinum particle size during long-term operation of HT-PEM fuel cell can be measured by X-ray diffraction (XRD) analysis [78, 90, 91] and by TEM imaging [75, 77, 82, 92]. The average particle size measured by TEM imaging is usually larger than that measured by XRD, because with TEM imaging the particles with diameter smaller than 1 nm can hardly be identified [93]. According to many researches, the growth rate of platinum particle in different electrode is different. Wannek et al. [78] reported that the increase in platinum particle size in cathode was larger than that in anode, over the same period of

operation. The same phenomenon was also observed by Qi and Buelte et al [94]. Usually the cathode potential is higher than anode potential. Higher potential brings about higher dissolution rate of platinum.

The operating parameters such as operating temperature can significantly influence the degradation of catalyst on the HT-PEM fuel cell. High operating temperature can accelerate the increase in platinum particle size and the decrease in ECSA. Therefore the performance decay rate of the HT-PEM fuel cell becomes higher with higher operating temperature as reported in the literature [76, 82, 83]. The kinetics of processes such as platinum dissolution, migration and agglomeration as well as the carbon corrosion, which lead to the degradation in platinum catalyst of HT-PEM fuel cell, can be enhanced by higher temperature. Moreover, the attachment of platinum particles on the carbon support surface can be weaken by the high temperature, which leads to more platinum particles detached from the carbon support surface. Except for the operating temperature, operating mode can also affect the degradation of platinum catalyst. Dynamic operation, such as load cycling, thermal cycling and start/stop cycling, can accelerate the degradation of catalyst of HT-PEM fuel cell. Yu et al. [95] reported that loss in ECSA of the HT-PEM fuel cell was much larger under load cycling condition and start/stop cycling condition than under constant load condition. The severe carbon corrosion caused by Load cycling and start/stop cycling operation is the main reason for the accelerated degradation in platinum catalyst of the HT-PEM fuel cell under these conditions.

Since the increase in platinum particle size is more severe when the particle diameter is small, the cell performance degradation caused by degradation in platinum catalyst mainly occurs in the initial stage of the lifetime of the HT-PEM fuel cell. This was confirmed by Zhai et al. [84] by conducting degradation test on HT-PEM fuel cell with different time spans. They observed that the increase in platinum particle size mainly occurred in the first 300 hour, and remained almost unchanged over the rest of the lifetime. At the same time, the cell performance showed a rapid decrease trend in the first 300 hours and a much slower decrease trend in the following time. Oono et al. [82] conducted a degradation test on a HT-PEM fuel cell with longer time span (16000 hours). The fast degradation was observed in the initial stage of the lifetime, which was ascribed to the increase in platinum particle size, especially in the cathode catalyst layer. When the platinum particle size is small in the initial stage of the lifetime, the Gibbs free energy of the particle is high which can result in more severe agglomeration. And the Gibbs free energy decreases with the increase in particle size, which explains the lower increase rate when the particle size becomes higher.

The degradation in catalyst of HT-PEM fuel cell can be also influenced by the platinum loading [96]. The usage of platinum in the catalyst layer can be minimized through modification of traditional methods. By minimizing the average platinum

particle size, sufficient performance of the PEM fuel cell can be achieved with lower platinum loading. However, the degradation in catalyst layer becomes more severe when the MEA is optimized towards lower platinum loading, because average platinum particle size growth is more severe with lower platinum loading. There is a trade-off relationship between the benefits from the reduced platinum loading and drawback from the higher degradation rate.

2.3.3. CARBON CORROSION

The porous carbon material is widely used in the PEM fuel cell as the support material for catalyst in the catalyst layer and to provide pathway for electron transfer and gas diffusion in the gas diffusion layer. The carbon can be corroded under typical operating conditions of the PEM fuel cell following Eq. (2.4):

$$C + 2H_2O \rightarrow CO_2 + 4H^+ + 4e^- \tag{2.4}$$

The equilibrium potential for this reaction is 0.207 V vs reference hydrogen electrode (RHE) in the acidic environment under room temperature [97], which means the carbon corrosion is thermodynamically feasible at the cathode potential of PEM fuel cell during operation. The carbon corrosion can lead to severe degradation in the catalyst layer of the PEM fuel cell. Firstly, the carbon corrosion weakens the attachment of platinum particles to the carbon support, which leads to the detachment of platinum particles from the carbon support surface. Thus the agglomeration and migration of platinum particle become more severe, resulting in severe decrease in ECSA and consequently the degradation in cell performance. Secondly, the void volume structure can be damaged by the carbon corrosion, leading to the blockage of pathway for gas diffusion and the increase in mass transfer resistance [98]. Thirdly, the corrosion or oxidation of carbon can decrease the hydrophobicity of the carbon surface, which can cause the electrode being blocked by phosphoric acid or water vapor. Lastly, corrosion of carbon support structure can increase the contact resistance, resulting in increasing ohmic resistance of the fuel cell.

Under typical operating conditions of the PEM fuel cell, the carbon corrosion proceeds very slowly. Therefore it only affects the durability of the PEM fuel cell over a long-term time span. The carbon corrosion rate in the PEM fuel cell can be evaluated by measuring the corrosion current, weight loss of the electrode or the CO_2 content in the exhaust gas of the PEM fuel cell. Lim et al. [99] investigated the carbon corrosion under different operating conditions and different platinum loading in the catalyst layer. They found that carbon corrosion rate became higher with higher operating temperature, higher relative humidity and higher platinum loading. Moreover, some operation modes of the PEM fuel cell which can result in high electrode potential, such as startup/shutdown and fuel starvation, can

accelerate the carbon corrosion significantly [95]. For the HT-PEM fuel cell, the high operating temperature brings about higher carbon corrosion rate. However, the low relative humidity can alleviate the carbon corrosion. Oh et al. [54] compared the carbon corrosion rate of HT-PEM fuel cell with that of the LT-PEM fuel cell, and the results revealed that carbon corrosion rate in the HT-PEM fuel cell was higher than in the LT-PEM fuel cell.

The stability of the carbon support can be improved by graphitization of the carbon material through high temperature treatment. The graphitized carbon material is widely used in PAFC to achieve better stability. For the HT-PEM fuel cell, the graphitized carbon material shows better stability under potential cycling condition. However, the expense of lower specific surface area of the graphite carbon material has to be paid [100].

2.3.4. LOSS OF PHOSPHORIC ACID

In the HT-PEM fuel cell, the PBI membrane has to be doped with PA to achieve high enough proton conductivity. The PA provides proton conductivity through the Grutthus Mechanism. In the catalyst layer of the HT-PEM fuel cell, the PA should be loaded as the electrolyte to provide the proton transfer pathway. The change in amount and distribution of PA in the membrane and electrodes of the HT-PEM fuel cell can influence the cell performance and the durability.

The PA loss rates of the HT-PEM fuel cell during long-term operation and its impact on performance degradation have been studied in the literature. By monitoring the PA content in exhaust water using inductively coupled plasma mass spectroscopy [101, 102] or chromatography [103], PA leaching rate is measured during long-term operation. PA leaching rate reported in these works ranges from 10^{-8} to 10^{-5} $mg \cdot cm^{-2} \cdot h^{-1}$, which is quite negligible and may not be the main reason for the performance degradation. With this leaching rate, even after 40,000 h lifetime operation less than 5% of PA will be leached out of the MEA. Yu et al [103] found that the PA leaching rate can be enhanced by high temperature and high current density. Lin et al. [104] reported that the pH value of water collected from the exhaust gas was about 5 in the first 30 h and increased to about 6 in the last 150 h, indicating the PA leaching mainly occurs in the beginning of the test. This can be explained by the excess PA in the MEA being squeezed into the flow field during single cell assembling and leached out during the operation. Although in [105] the authors believed that PA loss had a substantial influence over the entire lifetime of the fuel cell, because the PA loss rate was in good agreement with the cell voltage reduction rate. However this conclusion was based on the PA evaporation rate measured in a PAFC, which can hardly be applied to the HT-PEM fuel cell. Hartnig and Schmidt [106] reported that unstable bipolar plates exhibited high PA uptake from the MEA during fuel cell operation, which lead to acid loss from the catalyst layer and the membrane. This phenomenon suggests that PA loss

rate measured in the exhaust is lower than the actual PA loss rate because the PA captured in the bipolar plate cannot be measure in the exhaust.

To evaluate the PA content in the electrodes and the membrane, Kwon et al [107] proposed three techniques: CV, EIS and acid-based titration (ABT). In-situ CV and EIS as the indirect measurement methods have limitations in precise measurement of PA content. The change of ECSA evaluated by CV as well as the change of internal resistance measured by EIS during the operation can be used to deduce redistribution of PA in the electrodes. However other degradation behaviors such carbon corrosion in MEA can also cause similar change in CV and EIS. Thus they can only be regarded as supplementary PA distribution measurement methods. Ex-situ ABT can supply clear PA distribution between the membrane and electrodes; however it cannot reflect the acid distribution during operation conditions because it is carried out under room temperature. Nevertheless, it is still a good tool for evaluating the PA loss during long-term operation. Recently, the confocal Raman microscopy was employed to evaluate the spatial distribution of phosphoric acid distribution in the AB-PBI membrane for HT-PEM fuel cell [108]. With this method, the relation between the acid distribution in the membrane and the fuel cell performance can be investigated. However, the application of this method in the HT-PEM MEA has not been seen in the literature. Another method to evaluate the change in amount of PA in the HT-PEM during operation is in-situ synchrotron X-ray radiography [109]. At the operating temperature of 160 ^{o}C and high current load, the movement of liquid toward GDL in the HT-PEM fuel cell was visualized by X-ray tomographic microscopy. It is indicated that the loss of PA from the MEA is likely to be the main reason for the degradation at high current [110].

2.4. OPERATIONAL EFFECTS ON DEGRADATION OF HT-PEM FUEL CELLS

Except for the steady state operating condition, some practical environment operating conditions are known can accelerate the degradation of the HT-PEM fuel cell. In this section, the degradation mechanisms of the HT-PEM fuel cell under several stressed operating conditions including start/stop cycling, open circuit voltage, contamination and H_2 starvation are reviewed.

2.4.1. START/STOP CYCLING

The startup and shutdown operation of the HT-PEM fuel cell is believed can accelerate the carbon corrosion in the electrode. After extended shutdown, the air can diffuse from the atmospheric to the anode flow channel. Then in the startup process the H_2 is supplied to anode flow channel, resulting in the formation of the H_2/air interface. In the region where H_2/air interface is presented, the oxygen reduction reaction occurs in the anode, while the carbon corrosion and water

electrolysis reactions occur in the cathode because of local high potential (2 V) in the cathode [98]. The carbon corrosion in cathode causes severe damage to the cathode catalyst layer. This phenomenon is illustrated in Fig. 2.3.

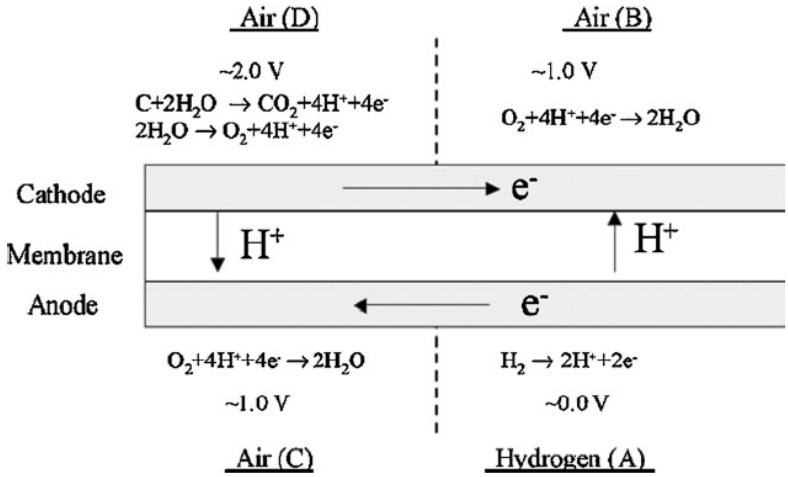

Fig. 2.3 – Schematic of reversal current model (reproduced from [98])

The degradation caused by start/stop cycling in the LT-PEM fuel cell has been widely investigated by many researchers. Ishigami et al. [111] conducted a simulated startup/shutdown cycling test by switching anode gas between H_2 and air. They found that the degradation caused by shutdown process was more severe than the degradation caused by startup process because H_2/air interface existed for a longer time during the shutdown process [112]. More researchers have investigated the effect of operating conditions on the degradation of PEM fuel cell under startup/shutdown cycles. The results revealed that the performance degradation was alleviated at lower humidity, lower temperature and with dummy load during shutdown process [113-115]. Takagi et al. [116] and Yu et al. [117] investigated the effect of gas shutoff sequence on the performance degradation rate. It was concluded that air should be closed before the closing of H_2 to prevent air permeation to the anode. Yu et al. [118] found that the closed cathode after shutdown of the HT-PEM fuel cell was beneficial for fuel cell durability.

Some researchers conducted start/stop cycling tests on PBI-based HT-PEM fuel cell. Schmidt and Baurmeister [89] operated a commercial HT-PEM fuel cell for more than 240 start/stop cycles in more than 6000 hours. The degradation rate of the HT-PEM fuel cell operated under start/stop cycling condition was much higher than that under steady-state condition. The increase in cathode mass transport resistance caused by carbon corrosion in cathode during start/stop processes was the main reason for the accelerated degradation. The simulated start/stop test in the HT-

PEM fuel cell was conducted by switching the anode gas between H_2 and air in intervals of 90 seconds [119]. The degradation rate of the fuel cell was similar to the fuel cell experienced realistic start/stop test with the same number of cycles.

To mitigate the degradation caused by startup/shutdown process, the time span with existence of H_2/air interface should be minimized. The inert gas such as N_2 can be purged into the electrodes after shutdown to expel the residual H_2 and air in anode and cathode, respectively. However, this strategy requires N_2 supply system which increases the complexity of the fuel cell system. Another mitigation method is to apply the auxiliary load (dummy load) before startup or after shutdown, as proposed in the literature [115]. Residual H2 in anode can be consumed by the dummy load, preventing the presence of H_2/air interface.

2.4.2. OPEN CIRCUIT VOLTAGE

The open circuit voltage (OCV) is the voltage of fuel cell when it is disconnected from the load. Operating the fuel cell under OCV condition can enhance the MEA chemical degradation, especially for the membrane. Under OCV condition, the hydrogen peroxide (H_2O_2) can be generated by the reaction of hydrogen and oxygen at anode catalyst layer, which leads to the chemical degradation of the polymer electrolyte membrane, as discussed in Section 2.2.1. The degradation in membrane can result in the thinning of the membrane, increasing the gas crossover through the membrane, which in turn accelerates the formation of H_2O_2. In addition, the cathode potential is higher under OCV condition than with certain current load, therefore the degradation in catalyst layer is more severe under OCV condition. Moreover, the cathode potential becomes higher under OCV conditions than with current load, which can lead to significant carbon corrosion in cathode of the fuel cell.

The degradation caused by OCV operation has been investigated in the literature. A 1200 h degradation test on a six-cell short stack was conducted under close to OCV (10 mA/cm^2) conditions by Wu et al. [120]. They found that the performance decay rate in the first 800 hours was much lower than that in the following 400 hours. The degradation mechanism for the first period was ascribed to catalyst degradation, while for the second period membrane failure was assumed to be the main reason for degradation. Teranishi et al. [121] observed the degradation under OCV condition mainly occurred in the cathode through EIS measurement and SEM observation. Qi and Buelte [94] investigated the effect of OCV on the performance degradation of a PBI HT-PEM fuel cell. The OCV of the fuel cell increased in the first 35 min and then declined thereafter. EIS result showed significant catalyst activity loss and increase in mass transport. Moreover, the platinum particle size in the cathode increased by 430% after the test.

2.4.3. IMPURITIES IN THE ANODE GAS

To increase the fuel flexibility and overcome the difficulties in H_2 storage, the H_2-rich reformate gas produced from light fossil fuels, such as ethanol, methanol and natural gas, is often adopted as the anode gas for the HT-PEM fuel cell. The H_2-rich reformate gas contains impurities, including CO, CO_2, water vapor and unconverted light fossil fuel, which can cause degradation in cell performance of the HT-PEM fuel cell. The contamination mechanisms of impurities to the HT-PEM fuel cell include: (a) strong adsorption on the catalyst surface, (b) decomposition into CO and then adsorbed on the catalyst surface and (c) dilution effect. The poisoning mechanisms of different typical impurities on HT-PEM fuel cell are reviewed.

2.4.3.1 Carbon monoxide

The CO is the typical impurity in reformate from light fossil fuel. The poisoning mechanism of the CO is the fast and strong adsorption on the platinum surface, which hinders the adsorption of H_2 on the catalyst surface and the following reaction. For LT-PEM fuel cell, it is reported that the CO with concentration of 50 – 70 ppm can cause 85% of cell voltage loss [122]. The tolerance of CO can be enhanced by higher temperature because of the exothermic nature of CO adsorption process. Therefore the HT-PEM fuel cell shows better tolerance to CO than its low temperature counterpart. In the temperature range of 180 – 210 ^oC, the HT-PEM fuel cell can be operate with CO concentration up to 5% [40, 123]. By higher operating temperature and lower current density, the CO poisoning effect can be alleviated [124]. The platinum loading, fuel utilization and the flow channel geometry can influence the CO poisoning [125]. Being diluted by N_2 can deteriorate the CO poisoning to a large extend [126]. Except for fast degradation in cell performance, the CO can also cause heterogeneity in current density distribution. In regions near the fuel inlet the current density increases, while in regions near the fuel outlet the current density drops [127]. Under higher CO concentration and higher current load conditions, the current density becomes more uneven. Engl et al. [128, 129] reported that the CO in the reformate gas can help to alleviate the carbon corrosion induced by startup/shutdown operation.

The CO poisoning on the HT-PEM fuel cell was widely investigated by numerical modeling. In the CO poisoning model developed by Bergmann et al. [130], the adsorption/desorption of CO was treated as a Frumkin isothermal process due to the interaction of adsorbed and non-adsorbed CO molecules. While in the model developed by Jiao et al. [131], the adsorption/desorption of CO was assumed to follow the Langmuir kinetics. On the base of the model in [131], the effect of flow channel configuration on the CO poisoning was studied [132]. The results suggested that the cell voltage loss caused by CO was more severe with interdigital and serpentine flow channel than with parallel flow channel. In the model developed by Oh et al. [133], the H_2 adsorption kinetics was treated as a function of

CO coverage, which can improve the simulation results. The model considering the effect of CO to the transient behaviors of the HT-PEM fuel cell during startup process was developed by Rasheed and Chan [134]. The results revealed the high current load and CO concentration and low temperature increase rate should be avoided to prevent sudden drop in cell voltage during startup process.

Several methods have been developed in order to minimize the poisoning effect of CO to the PEM fuel cells. Generally, the higher operating temperature, employment of CO tolerance catalyst and air bleeding are the common methods to mitigate the CO poisoning effect. High operating temperature can effectively reduce the performance loss of the HT-PEM fuel cell caused by CO poisoning. However, high temperature brings about more severe degradation on all components of the HT-PEM fuel cell, which could shorten the lifetime. Therefore the optimum operating temperature needs further investigation to take both CO tolerance and durability into account. Alloying the platinum with the second or even the third element to form binary or ternary platinum alloy can improve the CO tolerance [135]. The enhanced CO oxidation by the addition of the second or the third element is ascribed to the mechanism for the improving CO tolerance. Modestov et al. [136] investigated the CO oxidation on pure Pt and Pt-Ru surface in high temperature PBI/H_3PO_4 MEAs. The results showed the CO oxidation rate on Pt-Ru catalyst surface is 20 times higher on pure Pt surface at the same electrode potential. Although the Pt alloys show better CO tolerance than pure Pt, the stability and activity of platinum alloys are lower [137], which need to be improved in the future. Air bleeding is a simple method to eliminate the CO poisoning effect to the PEM fuel cell. By introducing low level of oxidant such as air or O_2, the CO can be eliminated by selective oxidation. For LT-PEM fuel cell, it was reported the cell performance loss caused by 200 ppm CO can be recovered by 5% air bleeding. The application of air bleeding on HT-PEM fuel cell has not been seen in the literature.

2.4.3.2 Carbon dioxide

The CO_2 is a typical byproduct in the steam reforming process. Its concentration in the reformate gas can be around 25%vol. The main poisoning mechanism of CO_2 in the PEM fuel cell is the dilution. Moreover, the CO_2 can be converted to CO through reverse water gas shift reaction.

Under the typical operating conditions of LT-PEM fuel cell, the CO concentration formed through reverse water gas shift reaction by the gas mixture of 75% H_2 and 25% CO_2 can be in the range of 20 – 100 ppm, which can be harmful to the cell performance [138]. It was reported the CO produced from reverse water gas shift reaction can cover more than half of the catalyst surface area under the operating temperature of 50 – 70 ^oC [139]. Under the operating conditions of HT-PEM fuel cell, the CO concentration formed through reverse water gas shift reaction can be even higher. On one hand, the operation of HT-PEM fuel cell does not rely on

humidification. The absence of water in anode fuel stream can shift the equilibrium of reverse water gas shift reaction to the formation of CO. On the other hand, higher operating temperature favors the formation of CO through reverse water gas shift reaction because of the endothermic nature of this reaction. However, Li et al. [124] observed that the cell performance showed no significant change when replacing the CO_2 in the H_2 by N_2.

2.4.3.3 Other impurities

The unconverted fuel is usually presented in the reformate gas because the conversion of fuel in a reformer can hardly go to 100%. Methanol is a popular fuel used for H_2 production via reformation. The influence of unconverted methanol in the anode fuel stream has been investigated in the literatures [140, 141]. Araya et al. [140] conducted a long-term durability test on a HT-PEM fuel cell in which the concentrations of methanol-water vapor mixture varied in the range of between 3 % and 8 %. The performance decay rate of the fuel cell was between -900μV/h and -3400μV/h in this test. The poisoning mechanism of methanol can be either the directly adsorbing on the platinum catalyst surface or the decomposing into CO which strongly absorbing on the platinum surface. In a recent literature [141] they characterized the performance of a high temperature PEM fuel cell at varying temperatures and methanol concentrations in anode fuel stream. Overall negligible effect was observed for methanol concentration below 3% in the operating temperature range between 140 ^{o}C and 180 ^{o}C.

The effect of chloride as the contaminant in air side of a HT-PEM fuel cell on the performance and durability was studied by Ali et al [29]. It is found that introducing HCl into the air humidifier can decrease the fuel cell performance; however the degradation is mostly reversible. The degradation of the fuel cell under potential cycling condition was accelerated by the presence of chloride.

Sulfur containing species such as hydrogen sulfide and sulfur oxide are also typical impurities presented in the fuel and air stream of the PEM fuel cell. The sulfur poisoning mechanism for the low temperature PEM fuel cell has been widely investigated. Like the CO, the sulfur containing species strongly adsorb on the active sites of the catalyst, preventing hydrogen or oxygen from adsorbing on the catalyst surface. It is suggested that the hydrogen sulfur concentration should be below 1 ppm for low temperature PEM fuel cell [142]. For PBI based high temperature PEM fuel cell, very limited work about the sulfur poisoning can be found. Schmidt and Baurmeister investigated the effect of CO and hydrogen sulfur on the cell performance and degradation of the high temperature PEM fuel cell [143]. At the operating temperature of 180 ^{o}C, at least 10 ppm hydrogen sulfur can be tolerated. The high temperature PEM fuel cell was operated for 3000 hours on reformate gas containing 2% CO and 5 ppm hydrogen sulfur with similar degradation rate to that for operated with pure hydrogen.

2.4.4. GAS STARVATIONS

Gas starvation of the fuel cell refers to the under supply of H_2 in anode or air in cathode. The situation which the overall gas stoichiometry is greater than 1.0 and local region of the fuel cell is starved of gas is call 'local gas starvation'. The situation which the overall gas stoichiometry is less than 1.0 is called 'overall gas starvation'.

The local H_2 starvation can be caused by gas maldistribution between different regions of a single fuel cell and the startup operation after long-term shutdown. Consequences and degradation mechanisms of local H_2 starvation is similar to degradation caused by startup/shutdown process, e.g. the reverse current decay mechanism. The carbon corrosion in cathode catalyst layer can be caused by the local H_2 starvation. Inhomogeneous current density distributions are observed during local H_2 starvation and can reflect the severity of local H_2 starvation [144, 145].

The overall H_2 starvation can be caused by many factors [146]: uneven H_2 distribution between different cells within a stack, fault in control of fuel supply system and sudden increase in current load. The fuel starvation is detrimental to the performance and durability of the PEM fuel cell. When the fuel cell is starved of H_2, the anode potential increases to be higher than cathode potential, which results in the cell reversal [147]. Under this condition the fuel cell consumes energy from other cells in the same stack, instead of generating electricity. More importantly, the high anode potential triggers the carbon corrosion and water electrolysis reactions in the anode catalyst layer. The occurrence of carbon corrosion and water electrolysis reactions are proven by the existence of O_2 and CO_2 in anode exhaust gas under H_2 starvation condition [148]. The carbon corrosion causes loss of platinum catalyst and the decrease in ECSA.

The air starvation is believed to be less harmful to the PEM fuel cell than the fuel starvation [149]. Under air starvation condition, the cathode potential decreases to be lower than the anode potential, which also results in the cell reversal [150]. Similar to the fuel starvation, air starvation causes the increase in current density in upstream regions and decrease in downstream regions.

2.5. MOTIVATIONS AND OBJECTIVES OF THE CURRENT PROJECT

Although the HT-PEM fuel cell shows many advantages over its low temperature counterpart, the great challenge on the degradation brought by the high operating temperature of the HT-PEM fuel cell is still the main obstacle which is hindering its successful commercialization. The performance degradation of the HT-PEM fuel

cell is inevitable during the operation process; however with better and more comprehensive understanding of the degradation mechanisms, the performance decay rate can be minimized. This project aims to gain better understanding of the degradation mechanisms of the HT-PEM fuel cell under non-ideal operating conditions, including start/stop cycling, impurities in anode stream and H_2 starvation. These operating conditions are related to the real-life application of the HT-PEM fuel cell. By investigating the degradation and failure modes of the HT-PEM fuel cell under these operating conditions, this project can contribute to the development of the HT-PEM fuel cell in terms of prolonging its lifetime.

2.6. SUMMARY

The HT-PEM fuel cell shows enhanced tolerance to the impurities such as CO in the anode stream because of the high operating temperature. Therefore it can directly utilize the reformate gas produced from fuel which usually contains CO with concentration in the range of 1 – 5 %vol. However, the impurities in the anode stream and high operating temperature bring about great challenges to the lifetime and durability of the HT-PEM fuel cell. In this section the degradation mechanisms of different components of the HT-PEM fuel cell are reviewed, giving the scientific background of this project. In the following sections, the experiments about degradation of HT-PEM fuel cell under different operating conditions are presented, including the methodologies, the results and the conclusions of these experiments.

CHAPTER 3. METHODOLOGIES

This section first describes the experimental setup used in this project, including the MEA, the single cell setup, the fuel cell test station and other instruments for fuel cell characterization. Then the in-situ and ex-situ characterization techniques used in this project are introduced. Lastly, the detailed experimental procedures of all the experiments conducted in this project are described.

3.1. EXPERIMENTAL SETUP

3.1.1. MEA

The commercially available HT-PEM membrane electrode assembly Dapozol G77 produced by Danish Power System was used in this project. This type of MEA is based on a 40 μm PBI membrane doped with phosphoric acid with the doping level of around 9 per repeat PBI unit. The active cell area is 46.2 cm^2 and the platinum loading on both anode and cathode are 1.5 mg/cm^2. The gas diffusion layer is woven of carbon fiber with the thickness of 250 μm. The operating temperature of this type of MEA is in the range of 120 – 180 ^oC.

3.1.2. SINGLE CELL SETUP AND CURRENT DENSITY DISTRIBUTION MEASUREMENT

The MEA was sandwiched between two graphite flow plates with double serpentine flow channel and two stainless steel end plates to form a single cell setup. Teflon gaskets with thickness of 250 μm and the assembly torque of 300 N·m were adopted to ensure the gas tightness and proper compression on the MEA during assembling. Four heaters (4×75 W) imbedded in the end plates can be used to heat up and maintain the operating temperature of the single cell. The picture and the schematic plot of the single cell setup are shown in Fig. 3.1.

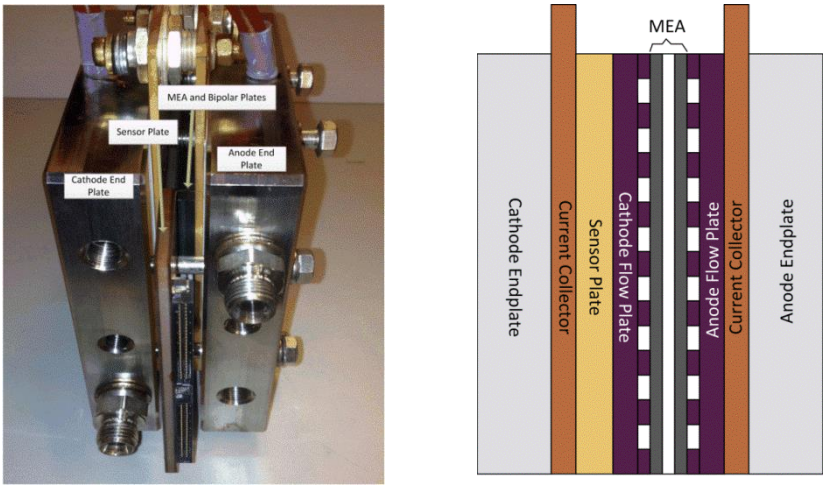

(a) *(b)*

Fig. 3.1 – The photo (a) and the schematic plot (b) single cell setup used in this PhD project

In the experiment of H_2 starvation investigation, the current density distribution was measured. A segmented sensor plate which is developed by the company S++ was installed between the flow plate and the end plate in cathode side to measure the current density distribution. The 100 segments in the sensor plate ensure the high enough resolution in current density measurement. In Fig. 3.2 the configuration of the segments in the sensor plate (red line) and the flow channels in the flow plates in both anode and cathode are illustrated.

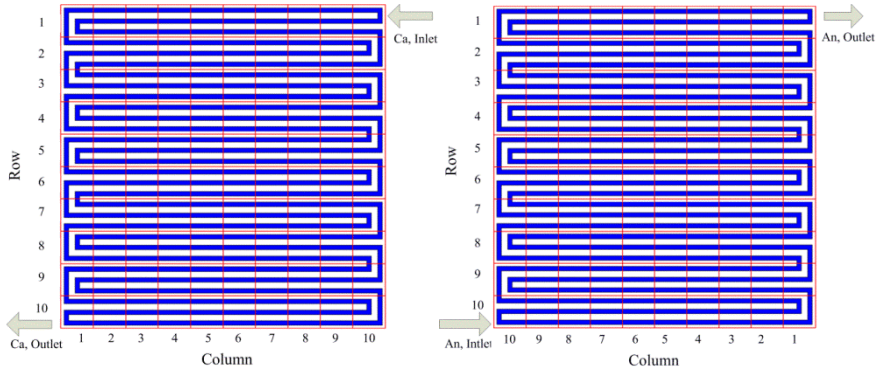

(a) *(b)*

Fig. 3.2 – The scheme of segmented sensor plate (red line) and flow channel (blue line) and configuration of gas flow in cathode (a) and anode (b).

The measurement of the local current density is based on the relationship between the permeability of the magnetically soft material and the magnetic field strength and temperature. On each segment there is a coil (L_1) which the measured current flows through and another pair of coil (L_2 and L_3). The current which needs to be measured flows through soft magnetic coil L_1, while a small alternating current is imposed in L_2. The current in coil L_1 results in a magnetic field which strength determines the induced voltage in L_3. Based on the induce voltage in L_3 and other known parameters, the measured current can be calculated. The measured local current values can be then stored in the computer by a data acquisition board connected with the sensor plate. This sensor plate allows a minimum measurement interval of 0.5 s, which ensures the dynamic behavior in local current density can be recorded.

Compared with other local current density measurement techniques such as segmented MEA and segmented flow plate, the technique used in this project is non-invasive to the components of the fuel cell, and therefore does not have interference with the operation of the fuel cell [151]. However it should be mentioned that the accuracy of the measurement can be affected by the lateral current flowing in the flow plate, although a thin flow plate (2 mm) is adopted for the single cell setup to minimize the influence of the lateral in-plane current.

3.1.3. FUEL CELL TEST STATION

The experimental setup used to control the operating parameters and characterize the fuel cell is illustrated in Fig. 3.3. A fuel cell test station FCATS G60 from GreenLight Innovation (Canada) is used to control the operating parameters of the fuel cell including gas stoichiometries in both anode and cathode, operating temperature, back pressure in both anode and cathode and the current load of the fuel cell. The H_2, N_2, carbon monoxide (CO) and carbon dioxide (CO_2) can be all fed into the anode of the fuel cell with any specific gas composition by controlling flow rate of each gas composite via the flow rate controller. Additionally, the gas mixture in anode pipe can be humidified by a bubble humidifier with precise control of the dew point temperature. The water content in anode gas is therefore controlled by the dew point temperature. To investigate the effect of methanol on the performance and endurance of the fuel cell, a metering pump and an evaporator is adopted in the test station to introduce methanol vapor into the anode gas with precise flow rate control.

An auxiliary power supply (SM 52-AR-60, DELTA ELECTRONIKA) is connected with the electronic load and the fuel cell in series, to study the cell reversal behaviors in H_2 starvation experiments. The Gamry device Reference 3000 (Gamry Instruments, USA) is used to perform the electrochemical impedance spectroscopy (EIS) and cyclic voltammetry (CV) to evaluate the performance and characterize the internal resistances of the fuel cell. The detailed measurement principles and

procedures of the EIS and CV are introduced in Section 3.2.2 and 3.2.3, respectively.

A quadrupole mass spectrometer (OmniStar GDS 301, Pfeiffer Vacuum) is connected with the anode exhaust pipe to analyze the anode exhaust composition under H_2 starvation conditions.

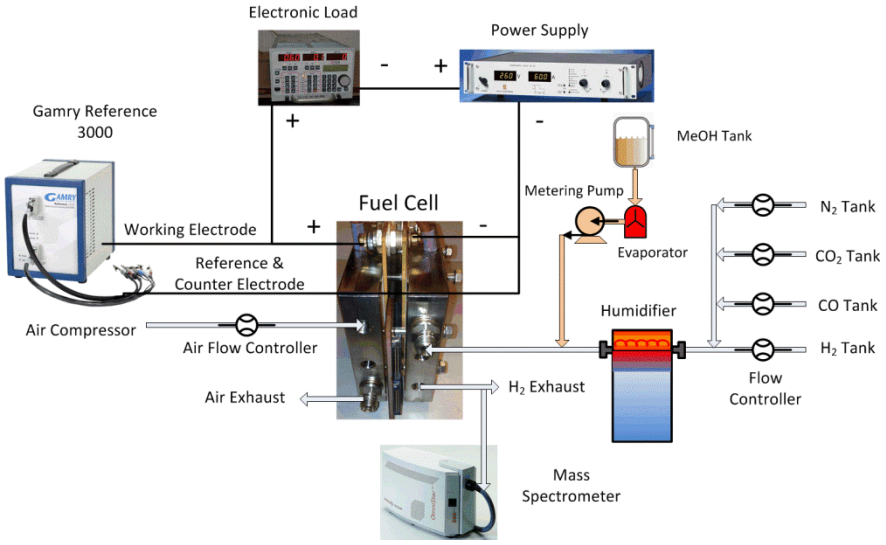

Fig. 3.3 – The scheme of the experimental setup

3.2. CHARACTERIZATION TECHNIQUES FOR THE HT-PEM FUEL CELLS

In this section, both in-situ and ex-situ characterization techniques adopted in this PhD project are introduced.

3.2.1. POLARIZATION CURVES

To yield the performance loss with different current load (or current density) under operating conditions, the plot of cell voltage versus current load (or current density) of the fuel cell, namely the polarization curve, can be measured and presented. It is the most commonly method to evaluate the cell performance under steady state conditions and give the information about the performance loss under different current density regions. A typical polarization curve of high temperature PEM fuel cell is illustrated in Fig. 3.4. Normally, the shape of the polarization curve varies under different current density regions. The cell voltage drops rapidly under low current density region due to the kinetic overpotential of the oxygen reduction

reaction (ORR) in cathode and hydrogen oxidation reaction (HOR) in anode, namely the activation loss. The activation loss increases sharply in the low current density region and remains almost stable in the intermediate and high current density regions. In the intermediate current density range the cell voltage decreases linearly according to the ohm's law, as the cell voltage loss is mainly caused by ohmic resistance of the fuel cell. Under high current density, the mass transfer resistance of the reactant gas in GDL and CL becomes higher and dominate the cell voltage loss. The cell voltage drops rapidly again due to the limitation in gas transfer rate in this region.

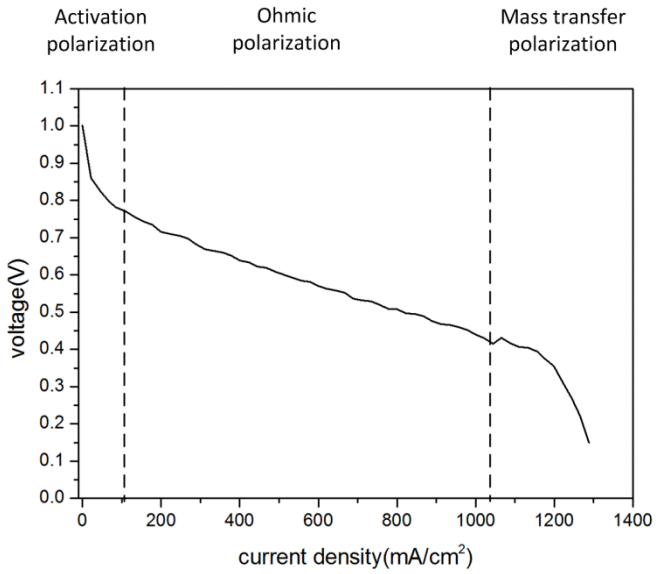

Fig. 3.4 – A typical polarization curve of the HT-PEM fuel cell

In this project, the polarization curves were often measured to evaluate the change in cell performance before and after the degradation tests. The current density was controlled by the electronic load and the cell voltage was measured at each current density value.

The Tafel plots which describe the relationship between ohmic-loss-corrected voltage ($E_{\text{IR-free}}$) and the current density in logarithmic coordinates were presented on the basis of the polarization curves. The ohmic-loss-corrected voltage can be calculated according to Eq. (3.1) [152]:

$$E_{IR-free} = E_{cell} + I \cdot R_{cell} \tag{3.1}$$

where E_{cell} is the cell voltage, I is the current load and R_{cell} is the ohmic resistance of the fuel cell. In the low current density region, the $E_{IR\text{-}free}$ is only related to the activation overpotential for ORR in cathode and HOR in anode. Given the fact that the exchange current density of HOR is 5-6 orders of magnitudes higher than that of ORR, the activation overpotential in cathode dominates the cell voltage loss in low current density region. However, it should be noted that when the impurities such as CO and CO_2 are presented in the anode stream, the anode overpotential is increased significantly. In this case the anode activation overpotential also contributes to the cell voltage loss in low current density region. The activation overpotential can be calculated according to the Eq. (3.2):

$$\eta_{act} = b \cdot \log(i) \tag{3.2}$$

where b is the Tafel slope and i is the current density. Therefore the $E_{IR\text{-}free}$ should decrease linearly in the low current density region in the semi-logarithmic Tafel plot. And in the high current density region the mass transfer limitation can cause the deviation of the $E_{IR\text{-}free}$ from the linearity. A typical Tafel plot of high temperature PEM fuel cell is illustrated in Fig. 3.5.

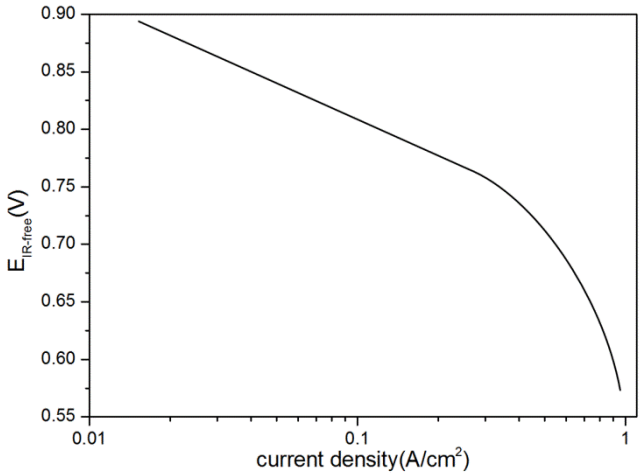

Fig. 3.5 – A typical Tafel plot of the HT-PEM fuel cell

From the polarization curves the cell voltage loss caused by resistances from different reaction processes can be observed in different current density regions. However the individual contribution of each resistance on the cell voltage loss is difficult to distinguish from each other because of the overlap of different losses over the whole current density range. Especially when multi-step reactions, parallel reaction and additional reactions such as adsorption/desorption are all involved in

the operation of the fuel cell. Thus characterization technique with better resolution such as EIS needs to be applied.

3.2.2. ELECTROCHEMICAL IMPEDANCE SPECTRUM

The electrochemical impedance spectrum (EIS), also known as alternate current (AC) impedance is another commonly used in-situ electrochemical characterization techniques in the field of fuel cell. When performing the EIS measurement, a sine-wave signal of current or voltage with small amplitude is superimposed on the fuel cell during operation with the frequency of the sine-wave signal sweeping from low frequency to high frequency. In the meantime the corresponding voltage or current response and its phase shift are measured and recorded. The complex function of the impedance can be illustrated according to Eq. (3.3) [153]:

$$Z = \frac{V_0}{I_0} e^{-j\phi} = \frac{V_0}{I_0}(\cos\phi - j\sin\phi) \tag{3.3}$$

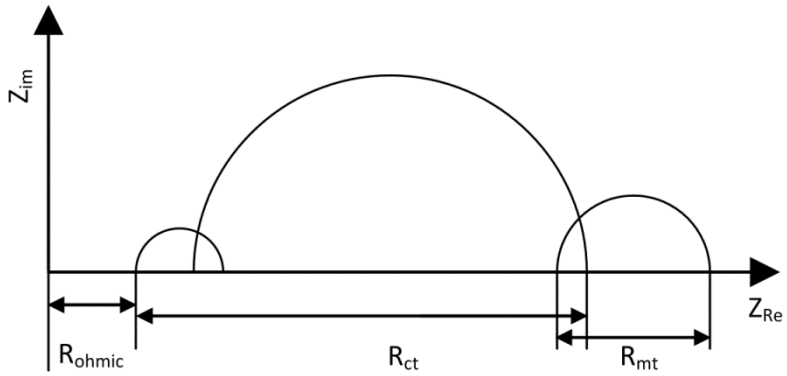

Fig. 3.6 – The typical impedance spectrum of the HT-PEM fuel cell

One of the most significant advantages of the EIS measurement is its capability to distinguish the contributions from different processes. The analysis in frequency domain can distinguish processes with different time constant [154]. For example the mass transfer process with relatively long time constant mainly contributes to the lower frequency range of the spectrum, while charge transfer which progresses much faster is related to the spectrum in higher frequency range. With such an analysis more useful information about the steady state operation and degradation of the fuel cell can be obtained. Another merit of the EIS measurement is that the operation of the fuel cell is not interrupted since the superimposed alternate current or voltage is much lower than the current or voltage generated by the fuel cell. In

addition, the short measurement time and non-intrusive nature of the EIS measurement make it very convenient in fuel cell characterization.

The obtained impedance spectrum can be fitted by the equivalent circuit (EC) model to extract the internal resistances resulted from different processes, which is the more meaningful information and can help for quantitative analysis [155]. The EC model is a network of ideal circuit elements such as resistors, capacitors and inductors, which can produce the same impedance as that produced by the fuel cell. It should be noted that for a certain impedance spectrum there may be not only one unique EC model which gives a nice fitting. Therefore when choosing the proper EC model, it is important that the EC model gives a reasonable interpretation of the processes involved with the reactions in the fuel cell.

The EIS measurement can be performed either in potentiostatic or galvanostatic mode. Generally there is no significant difference between these two measurement modes. In this project, galvanostatic mode measurements were performed by a Gamry device when the fuel cell was operated at steady state with current load of 9A. The amplitude of AC perturbation was set at 5% of the current load of the fuel cell. This amplitude is neither too high to interrupt the operation of the fuel cell nor too low to result in low signal noise ratio. The frequency of the AC signal ranges from 10 kHz to 0.1 Hz with 10 points per decade. In addition, the obtained impedance spectra were checked by means of Kramers-Kronig relations to verify the linearity of the response.

3.2.3. CYCLIC VOLTAMMETRY

The cyclic voltammetry (CV) is another commonly used electrochemical characterization technique for the fuel cell research which has the ability to quantify the catalyst activity of the fuel cell [156]. When performing the CV measurement, the potential of the working electrode is swept forth and back between two potential limits. The current response is recorded in the meantime. The plot of potential versus current (or current density) is the so-called cyclic voltammogram. A typical cyclic voltammogram is shown in Fig. 3.5. In this figure it can be observed there are several potential peaks which give information about the relative rates of reactions and adsorption/desorption processes in the catalyst layer of the fuel cell. The upward peak in the cyclic voltammogram between 0.2 and 0.4 V is related to the hydrogen desorption from the platinum catalyst surface. By assuming only a monolayer of hydrogen molecules adsorbed on the platinum surface with a charge density of 210μC/cm^2, the electrochemical active surface area can be calculated by the Equation (3.4) [76].

$$ECSA(cm^2 Pt / gPt) = \frac{charge(\mu C / cm^2)}{210(\mu C / cm^2 Pt) \times catalyst\_loading(gPt / cm^2)} \quad (3.4)$$

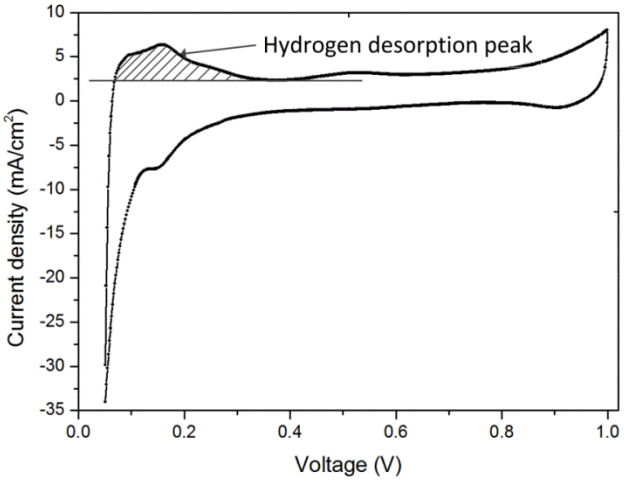

Fig. 3.7 – The typical cyclic voltammogram of a HT-PEM fuel cell in the potential range of 0.05 V and 1.0 V

In this project, when performing the CV measurement, the cathode was treated as the working electrode since the degradation in cathode is more severe and of more interest. While the anode was treated as reference and counter electrode. The H_2 and N_2 were fed to anode and cathode, respectively. The potential of the cathode was swept between 0.05 V and 0.5 V with a sweep rate of 0.01 V/s.

3.2.4. SCANNING ELECTRON MICROSCOPY

The scanning electron microscopy (SEM) can be used as a post-mortem analysis, which can characterize the microstructure of the MEA. It is believed that the changes in microstructure of the MEA illustrate the mechanisms of the degradation of the fuel cell, such as the thinning of the membrane and the catalyst layer, the cracking and delamination of the membrane, and carbon corrosion in the catalyst layer and the GDL.

In this project, the cross-section images of the MEA was characterized by the SEM (EVO LS15, Zeiss) operated at 20 kV. The MEA sample was prepared by cutting using a sharp knife.

3.2.5. X-RAY DIFFRACTION

The X-ray diffraction (XRD) is a common technique to study the structure of crystalline based on the constructive interference of monochromatic X-rays and the crystalline sample. For characterization of the fuel cell, it is widely used to estimate

the crystallite size of the platinum particles using Scherrer's equation on the basis of diffraction peaks [157]:

$$L = \frac{0.9\lambda}{\beta_{2\theta} \cos\theta_{\max}} \tag{3.5}$$

In this project the XRD analysis was performed on the catalyst samples scratched from the catalyst layer of the fuel cell. The experiment was conducted on an X-ray diffractometer (Empyrean, PANalytical) equipped with a Cu Kα1 (λ=1.540598 Å) X-ray source operated at 40 kV and 25 mA. The samples were scanned between 30^o and 90^o for 2θ with the scan rate of $2^o min^{-1}$.

3.2.6. MASS SPECTROMETRY

The mass spectrometry is an analytical chemistry technique which can help to identify the composition of the mixture by measuring the mass to charge ratio of the ionized fragments of the gas molecules and corresponding abundance. In a typical mass spectrometer, the gas molecules are first ionized by the collision with high energy electrons and knocking out one of the electrons to give a positive ion. Then the ionized fragments are accelerated to the same kinetic energy. With different deflection in the electromagnetic field, the fragments with different mass to charge ratio can be separated and detected by the detector separately. Higher strength of signal detected at a certain mass to charge ratio indicates more fragments with this mass to charge ratio.

In this project a quadrupole mass spectrometer (OmniStar GDS 301, Pfeiffer Vacuum) was used to analyze the gas composition of the anode exhaust of the fuel cell.

3.3. EXPERIMENTAL PROCEDURES

In Section 3.3, the break-in which is conducted in all the fuel cells used in this project is introduced first, followed by the experimental procedures of all the experiments conducted in this project.

3.3.1. BREAK-IN

The break-in (or activation/conditioning) process is needed for a HT-PEM fuel cell to achieve its best performance. Different break-in modes are introduced in the literature [158]. It was reported the continuous galvanostatic break-in brings about deeper activation and higher performance for the HT-PEM fuel cell, although the time needed for discontinuous break-in and potential cycling break-in is shorter [159]. In this project, a galvanostatic break-in as suggested by the manufacturer of

the MEA was performed on each single cell before the experiments. The operating temperature was set at 160 ^{o}C, and the stoichiometries at anode and cathode are 1.5 and 4, respectively. The current load of the single cell was maintained at 9A (200mA/cm^2). The cell voltage was monitored during the break-in, and a stable value on the cell voltage over a certain period (several hours) indicates the end of the break-in.

3.3.2. LONG-TERM DEGRADATION TEST

To investigate the degradation of the PBI/H_3PO_4 HT-PEM fuel cell under steady state and start/stop conditions and in the presence of methanol, degradation tests were performed on two HT-PEM fuel cells.

A 24-hour break-in was performed on the first cell, followed by the 100-hour operation under constant steady state condition with constant current load of 300mA/cm^2. After that, the fuel cell was operated at the 12-hour startup/12-hour shutdown condition for 120 hours. During the startup process, the H_2 and air were supplied after the fuel cell was first heated up to 120 ^{o}C. After the 12-hour operation, the heaters of the fuel cell were shut off. When the cell temperature deceased below 120 ^{o}C, the electronic load was disconnected and the gas supply was turned off. During the shutdown period, the fuel cell was cooled down to room temperature and exhaust was closed at anode and cathode. After the 120-h startup/shutdown cycling, the fuel cell was operated at steady state condition with methanol in the fuel stream to study the effect of methanol slip on the degradation of the HT-PEM fuel cell. The gas composition in this period was similar to that of the reformate gas produced from a methanol reformer, except that the CO_2 was eliminated to investigate the effect of methanol alone. The following reaction was considered for the steam reforming reaction in the methanol reformer:

$$CH_3OH + H_2O \rightarrow 3H_2 + CO_2 + (CH_3OH + H_2O)_{unreacted} \tag{3.6}$$

The steam to carbon ratio in the reformer was assumed to be 1.5, and side reactions which bring about the formation of CO such as methanol decomposition and reverse water gas shift were neglected. The methanol conversion rate was assumed to be 90%. Based on the assumptions made, the simulated reformate was consist of H_2, H_2O and methanol with volume fraction of 79.11%, 17.95% and 2.94%, respectively.

After the first single cell was designated the end of life because of a series of emergency stops of the test station, the degradation tests were performed on the second single cell. It experienced a 110-h break-in and a continuous test. After that, a continuous test and a reformate startup/shutdown test with simulated reformate as

fuel were carried out. The detailed procedure and operating conditions are listed in Table 3.1.

Table 3.1 – Procedure and operating conditions of degradation tests

Fuel Cell No.	Operating Modes	Operating Conditions	Duration	Electrochemical techniques
1	Break-in	160 °C $\lambda_{air}/\lambda_{H2}$=2.5/1.5 0.2A/cm^2	24 h	None
1	H_2 continuous	160 °C, $\lambda_{air}/\lambda_{H2}$=4/1.2 0.3A/cm^2	100 h	Polarization curves and EIS
1	H_2 startup/shutdown	Start: 160 °C $\lambda_{air}/\lambda_{H2}$=4/1.2 0.3A/cm^2 Stop: room temperature, no gas supply	120 h	Polarization curves and EIS
1	Reformate continuous	160 °C $\lambda_{air}/\lambda_{H2}$=4/1.2 0.3A/cm^2	108 h	Polarization curves and EIS
2	Break-in	160 °C $\lambda_{air}/\lambda_{H2}$=2.5/1.5 0.2A/cm^2	110 h	Polarization curves
2	H_2 continuous	160 °C $\lambda_{air}/\lambda_{H2}$=4/1.2 0.3A/cm^2	67 h	Polarization curves

2	Reformate continuous	160 °C, $\lambda_{air}/\lambda_{H2}$=4/1.2 0.3A/cm^2	48 h	Polarization curves
2	Reformate startup/shutdown	Start: 160 °C, $\lambda_{air}/\lambda_{H2}$=4/1.2 0.3A/cm^2 Stop: room temperature, no gas supply	120 h	Polarization curves

During the degradation test, the polarization curves and EIS measurement were performed every certain interval. In the test for the first cell, the polarization curves were conducted every 24 hours, while the EIS measurement was conducted every 8 hours. Unfortunately, the EIS measurement did not applied on the second cell due to the failure of the potentiostat.

3.3.3. CO POISONING TEST

The effect of CO in the fuel stream to the performance of the HT-PEM fuel cell and the influence of relative humidity and dilution conditions on the CO poisoning effect were investigated in the experiments introduced in this section.

In this work each experiment consists of two periods: poisoning period and recovery period. In the poisoning period impurities such as CO, CO_2 or N_2 were mixed with H_2, while in the recovery period the fuel cell was operated with pure H_2. Both poisoning period and recovery period lasted for 6 hours to ensure equilibrium state of CO adsorption and desorption. At the end of the poisoning period and recovery period in all experiments, the polarization curves and EIS were measured to quantify the cell performance and the internal resistances. In the poisoning period in all experiments, the CO concentration was set at 1% or 3% while the N_2 and CO_2 concentration was in the level of 20%, which concentration levels are in the typical range of those in the reformate derived from fossil fuels. The operating temperature was kept at 150 °C while the current load was at 10 A. The anode and cathode stoichiometries were both set at 3. It was reported that the cell performance loss caused by CO poisoning can be fully recovered with pure H_2 operation at the operating temperature of 130 °C. Therefore the same MEA can be used for all the experiments.

The detailed experimental procedure and operating conditions (anode gas composition and dew point temperature) are listed in Table 3.2. The effect of anode

humidification on the cell performance and the CO poisoning was first investigated in Experiment 1, 2 and 3 by introducing 3%vol CO into H_2 under different anode dew point temperatures (23 ^oC, 60 ^oC and 80 ^oC). The cell performance under different anode dew point temperatures was evaluated at the end of the recovery period of Experiment 1, 2 and 3. In Experiment 4, 5, 6 and 7 the influence of CO_2 on the cell performance and CO poisoning was studied. In Experiment 4 and 5, the dilution effect was induced by 20%vol CO_2 and N_2, respectively. The CO poisoning caused by 1%vol CO was evaluated in Experiment 6. In Experiment 7 both 1%vol CO and 20%vol CO_2 were introduced into H_2 to investigate the effect of CO_2 on CO poisoning. The combined effect of water vapor and dilution on the CO poisoning was studied in Experiment 8 and 9. The fuel cell was operated under different dew point temperature (23 ^oC and 60 ^oC) with the same anode gas composition (79%vol H_2, 1%vol CO, 20%vol CO_2). It should be noticed that the gas composition in the experiments in this section is on the basis of dry gas feed, which means increasing the dew point temperature can cause a dilution effect.

Table 3.2 – The anode gas compositions and dew point temperatures in each experiment

Exp No.	Gas compositions				$T_{DP,a}$ (^oC)
	H_2 (%)	CO (%)	CO_2 (%)	N_2 (%)	
1	97	3	0	0	23
2	97	3	0	0	60
3	97	3	0	0	80
4	80	0	20	0	23
5	80	0	0	20	23
6	99	1	0	0	23
7	79	1	20	0	23
8*	79	1	20	0	23
9*	79	1	20	0	60

* The cell performance in these two experiments showed obvious permanent degradation compared with the performance in other experiments because of the long term operation between Exp. 7 and Exp. 8.

3.3.4. H_2 STARVATION

The H_2 starvation has been proven can cause severe damage to the catalyst layer of the LT-PEM fuel cell. In this work, some experiments on a HT-PEM fuel cell under H_2 starvation conditions was conducted to investigate the effect of H_2 starvation to the performance and degradation of the HT-PEM fuel cell. In Section 3.3.4.1, the dynamic response of a HT-PEM fuel cell when H_2 starvation occurs is measured. The effects of H_2 starvation degree and current load to the dynamic response are also investigated. Then in Section 3.3.4.2, the degradation of a HT-PEM fuel cell under H_2 starvation condition is thoroughly investigated, including the degradation mechanisms.

3.3.4.1 Dynamic behaviors of the HT-PEM fuel cell under H_2 starvation conditions

After the galvanostatic break-in, the fuel cell was operated at 150 ^{o}C with anode and cathode stoichiometry of 3.0. To simulate the condition that the fuel cell was starved of H_2, the H_2 stoichiometry in anode was decreased below 1.0 (0.8 and 0.4) in all experiments, while the air stoichiometry in cathode was remained at 3.0. It is worth pointing out that the H_2/N_2 mixture (70%/30% in volume) was fed to anode. As reported in the literature [147] the H_2 can be drawn back into the anode flow channel of a single cell from the manifold in a fuel cell stack when this single cell was starved of H_2. In this work the long exhaust pipe of anode can act as the manifold in a fuel cell stack. Therefore employing the H_2/N_2 mixture can help to avoid 'vacuum effect'. The H_2 flow rate was determined by the stoichiometry value and the current load, while the N_2 flow rate was calculated according to the volume fraction of N_2 (30%vol) in the mixture. The total anode gas flow rate was the sum of H_2 flow rate and N_2 flow rate. Different starvation degree of H_2 was studied by decreasing the H_2 stoichiometry to different values. Additionally, the effect of current load to the H_2 starvation of the HT-PEM fuel cell was investigated. The detailed current load and H_2 stoichiometry are listed in Table. 3.3. Cell voltage and local current density were monitored and recorded during the H_2 starvation process in each experiment. The anode exhaust gas composition under different H_2 starvation conditions was analyzed by the mass spectrometer.

Table 3.3 – Operating conditions for the fuel cell during H_2 starvation experiments

Experiment No	Current load (A)	H_2 stoichiometry	Air stoichiometry
1	10	0.8	3
2	10	0.4	3
3	20	0.8	3
4	20	0.4	3

3.3.4.2 Degradation test of the HT-PEM fuel cell under H_2 starvation condition

An accelerated degradation test was conducted on a HT-PEM fuel cell to investigate the degradation of the HT-PEM fuel cell caused by H_2 starvation. The H_2/N_2 mixture was also adopted in this experiment for anode to avoid the 'vacuum effect'. When the cell voltage reached a stable level after the break-in, the H2 stoichiometry was cycled between the normal value of 3.0 and the low value of 0.8 every 2 min to simulate the frequent H_2 starvation during the fuel cell operation, while the air stoichiometry was remained at 3.0.

During the degradation test, the cell voltage and the anode exhaust gas composition were monitored. To figure out the degradation mechanism of the HT-PEM fuel cell caused by H_2 starvation, the polarization curves, EIS and CV were performed on the fuel cell before and after the degradation test. Post-mortem analysis techniques such as SEM and XRD were conducted on the tested MEA and a fresh MEA to characterize the structure change of the MEA caused by H_2 starvation.

3.4. SUMMARY

In this section, all the experimental setups which can be used to perform all the experiments conducted in this project are presented. With many characterization techniques used in this project, including polarization curves, EIS, CV, SEM, XRD and current density distribution measurement, the change in cell performance during all the experiments and the underlying degradation mechanisms can be investigated. The experimental procedures for all the experiments described in this section can give the readers an overview of how the topics about degradation of the HT-PEM fuel cell mentioned in Section 2.4 are investigated in this project. In the next section, the experimental results are presented and the underlying degradation mechanisms are discussed.

CHAPTER 4. RESULTS AND DISCUSSION

This section gives the main contributions of this project. First the results of the experiment about the long-term degradation under different operating conditions, including the presence of methanol in the anode stream, are presented in Section 4.1. Then Section 4.2 presents the experimental results about the CO poisoning on the HT-PEM fuel cell under different operating conditions. In Section 4.3 and 4.4, the effects of H_2 starvation to the cell performance and degradation are presented and discussed.

4.1. LONG-TERM DEGRADATION TEST WITH THE PRESENCE OF METHANOL

In this section, the results of the degradation tests with different operating conditions including the presence of methanol in the anode gas performed on two PBI/H_3PO_4 HT-PEM fuel cells are presented.

4.1.1. CELL VOLTAGE PROFILE

In Fig. 4.1 the voltage profile of the first fuel cell during the degradation test which consists of a H_2 continuous test, a H_2 start/stop test and a reformate continuous test. Before the degradation test, a 24-hour galvanostatic break-in was performed on the fuel cell. As can be seen from Fig. 4.1, there was an obvious increase in the cell voltage during the break-in in the first 24 hours. However, the cell voltage continued to increase during the H_2 continuous test, which indicates the break-in for this type of fuel cell should be longer than 24 hours for DPS Dapozol MEAs. According to the literature [158], the increased cell voltage during the break-in and the H_2 continuous test can be ascribed to the redistribution of phosphoric acid (PA) between the membrane and the electrodes. During the start/stop test, the cell voltage showed minor decreasing trend in the first two cycles, followed by a significant drop between the second and the third cycle, and then kept stable in the last three cycles. During the reformate continuous test, the cell voltage is significantly reduced by the presence of methanol in the anode gas. In addition, many downward spikes in the cell voltage profile in the reformate continuous test can be observed, which lead to a permanent damage to the fuel cell.

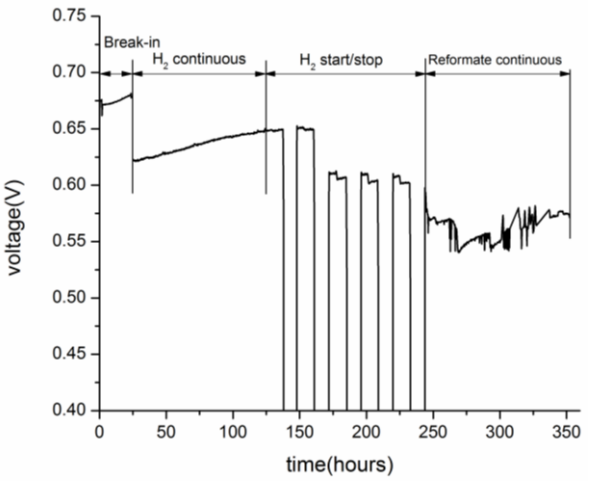

Fig. 4.1 – The voltage profile of the first MEA over time during the degradation test

A degradation test was performed on the second fuel cell after the first fuel cell was designated to an end of life. The voltage profile on the second fuel cell was illustrated in Fig. 4.2. A 100-hour break-in was performed to ensure the maximum cell performance can be achieved. In the following H_2 continuous test, the performance of the second fuel cell was better than the first one, which suggested the importance of a proper break-in procedure. The cell voltage remained almost stable with a minor increase (5 mV) in the 110-hour H_2 continuous test. After the H_2 continuous test, the cell voltage decreased by 13 mV in the 30-hour reformate continuous test. The cell voltage decay rate was -2.6mV/h during this period, which was similar to the value reported by Araya et al [140]. The downward spikes in cell voltage can also be observed in the first fuel cell, which deteriorate the cell performance. After a shutdown for 10 hours, the fuel cell was operated with pure H_2 for reconditioning. Then, a start/stop test with simulated reformate as the anode gas was conducted for 120 hours. The average cell voltage in each start period decreased slightly in the Reformate start/stop test.

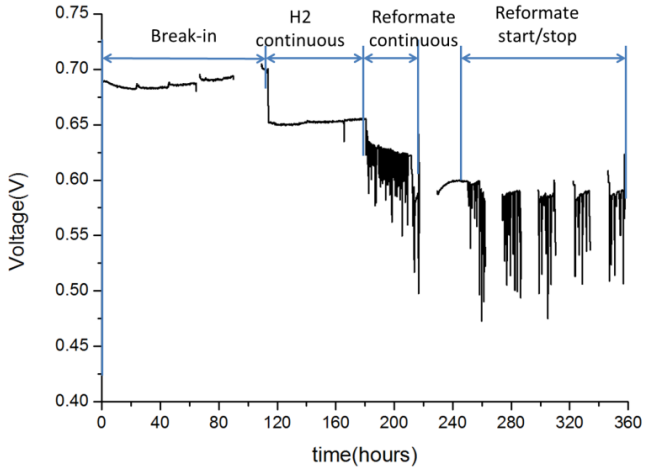

Fig. 4.2 – The voltage profile of the second MEA over time during the degradation test

4.1.2. POLARIZATION CURVES

The evolution of polarization curves of the first fuel cell throughout the H_2 continuous test and the H_2 start/stop test are shown in Fig. 4.3 (a) and Fig. 4.4 (a), respectively. As can be seen from these two figures, the cell performance improved during the H_2 continuous test and decreased after the second day of the H_2 start/stop test, which was in accordance with the cell voltage profile as shown in Fig. 4.1. To better understand and quantify the different sources of the performance losses during the degradation test, Tafel plots which illustrate the relationship between the ohmic drop corrected voltages ($E_{IR\text{-}free}$) and the current density in logarithmic form are presented in Fig. 4.3 (b) and Fig. 4.4 (b). The calculation procedure of $E_{IR\text{-}free}$ is introduced in Section 3.2.1. The linear decrease in $E_{IR\text{-}free}$ in the low current density range is mainly caused by the kinetic overpotential, especially in the cathode.

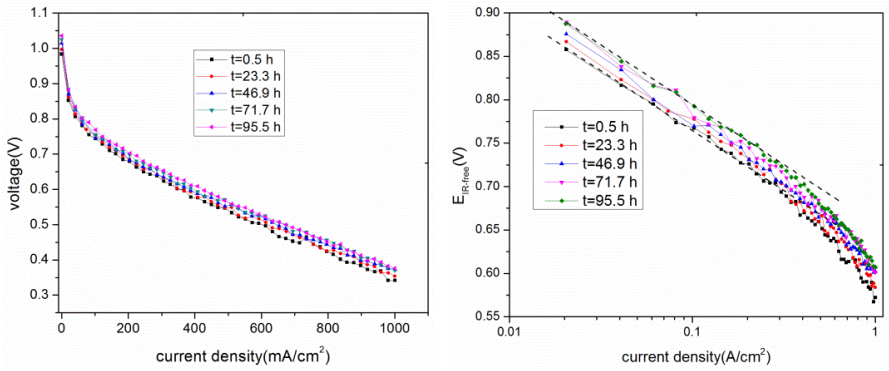

(a) *(b)*

Fig. 4.3 – Polarization curves (a) and Tafel plots (b) of the first fuel cell over time during the H_2 continuous test

The $E_{IR\text{-}free}$ curves shifted upward during the H_2 continuous test, and it shifted downward during the H_2 start/stop test. This indicated that the kinetic overpotential decreased during the H_2 continuous test and increased during the H_2 start/stop test. The enhanced kinetics of the electrode reaction could be contributed to the redistribution of PA during the break-in and the H_2 continuous test. The carbon corrosion triggered by high cathode potential during the startup and shutdown processes could contribute to the increase in the kinetic overpotential [95]. However, in this work there was an obvious decrease in cell performance measured between the second (t=128.6h) and the third cycle (t=154.1h). This significant drop in cell performance cannot be simply attributed to the carbon corrosion. The improper procedures for startup or shutdown could be the reason. More detailed analysis, about the reason for the drop in cell performance during H_2 start/stop test, will be given by the analysis of the EIS in Section 4.1.3. As can be seen from Fig. 4.4 (b) and Fig. 4.3 (b) the $E_{IR\text{-}free}$ curves deviated from the linearity in high current density range. During the H_2 start/stop test the enlarged deviation of $E_{IR\text{-}free}$ curves from the linearity proved the increase in mass transport loss caused by carbon corrosion in the startup and shutdown processes.

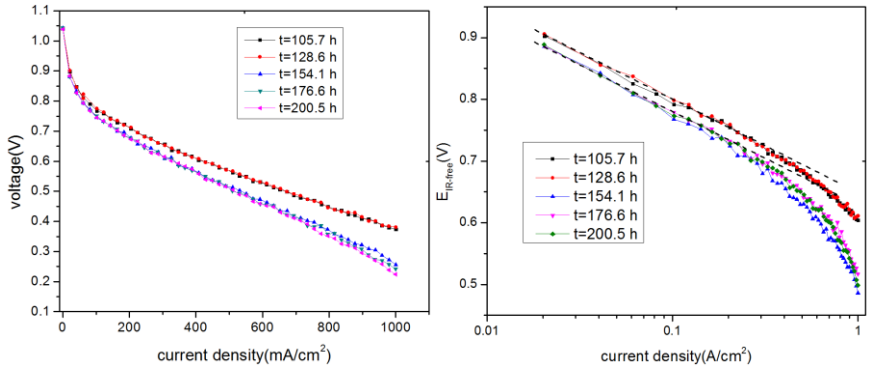

(a) *(b)*

Fig. 4.4 – Polarization curves (a) and Tafel plots (b) of the first fuel cell over time during the H_2 start/stop test

The evolution of polarization curves of the second fuel cell during the continuous test and the Reformate start/stop test are shown in Fig. 4.5 (a) and Fig. 4.5 (b), respectively. The cell performance remained almost stable during the H_2 continuous test (t=193 h, 141 h, 168 h), while it degraded significantly during the Reformate continuous test (t=193 h, 217 h). From the Tafel plot shown in Fig. 4.5 (b) it can be seen there was no obvious mass transport overpotential during the H_2 continuous test. The lower mass transport loss in the second fuel cell than in the first fuel cell can be one of the reasons for the higher performance resulted from the longer break-in. When the fuel cell was operated with simulated reformate as the anode gas, the kinetic overpotential increased, as well as the mass transport overpotential. The methanol presented in the anode gas can adsorb on the Pt surface, hindering the electro-oxidation of H_2. In addition, the intermediate from methanol oxidation reaction, such as CO, can strongly adsorb on the catalyst surface, which resulted in the increase in the kinetic overpotential in anode. Moreover, the dilution in H_2 caused by the presence of methanol and water vapor brought about the increase in mass transport overpotential. During the Reformate start/stop test the polarization curves showed no obvious change, which was in accordance with the voltage profile shown in Fig. 4.2.

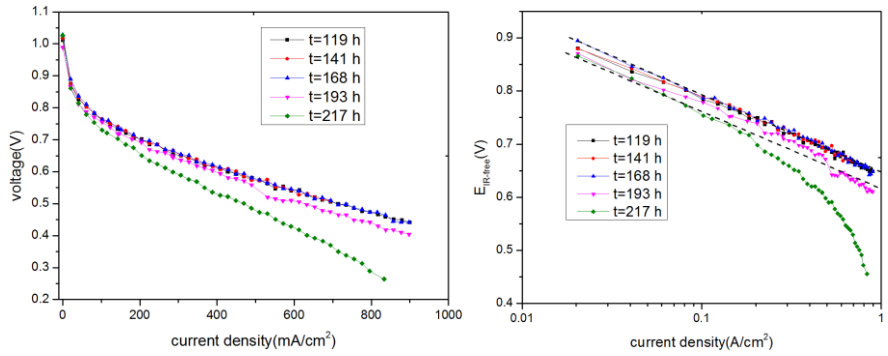

(a) *(b)*

Fig. 4.5 – Polarization curves (a) and Tafel plots (b) of the second fuel cell over time during the continuous test

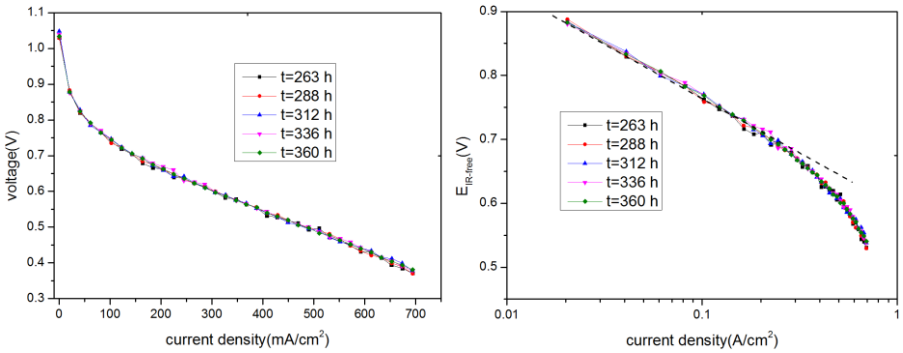

(a) *(b)*

Fig. 4.6 – Polarization curves (a) and Tafel plots (b) of the second fuel cell over time during the Reformate start/stop test

4.1.3. EIS

To better understand the degradation mechanisms and separate the different polarization losses, the impedance spectra were recorded during the degradation test for the first fuel cell and fitted to the EC model shown in Fig. 4.7. The EC model is consisted of two parallel resistor and capacitor loops connected in series with a resistor (R_{ohmic}) and an inductor (L_{stray}). The inductor represents the inductive loop in the impedance spectra in the highest frequency range, which can be ascribed to the measurement noise from connecting wires. R_{ohmic} represents the ohmic resistance of all components of the fuel cell and the contact resistance between different components. Two parallel resistor and capacitor loops represent the two

arcs in the impedance spectrum. The origin of the arc in the high frequency (R_{hf}) range has not reached a consensus. Most of researchers agree that it comes from the proton transfer resistance in the catalyst layer [160, 161]. The larger arc in the low frequency range (R_{lf}) can be attributed to the charge transfer resistance, mainly from the cathode because of sluggish ORR in cathode [162].

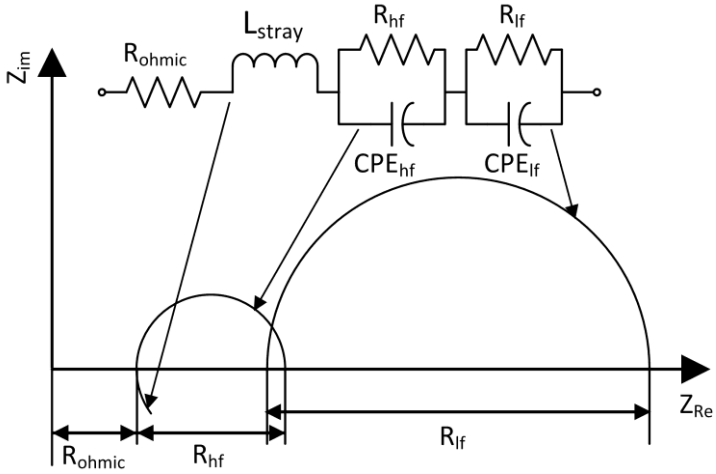

Fig. 4.7 – The EC model used to fit the measured impedance spectra

In Fig. 4.8 (a) the impedance spectrum of the fuel cell during the H_2 continuous test are illustrated, as well as the fitted resistances. There was no obvious arc related to the mass transfer in the lowest frequency range of the impedance spectrum in this work which was observed by many researchers [163]. In this work the mass transfer arc might be swallowed by the large charge transfer arc. During the H_2 continuous test, the most pronounced change in the impedance spectra was the shrinking of the charge transfer arc. As can be seen from Fig. 4.9 (b), there was an increase in the R_{hf} and a decrease in the R_{lf}. The decreasing R_{lf} indicated that the electrode reaction kinetic was enhanced by the redistribution in PA between the membrane and the electrodes. Excess PA in the electrode was removed via migration, which resulted in the increase in the ECSA in the catalyst layer, and therefore the decrease in charge transfer resistance. In the meantime, the decrease in amount of PA in the catalyst layer lead to a reduction in effective transfer path for proton passing through the electrolyte, which could be the reason for the increase in the R_{hf}. The R_{ohmic} was not significant affected during the H_2 continuous test.

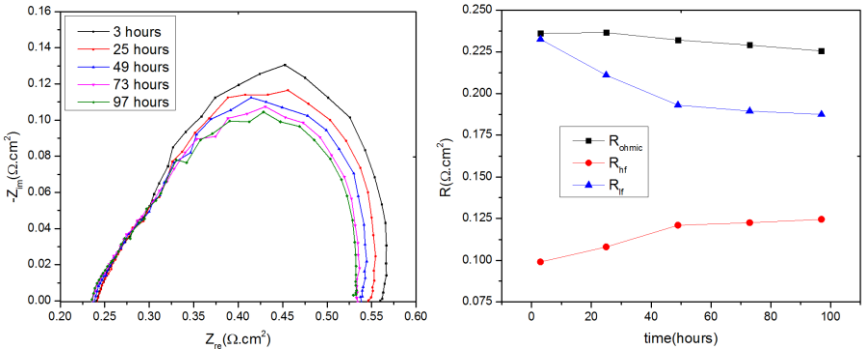

(a) *(b)*

Fig. 4.8 – Evolution of impedance spectra (a) and all the internal resistances (b) of the first fuel cell throughout the H_2 continuous test

The impedance spectra of the first fuel cell recorded during the H_2 start/stop test is illustrated in Fig. 4.9 (a). The impedance spectra remained almost unchanged in the first two days of operation (t=150 h and 128 h) and shifted right in the following three days (t=161 h, 184 h, 200 h). This indicated an increase in the ohmic resistance, which can also be observed in Fig. 4.9 (b). Besides R_{ohmic}, R_{hf} also showed an increasing trend during this period. The increase in R_{ohmic} and R_{hf} can be ascribed to the PA leached out of the fuel cell because the membrane resistance and the proton transfer resistance were related to the PA content in the membrane and in the electrodes, respectively. Improper startup and shutdown procedure could result in liquid water generated in the fuel cell, which brought about the PA being leached out by the liquid water. The R_{lf} did not change significantly, indicating the charge transfer resistance was not significantly affected by the start/stop operation.

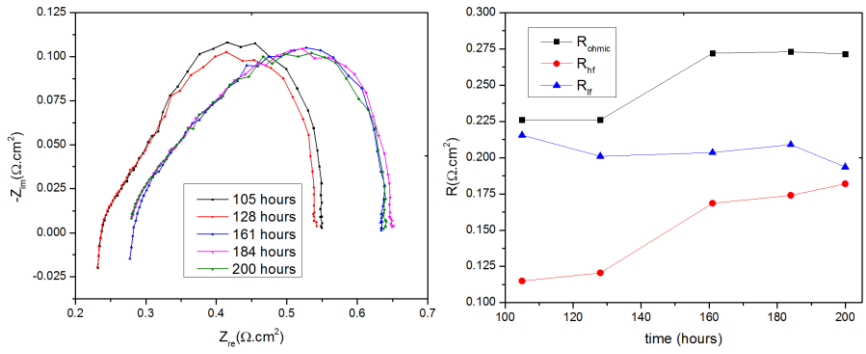

(a) *(b)*

Fig. 4.9 – Evolution of impedance spectra (a) and all the internal resistances (b) of the first fuel cell throughout the H_2 start/stop test

The effect of the presence of methanol and water in the anode gas on the impedance spectra are shown in Fig. 4.10 (a). The fitted resistances according to the EC model shown in Fig. 4.7 are illustrated in Fig. 4.10 (b). It can be seen that the presence of methanol brought about the opposite trend in change of R_{hf} and R_{lf}. The catalyst surface covered by methanol and the intermediate in the oxidation process could be the reason for the increase in R_{lf}. However the reason for the decrease in R_{hf} is not clear. The ohmic resistance was not impacted by the presence of methanol in the anode gas.

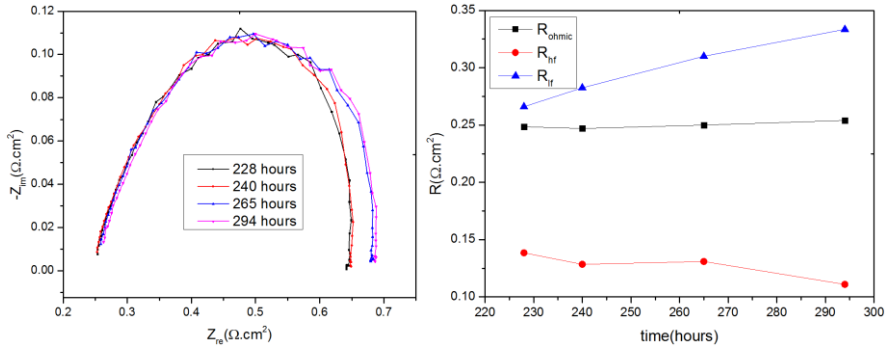

(a) *(b)*

Fig. 4.10 – Evolution of impedance spectra (a) and all the internal resistances (b) of the first fuel cell throughout the Reformate test

4.2. CO POISONING ON THE HT-PEM FUEL CELL

In this section the CO poisoning effect on the HT-PEM fuel cell was investigated under different anode relative humidities and different dilution conditions.

4.2.1. EFFECT OF ANODE HUMIDIFICATION ON THE CO POISONING

Fig. 4.11 illustrates the change in cell voltage under different CO concentrations and anode dew point temperatures in Experiment No. 1, 2 and 3. The anode gas was saturated with water vapor at different dew point temperatures by a humidifier in the fuel cell test station before the gas entered the fuel cell. As can be seen from this figure, the cell voltage dropped rapidly in the poisoning period in each experiment, and it was completed recovered at the end of the recovery period after pure H_2 operation for 6 hours. This means that the cell voltage at the end of the recovery period can be regarded as the voltage of the fuel cell operated without CO. By comparing the cell voltage in poisoning period in these three experiments, it can be

observed that higher anode dew point temperature brings about higher cell voltage with 3%vol CO in anode gas. On the other hand, when the fuel cell was operated with pure H_2 in the recovery period, the anode dew point temperature did not affect the cell voltage significantly in the dew point temperature range of 23 ^oC and 60 ^oC. When the dew point temperature increased to 80 ^oC, the cell voltage decreased. The opposite variation trend in cell voltage in the poisoning period and in the recovery period suggests that the cell voltage loss caused by CO poisoning can be reduced by higher anode dew point temperature. In Experiment No. 3 there were several downward spikes in cell voltage which can be ascribed to the blockage of anode flow channels by significant amount of water.

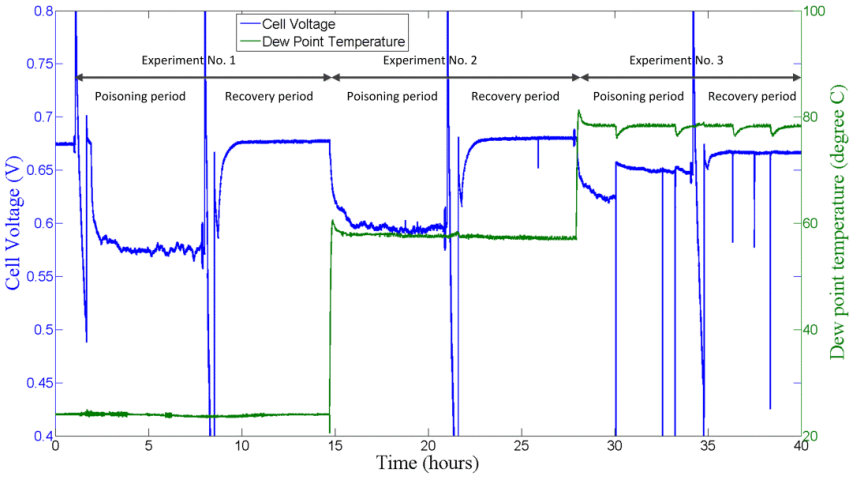

Fig. 4.11 – The change in cell voltage and anode dew point temperature in Experiment No. 1, 2 and 3. The CO poisoning period and performance recovery period are indicated in each experiment.

The polarization curves of the fuel cell at the end of the poisoning period and the recovery period in Experiment No. 1, 2 and 3 are illustrated in Fig. 4.12. It can be seen that without CO in the anode gas, the cell performance remained almost unchanged when the anode dew point temperature increased from room temperature to 60 ^oC, and it showed a minor decrease when the anode dew point temperature rose to 80 ^oC. When CO is introduced into the anode gas, the cell performance was improved by higher anode dew point temperature. In addition, as can be seen from the cell voltage loss caused by 3%vol CO at different anode dew point temperatures shown in Fig. 4.12 which was calculated by the difference between cell voltages operated with pure H_2 and 3%vol containing H_2, the cell voltage loss increased with the increase in current load and decreased with the increase in anode dew point temperature. The CO poisoning was alleviated by the increase in water content in anode gas.

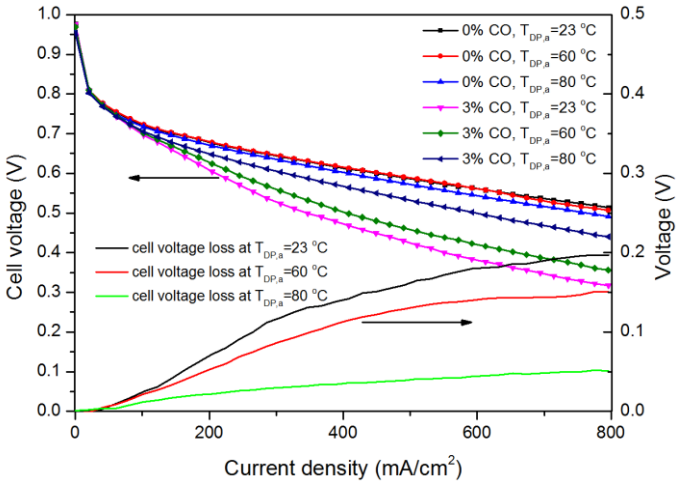

Fig. 4.12 – The polarization curves (lines with symbols) and cell voltage loss (lines) caused by the presence of CO under different anode gas dew point temperatures with and without CO.

The cell performance with the presence of CO is caused by the strong bond between the CO molecules and the catalyst surface which resulted in the reduction in the active surface area for hydrogen oxidation. Lower CO coverage on catalyst surface brings about lower cell performance loss. Removal of CO from the catalyst surface can be achieved by desorption of CO from the catalyst surface and the oxidation of CO.

In this work, the nominal CO concentration is on the basis of dry gas feed. When the dry gas was humidified, the CO concentration in the anode gas was actually decreased by the increased water content. The water content is equal to the ratio between the water vapor partial pressure and the gas total pressure. The gas total pressure can be assumed to be the atmospheric pressure (1.01×10^5 Pa), while the water vapor partial pressure can be calculated according to the Eq. (4.1) [164]:

$$p_s = C_1 \cdot \exp\left(\frac{A_1 \cdot T}{B_1 + T}\right) \tag{4.1}$$

where T is the dew point temperature. The coefficients' values are: A_1=17.625, B_1=243.04 °C, and C_1=610.94 Pa. According to the calculation, the actual CO concentration decreases from 3%vol with a dew point temperature of room temperature (23 °C) to 2.4%vol and 1.6%vol with a dew point temperature of 60 °C and with dew point temperature of 80 °C, respectively. The lower CO concentration resulted in the lower CO adsorption rate and higher CO desorption rate, which brought about lower CO coverage.

Except for the dilution effect, the higher water content is believed to accelerate the CO oxidation. The CO oxidation is the combination of electrochemical process and catalytic process [135].The electrochemical oxidation of CO involves the following reactions:

$$CO + M \rightarrow M - CO_{ads} \tag{4.2}$$

$$H_2O + M \rightarrow M - OH_{ads} + H^+ + e^- \tag{4.3}$$

$$M - CO_{ads} + M - OH_{ads} \rightarrow 2M + CO_2 + H^+ + e^- \tag{4.4}$$

Here the M stands for the available catalyst sites for CO adsorption. The potential for electrochemical oxidation of CO is usually higher than the anode potential. The CO oxidation peak potential is in the range of 0.35 V and 0.40 V versus reference hydrogen electrode at the temperature of 180 ^{o}C [165]. In this study the anode overpotential which can be regarded as the cell voltage loss shown in Fig. 4.12 is lower than the CO oxidation peak potential. Therefore it could be deduced that the electrochemical oxidation rate of CO is pretty slow under the operating conditions of the HT-PEM fuel cell. Moreover, Modestov et al. [136, 166] investigated the CO oxidation on Pt surface in the HT-PEM fuel cell. The CO electrochemical oxidation rate was quantified by slow scan rate voltammetry in the typical operating temperature range of the HT-PEM fuel cell, and the results proved that the CO electrochemical oxidation is too slow to influence the CO tolerance of the HT-PEM fuel cell operated with H_2 containing a few percent of CO.

The CO can also be oxidized through the water gas shift reaction as follow:

$$CO + H_2O \rightarrow H_2 + CO_2 \tag{4.5}$$

The water gas shift reaction is a moderately exothermic reversible reaction, thus it can be accelerated at low temperature. This reaction is widely used to reduce the CO concentration in the reformate. It is reported that the CO concentration in the reformate gas in the level of 10 – 20 %vol can be reduced to around 1 %vol after oxidation process in a fuel processor in the temperature range of 200 – 300 ^{o}C [167]. In this work the temperature is around 150 ^{o}C, thus the CO conversion rate can be even higher. When the fuel cell was not humidified in this work, the amount of water vapor in the anode is limited. The water content in the anode increased with the humidification, which promoted the CO oxidation through water gas shift reaction.

The electrochemical impedance spectra of the fuel cell measured at the end of the poisoning period and the recovery period in Experiment No. 1, 2 and 3 are

illustrated in Fig. 4.13. The EC model shown in Fig. 4.14 is used to fit the measured impedance spectra. The ohmic resistance (R_{ohmic}) can be attributed to the ohmic resistance of the membrane and the contact resistance between the membrane and the electrodes. The big arc in the high and intermediate frequency range represents the charge transfer resistance (R_{ct}) and the small arc in the low frequency range stands for the mass transfer resistance (R_{mt}). All the fitted resistances are illustrated in Fig. 4.15.

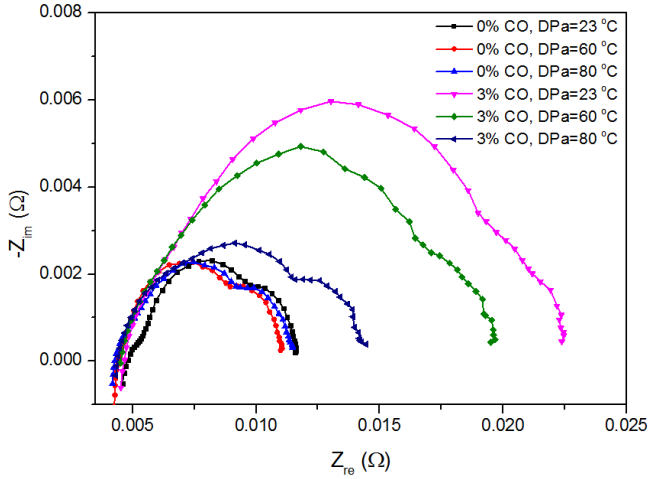

Fig. 4.13 – The electrochemical impedance spectra of the fuel cell operated with different anode gas dew point temperatures with and without CO in anode stream.

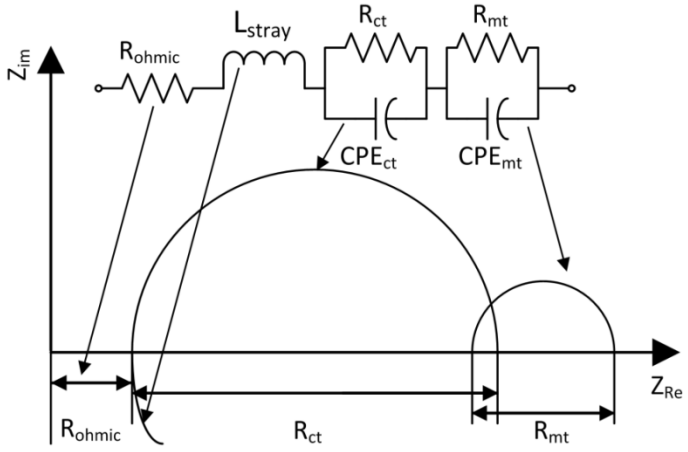

Fig. 4.14 – The EC model used to fit the obtained impedance spectra

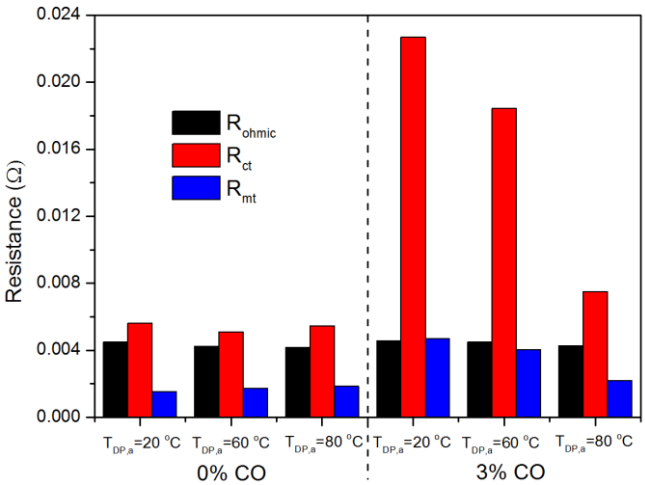

Fig. 4.15 – The corresponding fitted resistances of the fuel cell calculated from the spectra shown in Fig. 4.12.

It can be seen from Fig. 4.15 that the internal resistances of the fuel cell were not affect by the anode dew point temperature when the fuel cell was operated with pure H_2. There was a slight decrease in ohmic resistance and a minor increase in mass transfer resistance with the increase in anode dew point temperature. The increased water content enhanced the hydration state of the membrane and suppressed the self-dehydration of the PA, which resulted in the decrease in ohmic resistance. On the other hand, the increased water content diluted the H_2, which brought about the increase in mass transfer resistance. In high anode dew point temperature range (80 ^oC), the increase in mass transfer resistance surpassed the decreased in ohmic resistance, resulting in the slight decrease in cell performance.

When 3%vol of CO was introduced into the anode gas, the impedance spectra were significantly influenced by the increase in anode dew point temperature. The charge transfer resistance and the mass transfer resistance reduced with higher anode dew point temperature, while the ohmic resistance remained almost unchanged. With higher anode dew point temperature, the CO coverage on the catalyst surface was reduced by the decreased CO concentration and accelerated CO oxidation, which resulted in the increase in ECAS for hydrogen oxidation reaction. This explains the decrease in charge transfer resistance. The lower CO coverage on the catalyst surface makes the diffusion path of hydrogen molecules shorter, which brings about lower mass transfer resistance.

4.2.2. EFFECT OF CO_2 ON CELL PERFORMANCE AND CO POISONING

The CO_2 is a typical byproduct of the reforming process which is usually contained in the reformate gas. In this section the effect of CO_2 dilution on the cell performance and the CO poisoning are investigated. For the low temperature PEM fuel cell, the poisoning mechanism of the CO_2 is the combination of dilution effect and the formation of CO through reverse water gas shift reaction as follow [168]:

$$H_2 + CO_2 \rightarrow CO + H_2O \tag{4.6}$$

According to the thermodynamic calculation, the CO concentration in the range of 20 – 100 ppm can be generated in the gas mixture of H_2 (80%vol) and CO_2 (20%vol) in the temperature of 80 ^oC [138]. Under the typical operating temperature of the HT-PEM fuel cell, the formed CO concentration can be even higher because of the endothermic nature of the reverse water gas shift reaction. Li et al. [124] estimated that the CO concentration generated from CO_2 reduction can be up to 1%vol for HT-PEM fuel cell. However, from Fig. 4.16 it can be observed that the 20%vol CO_2 in anode gas only caused a minor decrease in cell performance. When the CO_2 was replaced by the N_2 which can be regarded as inert gas in the fuel cell, the cell performance loss remained almost unchanged. This phenomenon indicated that the CO_2 merely caused dilution effect to the HT-PEM fuel cell because the CO formed via reverse water gas shift reaction was not high enough to affect the cell performance.

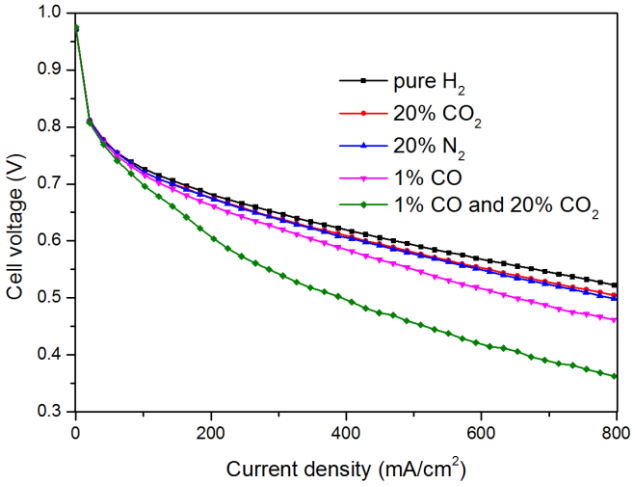

Fig. 4.16 – The polarization curves of the fuel cell operated with pure H_2, 20%vol CO and 20%vol N_2 contained H_2, 1%vol CO contained H_2 and 1%vol CO and 20%vol CO_2 contained H_2

The effect of CO_2 to the CO poisoning can be investigated by comparing the cell performance when it was operated with 1%vol CO containing H_2 with and without 20%vol CO_2 dilution. The 1%vol CO caused larger cell performance loss than the 20%vol CO_2. And the cell voltage loss caused by 1%vol CO and 20%vol CO_2 was higher than the sum of that caused by 1%vol CO and 20%vol CO_2 individually. For example at current density of 200mA/cm^2, the cell voltage loss was 6 mV with 20%vol CO_2 in H_2 and 19 mV with 1%vol CO, while the voltage loss of 76 mV was observed with both 20%vol CO_2 and 1%vol CO. The CO poisoning can be deteriorated by CO_2 dilution even if the CO_2 dilution alone only has minor effect on the cell performance. The cell voltage loss in this work resulted from the rise in anode overpotential because the impurities only appeared in the anode side. According to the modeling work of Springer et al. [169], the anode overpotential (η_a) appears in an inverse hyperbolic sine relationship with the hydrogen coverage on the catalyst surface (θ_H) as shown in Eq. (4.7):

$$\eta_a = \frac{RT}{\alpha F}\sinh^{-1}\left(\frac{i}{2k_{eh}\theta_H}\right) \tag{4.7}$$

According to Eq. (7), the anode overpotential increases with the decrease in hydrogen coverage, and the increase becomes more significant in low hydrogen coverage range. When the H_2 was diluted by 20%vol CO_2 in this work, there was a minor decrease in hydrogen coverage because of dilution effect. The hydrogen coverage still stayed at the high level where its influence on the anode overpotential was minor. With 1%vol CO alone, the strong adsorption of CO on the catalyst surface reduced the hydrogen coverage to a large extend, resulting in an obvious increase in anode overpotential. When the 20%vol CO_2 was added to the 1%vol CO containing H_2, the decrease in the hydrogen coverage resulted in a large increase in anode overpotential because the hydrogen coverage was in the low level.

In Fig. 4.17, the impedance spectra of the fuel cell when the H_2 is diluted by the CO_2 and N_2 are illustrated, and the fitted resistance values are shown in Fig. 4.18. It can be seen from Fig. 4.18 that the 20%vol CO_2 alone only brought about an increase in mass transfer resistance with the ohmic resistance and charge transfer resistance unchanged. The impedance spectrum of the fuel cell operated with 20%vol CO_2 is similar to that of the fuel cell operated with 20%vol N_2.

The impedance spectra and the fitted resistances of the fuel cell operated with 1%vol CO containing H_2 with and without CO_2 dilution are illustrated in Fig. 4.17 and Fig. 4.18, respectively. The 1%vol CO only brought about the increase in charge transfer resistance compared with the fuel cell operated with pure H_2, which was derived from the reduction in ECSA because of CO adsorption on the catalyst surface. When the 20%vol CO_2 was added to the 1%vol CO containing H_2, a significant increase in the charge transfer resistance can be observed, along with the

moderate increase in mass transfer resistance. The increase in mass transfer caused by 1%vol CO and 20%vol CO_2 was comparable to that caused by 20%vol CO_2 alone. Thus it can be deduced that the additional cell performance loss caused by 1%vol CO and 20%vol CO_2 mainly came from the increase in charge transfer resistance.

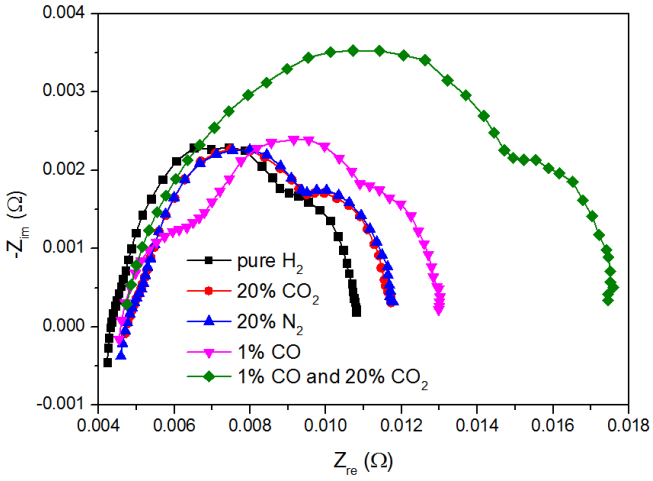

Fig. 4.17 – The electrochemical impedance spectra of the fuel cell operated with pure H_2, 20%vol CO and 20%vol N_2 contained H_2, 1%vol CO contained H_2 and 1%vol CO and 20%vol CO_2 contained H_2

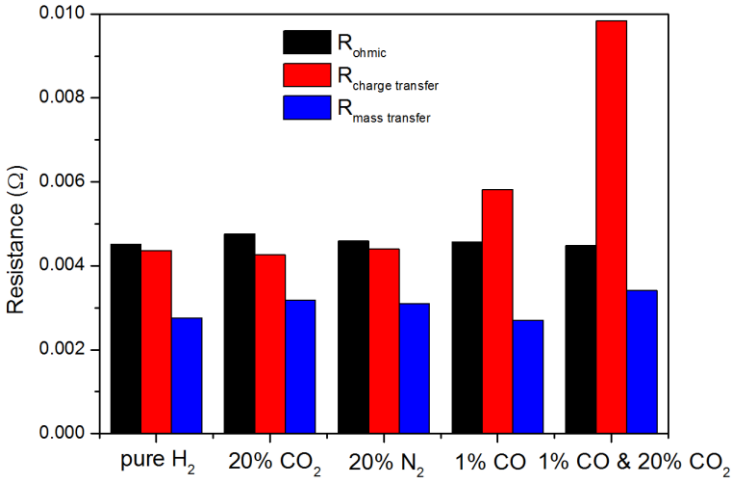

Fig. 4.18 – The corresponding fitted resistances of the fuel cell calculated from the spectra shown in Fig. 4.17.

4.2.3. EFFECT OF HUMIDIFICATION ON CO POISONING WITH THE PRESENCE OF CO_2

In Fig. 4.19 the effect of anode humidification on the CO poisoning with the presence of CO_2 is illustrated. It should be mentioned that the fuel cell was degraded to a large extend before Experiment No. 7 and 8 due to the long-term operation and several emergency stops of the fuel cell test station. Thus the cell performance in these two experiments was lower than the performance in previous experiments. However, the cell performance still can be compared within these two experiments. It can be seen that the cell performance loss caused by 1%vol CO and 20%vol CO_2 was reduced by increasing the anode dew point temperature, which suggested that the CO oxidation can still be enhanced by the increase in water content via water gas shift reaction even with the presence of CO_2. Although the presence of CO_2 could inhibit the water gas shift reaction to some extent, the addition of water can still shift the equilibrium of water gas shift reaction to the way of CO oxidation.

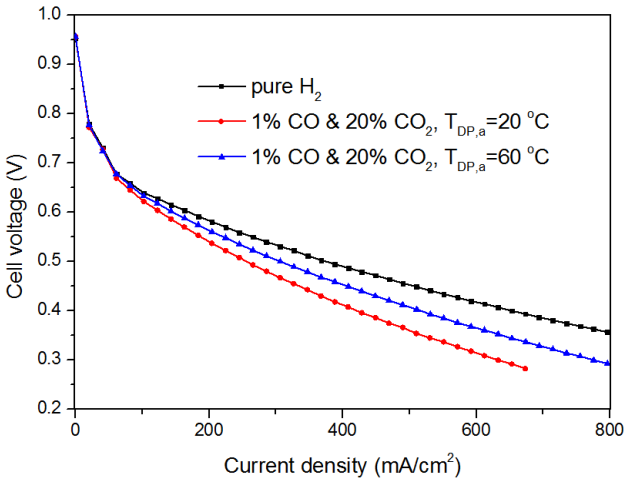

Fig. 4.19 – The polarization curves of the fuel cell operated with pure H_2, and 1%vol CO and 20%vol CO_2 contained H_2 under different anode gas dew point temperatures

The impedance spectra and the fitted resistances of the fuel cell operated with H_2 containing 1%vol CO and 20%vol CO_2 with and without anode humidification are presented in Fig. 4.20 and Fig. 4.21, respectively. The increase in charge transfer resistance caused by 1%vol CO and 20%vol CO_2 was reduced by humidifying the anode gas, while the mass transfer resistance was more or less unchanged with the increase in water content. Although the addition of water vapor can cause dilution effect, the reduced CO coverage on catalyst surface because of enhance CO oxidation resulted in shorter diffusion path for H_2 in the catalyst layer. The negative

effect of water vapor on mass transport resistance may be offset by the positive effect.

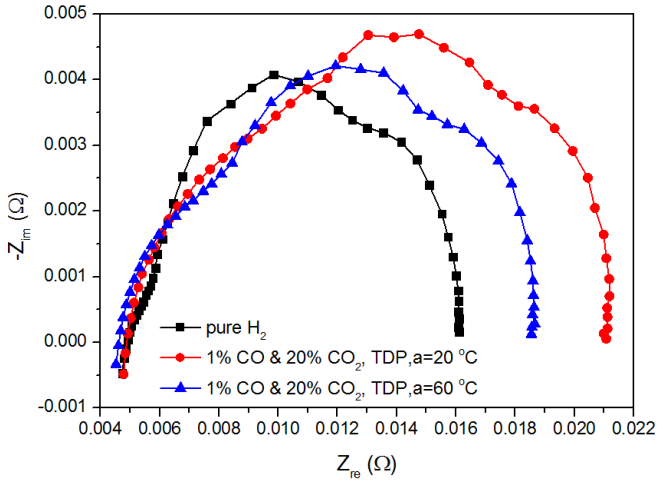

Fig. 4.20 – The electrochemical impedance spectra of the fuel cell operated with pure H_2, and 1%vol CO and 20%vol CO_2 contained H_2 under different anode gas dew point temperatures

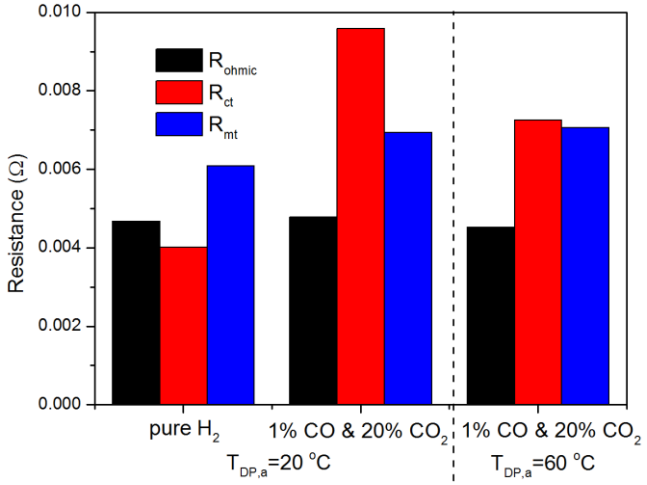

Fig. 4.21 – The corresponding fitted resistances of the fuel cell calculated from the spectra shown in Fig. 4.20

4.3. H_2 STARVATION TESTS ON HT-PEM FUEL CELLS

In this section, the dynamic response of the cell voltage and the local current densities of a HT-PEM fuel cell were investigated under different H_2 starvation conditions.

4.3.1. CELL BEHAVIORS UNDER H_2 STARVATION CONDITIONS

Fig. 4.22 illustrates the cell voltage profile and the change in local current density in different regions when the H_2 stoichiometry decreased from 3.0 to 0.8 which triggered the H_2 starvation of the fuel cell. In Fig. 4.22 the notation 'i_Rn' (n=1, 2 … 10) represents the average current density in each row of the segments as illustrated in Fig. 3.1. The notations from 'i_R10' to 'i_R1' represent the current density from upstream regions to downstream regions. As can be seen from the cell voltage profile, it remained stable in the first 5 seconds because of the residual H_2 in the gas diffusion layer and the flow channels in the anode. After the first period, the cell voltage dropped rapidly due to the H_2 depletion under H_2 starvation condition. Then the cell voltage remained at a stable level where the voltage value became negative. The cell polarity was reversed under the H_2 starvation condition, which phenomenon was reported in the literature [148, 170]. The decreasing cell voltage under H_2 starvation condition can be ascribed to the increase in anode overpotential. The anode and cathode potential (E_a, E_c) of the fuel cell can be written as the following equations [171]:

$$E_a = E_{eq,a} + \eta_a \tag{4.8}$$

$$E_c = E_{eq,c} - \eta_c \tag{4.9}$$

where $E_{eq,a}$ and $E_{eq,c}$ are equivalent potential of anode and cathode, and η_a and η_c are overpotential which resulted from the charge transfer resistance and mass transfer resistance in anode and cathode, respectively. When the anode of the fuel cell was starved of H_2, the anode overpotential increased, resulting in the increase in anode potential. Meanwhile, the cathode overpotential was not affected. Therefore the increase in anode potential resulted in the decrease in cell voltage. When the anode potential became higher than the cathode potential, the cell polarity was reversed. The negative cell voltage suggested that the fuel cell consumed energy provided by the auxiliary power supply, instead of generating electricity. In the real-life application, the energy can be provided by other cell in the same stack or other series connected stacks.

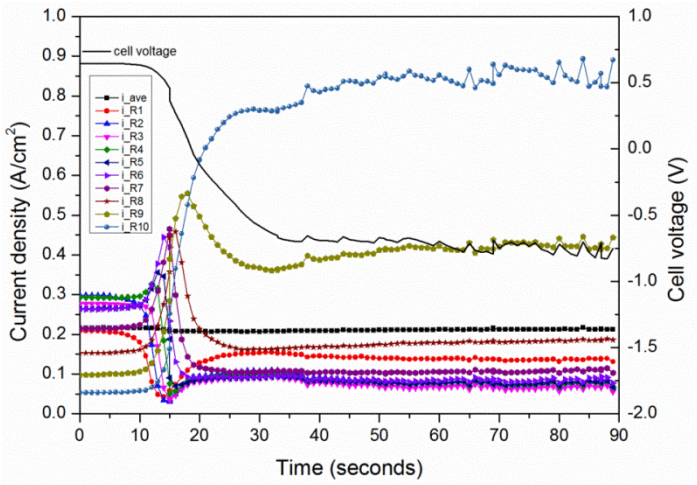

Fig. 4.22 – Dynamic response of cell voltage and local current density when H_2 stoichiometry decreased from 3.0 to 0.8 with the current load of 10A

Under the H_2 starvation condition, the amount of H_2 was not high enough to maintain the current load, thus the carbon corrosion reaction and the water electrolysis reaction would occur to provide the electrons and the protons. These two reactions follow the Eq. (4.10) and Eq. (4.11):

$$C + 2H_2O \rightarrow CO_2 + 4H^+ + 4e^-, E^0 = 0.207V_{RHE} \quad (4.10)$$

$$2H_2O \rightarrow O_2 + 4H^+ + 4e^-, E^0 = 1.229V_{RHE} \quad (4.11)$$

The standard potential for carbon corrosion reaction is 0.207 V vs relative hydrogen electrode, which is lower the anode potential when the fuel cell is operated under normal operating condition. Under the H_2 starvation condition, the high anode potential accelerates the carbon corrosion reaction, resulting in severe degradation in anode catalyst layer. During the experiment the gas composition of anode exhaust was measured by a mass spectrometer, and the results were shown in Fig. 4.23. No H_2 existed the anode exhaust suggested that the H_2 was depleted. The anode exhaust was consisted of N_2 and CO_2. The N_2 came from the anode inlet gas, while the CO_2 was generated by the carbon corrosion reaction. In this experiment there was no O_2 in the anode exhaust, indicating the anode potential was not high enough to trigger the water electrolysis reaction.

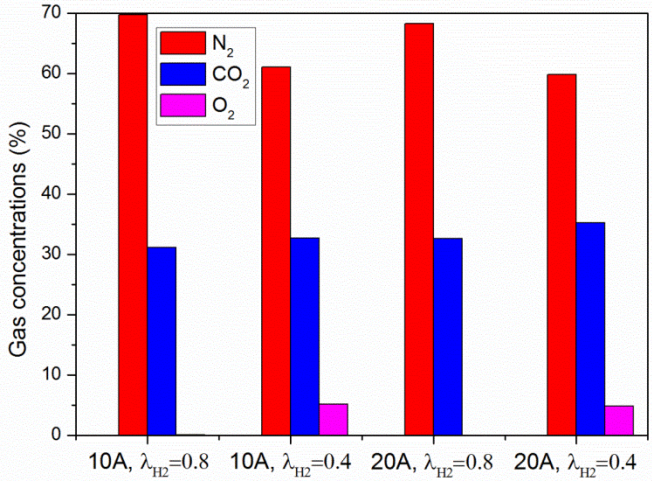

Fig. 4.23 – Gas composition of anode exhaust under different H_2 starvation conditions

The change in current density in this experiment followed the change in cell voltage as shown in Fig. 4.22. In the first 5 seconds, the local current densities remained stable. When the cell voltage started to decrease, the current density in downstream regions decreased, while in other regions it showed the increasing trend. When the H_2 stoichiometry decreased to 0.8 in this experiment, the H_2 started to deplete in downstream regions, resulting in the increase in mass transfer resistance in these regions. The current tended to flow through upstream regions where the mass transfer resistance was lower, which resulted in the increase in current density in upstream regions. With the further decrease in cell voltage, the decrease in current density spread from downstream regions to the upstream region because in some upstream regions the H_2 depleted. When the cell voltage stayed stable in the lowest level, the local current density in different regions stopped diverging. The current density distributions of the fuel cell in different time during the experiment are illustrated in Fig. 4.24. At the beginning of the experiment, the current density was evenly distributed on the electrode surface when the fuel cell was operated with normal H_2 stoichiometry. When the cell voltage decreased to 0 V, the obvious heterogeneity in current density distribution can be observed as can be seen from Fig. 4.24 (b). The current density in upstream was the highest, decreasing along the anode flow channels, and became the lowest in downstream regions. When the cell voltage decreased to the lowest level, the heterogeneity in current density became more severe. As in more regions the H_2 was depleted, most of current flowed through a small regions near the inlet, resulting in quite high current density in upstream regions.

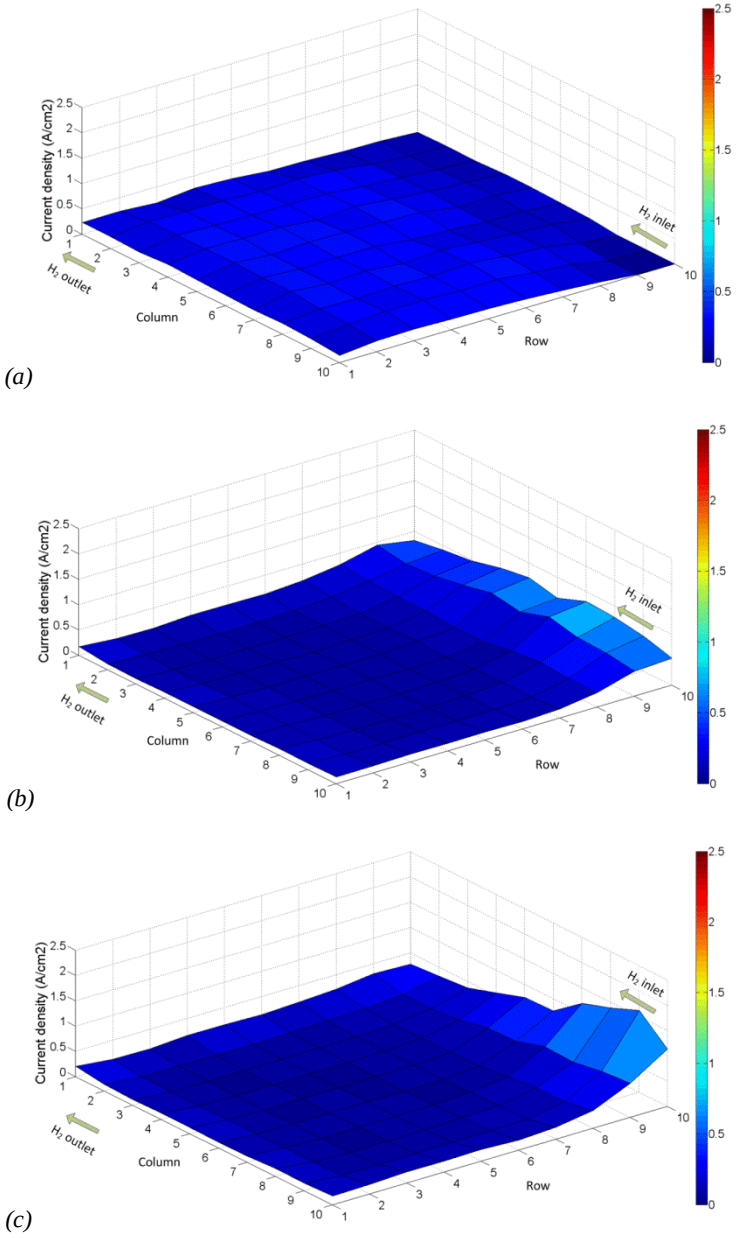

Fig. 4.24 – Current density distribution profiles of the fuel cell in different time ((a): t=0s; (b): t=16s when the cell voltage decreases to 0 V; (c): t=60s when the cell reversal occurs and the cell voltage reaches the lowest level) during the H_2 starvation process under H_2 stoichiometry of 0.8 and current load of 10 A.

4.3.2. EFFECT OF H_2 STOICHIOMETRY

The change in cell voltage and the local current density when the H_2 stoichiometry decreased to 0.4 are illustrated in Fig. 4.25, to investigate the effect of H_2 stoichiometry on the H_2 starvation. The change in cell voltage in this experiment was similar to that in the experiment when the H_2 stoichiometry was decreased to 0.4. In this experiment the H_2 stoichiometry was lower, indicating the more severe H_2 starvation. With more severe H_2 starvation, the cell voltage dropped more rapidly, and the lowest cell voltage was lower, as shown in Table 4.1. Under lower H_2 stoichiometry condition, lower current was provided by the H_2 oxidation reaction, thus more current should be provided by the carbon corrosion reaction and the water electrolysis reaction. Therefore the anode potential should be higher to increase the reaction rate of carbon corrosion and water electrolysis, resulting in lower reversed cell voltage and more severe cell reversal.

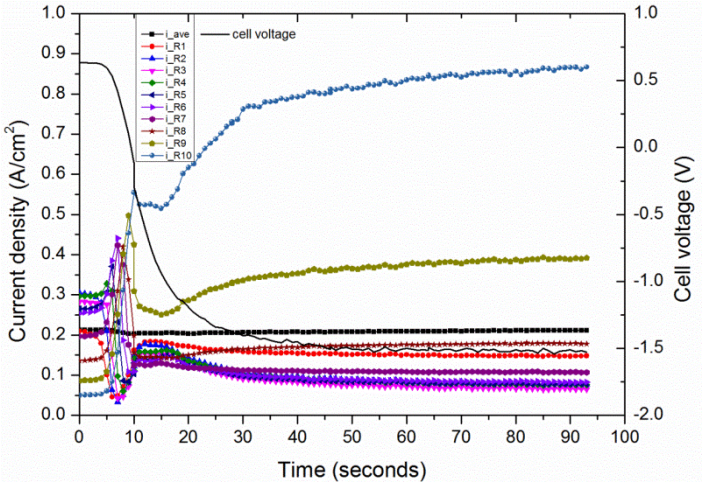

Fig. 4.25 – Dynamic response of the cell voltage and the local current density when H_2 stoichiometry decreased from 3.0 to 0.4 with the current load of 10A

Table 4.1 – Values for cell voltage and local current density under different operating conditions

Operating conditions	Time needed for cell reversal (s)	Reversed cell voltage (V)	Difference between highest and lowest local current density (A/cm^2) **
10A, λ_{H2}=0.8	19	-0.75	1.59
10A, λ_{H2}=0.4	15	-1.50	2.45
20A, λ_{H2}=0.8	17	-1.20*	2.00
20A, λ_{H2}=0.4	12	-2.30	2.52

** This value is the average cell voltage between 40 seconds and 115 seconds*

*** These values are measured when the cell voltage decreased to the lowest value in each experiment*

From Fig. 4.23 it can be seen that the anode exhaust consisted of N_2, CO_2 and O_2 in this experiment. The higher anode potential in this experiment triggered the water electrolysis, which generated the O_2 in the anode exhaust. In addition, the CO_2 concentration was higher in this experiment, which means lower H_2 stoichiometry brought about higher carbon corrosion rate.

The change in local current density at H_2 stoichiometry of 0.4 is similar to that at H_2 stoichiometry of 0.8 as shown in Fig. 4.25. The local current density showed increase trend in upstream regions and decrease trend in downstream regions. The change in local current density brought about the current density distribution shown in Fig. 4.26. Compared with the current density distribution at the H_2 stoichiometry of 0.8, the area with high current density was much less in this experiment at the H_2 stoichiometry of 0.4. In addition the difference between the highest and lowest local current density values was higher at the H_2 stoichiometry of 0.4 than at the H_2 stoichiometry of 0.8. With higher current load, the polarization losses such as mass transfer loss and activation loss were higher, resulting in lower cell voltage and more severe cell reversal. Lower cell voltage in this work suggested higher anode potential and consequently higher carbon corrosion rate, which suggested that the performance degradation caused by H_2 starvation can be more severe with higher current load.

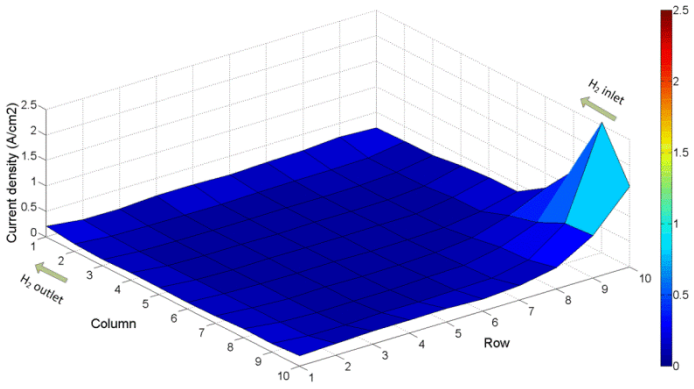

Fig. 4.26 – The current density distribution profile of the fuel cell when the cell reversal occurred and the cell voltage decreased to the lowest level during the H_2 starvation process under the H_2 stoichiometry of 0.4 and current load of 10 A

4.3.3. EFFECT OF CURRENT LOAD

To investigate the effect of current load of the fuel cell on the cell behaviors under H_2 starvation conditions, the change in cell voltage and local current density when H_2 starvation occurred with the current load of 20 A are illustrated in Fig. 4.27. It can be observed that the variation trend in cell voltage was similar with different current loads, by comparing Fig. 4.27 with Fig. 4.23 and Fig. 4.25. The current load affected the cell voltage drop rate and the reversed cell voltage value. As can be seen from Table 4.1, the cell voltage dropped faster with current load 20A than with current load of 10A, which can be contributed to the higher consumption rate of H_2 with higher current load. The lowest cell voltage with the same H_2 stoichiometry was lower with higher current load, which revealed that higher current load brought about more severe cell reversal.

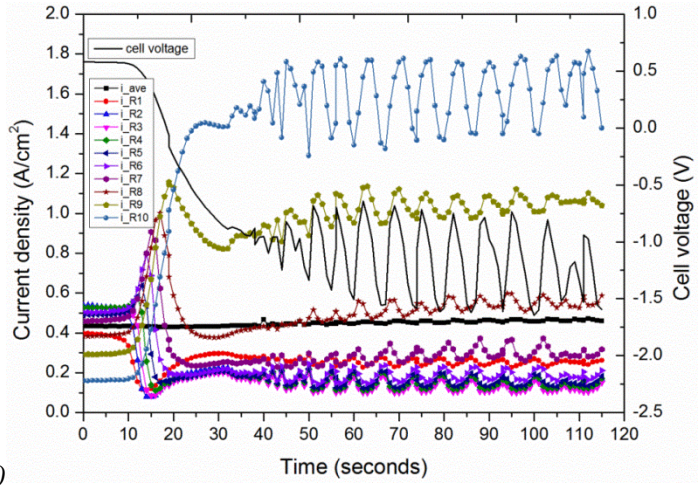

(a)

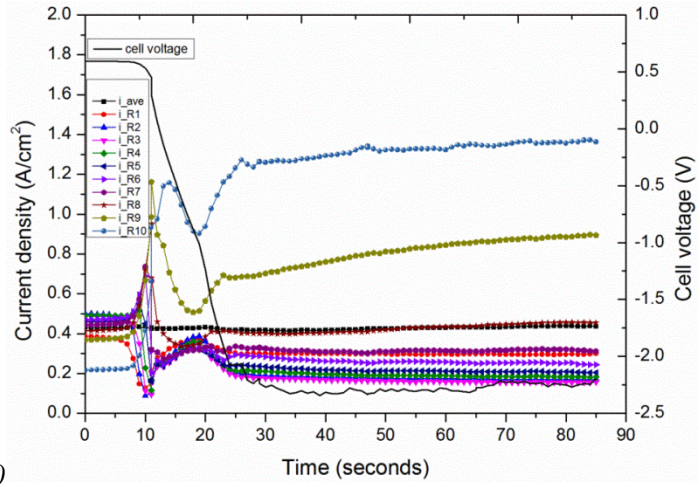

(b)

Fig. 4.27 – The dynamic response of the cell voltage and the local current density when the H_2 stoichiometry decreased to 0.8 (a) and 0.4 (b) with current load of 20 A

The change in local current density was not significantly affected by the current load, except for the diverging rate between different regions and the difference between the highest and lowest local current values. Higher current load brought faster diverging rate and higher difference between the highest and lowest local current values.

The current load also affected the anode exhaust composition under H_2 starvation conditions as can be seen from Fig. 4.23. It can be seen that with the same H_2 stoichiometry the anode exhaust gas composition was similar with different current

loads. Higher current load resulted in a slight increase in CO_2 concentration. It should be mentioned that the gas flow rate was higher with higher current load, thus the amount of CO_2 generated from carbon corrosion was higher with higher current load, indicating a higher carbon corrosion rate.

The current density distribution with current load of 20 A was similar to that with current load of 10 A with the same H_2 stoichiometry. In a small area in upstream the current density was quite high, while in most regions the current density was very low. The local current density in upstream regions was higher with higher current load, by comparing Fig. 4.28 and Fig. 4.24 and Fig. 4.26. Therefore the difference between the highest and lowest current density was higher with higher current load, confirmed by Table 4.1.

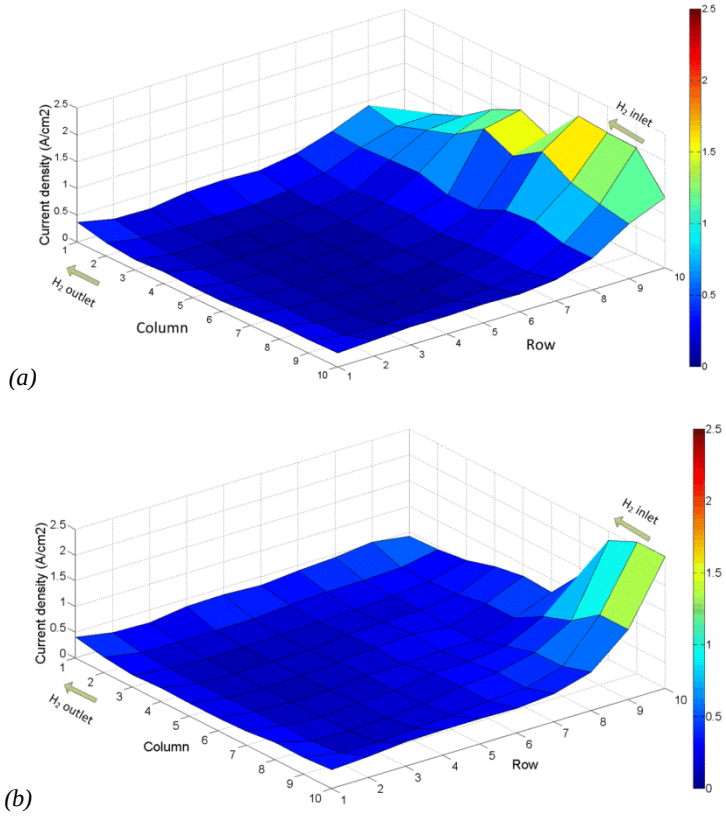

Fig. 4.28 – The current density distribution profile of the fuel cell when the cell reversal occurred and the cell voltage decreased to the lowest level during the H_2 starvation process under the H_2 stoichiometry of 0.4 and current load of 10 A

4.4. ACCELERATED DEGRADATION TEST OF A HT-PEM FUEL CELL UNDER H_2 STARVATION CONDITION

In this work, the effect of cell reversal caused by H_2 starvation to the degradation in a HT-PEM fuel cell was experimentally investigated.

4.4.1. CELL VOLTAGE DEGRADATION

As can be seen from Fig. 4.29, the fuel cell experienced 19 H_2 starvation cycles in 90 minutes. In each cycle when the H_2 stoichiometry decreased to 0.8, the cell voltage dropped dramatically and eventually got reversed. When the H_2 stoichiometry returned to 3.0, the cell voltage can be recovered. The repeated H_2 starvation operation of the fuel cell resulted in continuous decrease in cell performance. The degradation in fuel cell caused by H_2 starvation was better illustrated in Fig. 4.30, in which showed the average cell voltage at H_2 stoichiometry of 3.0 in each cycle. The cell voltage at the H_2 stoichiometry of 3.0 decreased from 0.59 V to 0.39 V in 90 minutes. The severe degradation of the HT-PEM fuel cell under H_2 starvation condition in this work can be related to the reversed cell polarity.

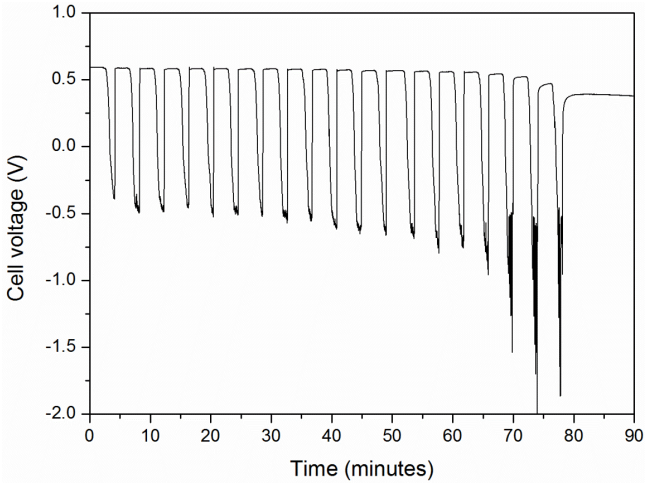

Fig. 4.29 – The cell voltage profile of the HT-PEM fuel cell during the H_2 starvation degradation test

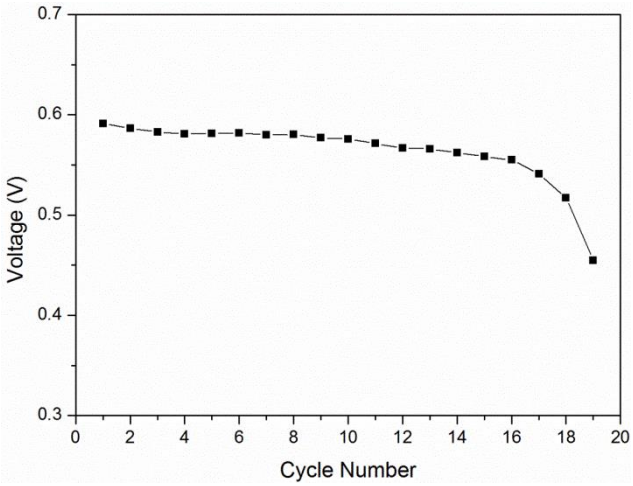

Fig. 4.30 – The change in average cell voltage at the H_2 stoichiometry of 3.0 in each cycle

The cell performance degradation of Nafion membrane based LT-PEM fuel cell caused by H_2 starvation was reported in the literature [170, 172]. It was observed that the anode potential increased rapidly which the cathode potential became a bit lower than the normal value, brought about cell reversal of the fuel cell. The high potential in anode would cause the carbon corrosion and even the water electrolysis reactions, resulting in severe degradation in anode catalyst layer. Given the fact that the electrode structure and catalyst material of HT-PEM fuel cell is similar to those of the LT-PEM fuel cell, the degradation mechanism of the HT-PEM fuel cell under H_2 starvation condition was also related the carbon corrosion in anode catalyst layer caused by cell reversal. From Fig. 4.29 it can be observed that the cell reversal became more and more severe with the increase in the cycle number, especially in the last three cycles, which indicated higher carbon corrosion rate and more severe damage to the anode catalyst layer. Therefore in the last three cycles the cell performance declined significantly.

The gas compositions of anode exhaust measured by the mass spectrometer in two different cycles (cycle 9 and cycle 19) are illustrated in Fig. 4.31, as well as the change in cell voltage. Under normal H_2 stoichiometry of 3.0, the anode exhaust was consisted of H_2 and N_2 with concentration of 63%vol and 37, respectively. When the H_2 stoichiometry decreased to 0.8, the H_2 concentration dropped rapidly to 0%vol, while the N_2 concentration started to increase correspondingly. This indicated that the H_2 was depleted in the fuel cell under H_2 starvation condition. Meanwhile, the CO_2 emerged with concentration around 20%, which was generated by the carbon corrosion reaction. In cycle 19, higher amount of CO_2 was generated, as indicated by higher CO_2 concentration and longer time for CO_2 generation, which suggested more severe carbon corrosion in anode catalyst. It can be

concluded that with the increase in the number of cycle, more severe cell reversal brought about higher carbon corrosion rate and more severe damage to the anode catalyst layer, which explained the higher performance decay rate at the end of the test.

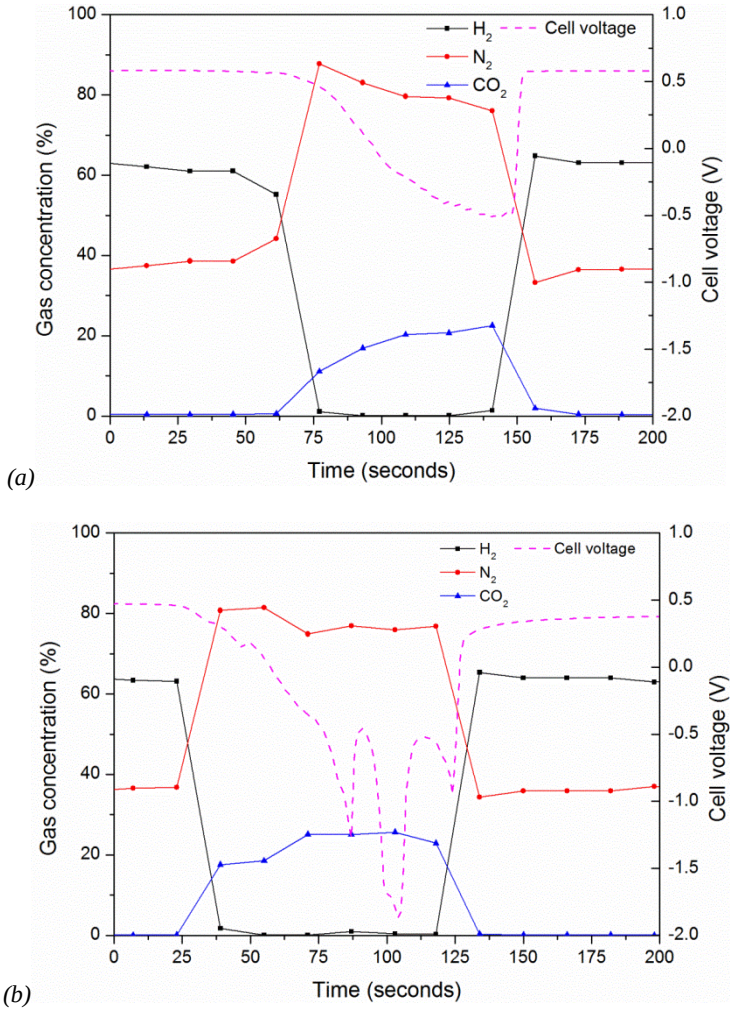

Fig. 4.31 – The response in anode exhaust composition (solid line) and cell voltage (dashed line) in cycle 9 (a) and cycle 19 (b)

4.4.2. ELECTROCHEMICAL ANALYSIS

The polarization curves of the fuel cell measured before and after the degradation test are illustrated in Fig. 4.32, to better show the effect of H_2 starvation on the

performance degradation of the HT-PEM fuel cell. The open circuit voltage (OCV) remained almost unchanged before and after the test, as can be seen from Fig. 4.32. However, the cell voltage in medium and high current density range showed larger decrease, which suggested the performance loss in ohmic and mass transfer regions was more significant. The OCV of the fuel cell in real application is always lower than the voltage value calculated by the Nernst equation because of mixed cathode potential and H_2 crossover [173]. The mixed potential is caused by the oxidation of Pt in cathode, which results in lower potential in cathode side. H_2 can diffuse from anode to cathode through the membrane, which reacts with the O_2 in cathode and results in the decrease in cathode potential. In this experiment the unchanged OCV indicated that the H_2 crossover rate was not significantly affected. Therefore the membrane was not affected by the cell reversal caused by H_2 starvation.

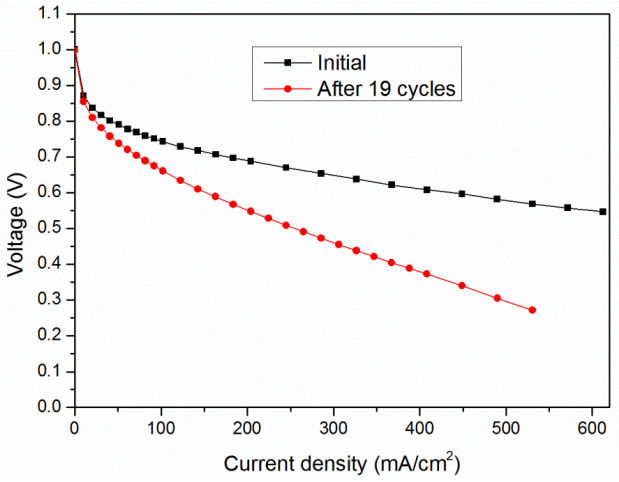

Fig. 4.32 – The polarization curves of the fuel cell measured before and after the H_2 starvation degradation test

The electrochemical impedance spectra measured in the beginning of the test and after the H_2 starvation test with current load of 20 A was illustrated in Fig. 4.33. The ohmic resistance can be measured by the x-axis intercept of semi-circle in the high frequency region, and the charge transfer resistance can be calculated by the diameter of the semi-circle. The impedance spectrum shifted right after the degradation, with an obvious increase in the size of the semi-circle, as can be seen from Fig. 4.33, which suggested both the ohmic resistance and the charge transfer resistance was increased by the degradation caused by H_2 starvation. The ohmic resistance of the fuel cell is the sum of the ohmic resistance of all components and contact resistance between different components. Since the membrane was not significantly affected, the increase in contact resistance caused by carbon corrosion could be the reason for the increase in ohmic resistance. The carbon corrosion can

weaken the attachment of platinum particles on the carbon support surface, resulting in detachment and migration of platinum particles. Moreover, the high anode potential under H_2 starvation condition accelerated the platinum solution. Both the migration and solution of platinum can cause the decrease in ECSA, and consequently the charge transfer resistance. The decrease in ECSA can be confirmed by the change in cyclic voltammogram shown in Fig. 4.34. The ECSA calculated from the hydrogen desorption peak between 0.1 V and 0.4 V in the voltammogram decreased after the degradation test. It should be mentioned that the ECSA was only evaluated in the cathode by CV, while the increase in charge transfer resistance originated from both anode and cathode. Although the CV was not performed in anode in this work, the decrease in ECSA of anode can be confirmed by the post-mortem analysis.

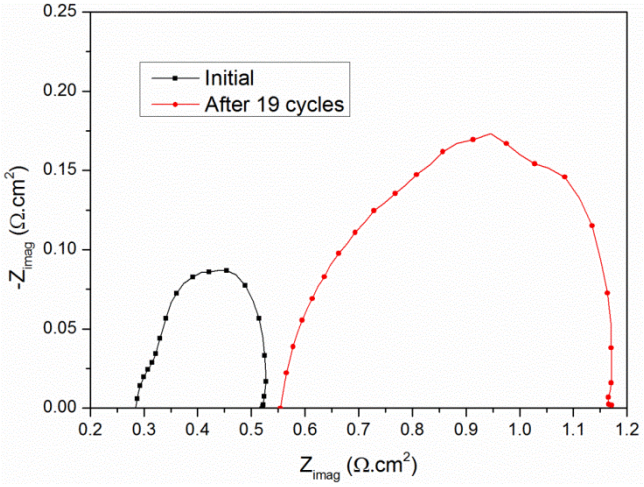

Fig. 4.33 – The electrochemical impedance spectra measured in the beginning of the test and after the H_2 starvation test with current load of 20 A

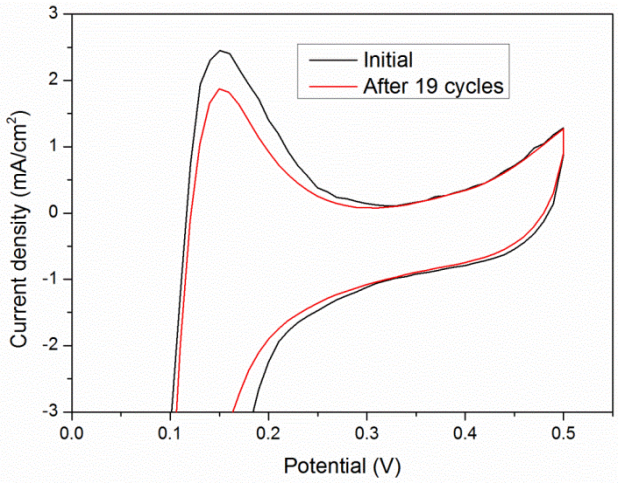

Fig. 4.34 – The cyclic voltammograms of the fuel cell measured in the beginning of the test and after the H_2 starvation test

4.4.3. POST-MORTEM ANALYSIS

The images of cross section of a pristine MEA and the MEA which experienced the degradation test are shown in Fig. 4.35 (a) and (b), respectively. It can be observed that the GDL and catalyst layer in the cathode were not impacted significantly by the degradation test. While in the anode catalyst layer the massive loss in the platinum can be observed, as the area of white part decreased significantly after the degradation test. Moreover, there was a gap between the catalyst layer and the GDL in the anode side of the tested MEA. Both the loss in the platinum and the carbon fiber in the anode were caused by severe carbon corrosion under H_2 starvation condition. In the catalyst layer the carbon corrosion could weaken the attachment of the platinum to the carbon support, leading to severe platinum agglomeration and migration. In addition, the loss of platinum can also be attributed to the high anode potential. In this experiment the anode potential became quite high under H_2 starvation condition, thus severe Pt dissolution, migration and redeposition occur in the anode catalyst layer, resulting in both increase in Pt particle size and loss of Pt in anode catalyst layer. The loss in platinum on the anode could lead to a massive decrease in the ECSA of the anode side, which can explain the increase in the charge transfer resistance after the degradation test. The observed gap between the catalyst layer and the GDL in the anode apparently increased the contact resistance between the two components of the MEA, resulting in the increase in the ohmic resistance shown in Fig. 4.33.

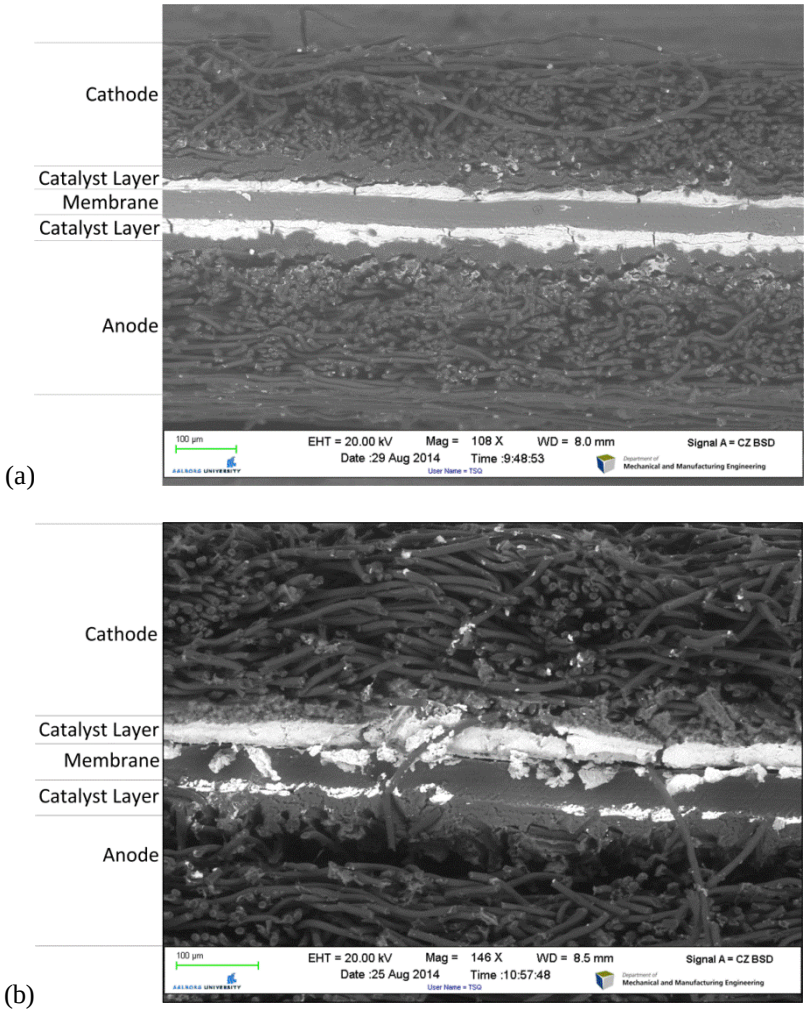

Fig. 4.35 – The cross-section images of an untested MEA (a) of a tested MEA (b) taken by a SEM

The XRD patterns of the platinum particles from anode and cathode of a pristine MEA and the MEA experienced the degradation test are illustrated in Fig. 4.36. The characteristic diffraction peaks at 2θ angles of 39.91, 46.42, 67.69, 81.45 degrees are associated with the Pt (111), (200), (220), (311) lattice planes, respectively [157]. The average size of platinum particle (L) in cathode and anode of the fuel cell can be calculated from the Scherrer's equation as shown in Eq. (3.5) on the basis of all the diffraction peaks.

According to the calculation results, the average platinum particle sizes were 4.40 nm and 4.38 nm in anode and cathode of the pristine MEA, respectively. While the average platinum particle sizes was increased to 5.81 nm and 5.47 nm in anode and cathode in the tested MEA, respectively. The increase in the platinum particle size in cathode side was in accordance with the decrease in the ECSA which was proved by the CV measurement as shown in Fig. 4.34. The increase in the anode platinum particle size can be explained by the carbon support corrosion which accelerated the platinum agglomeration.

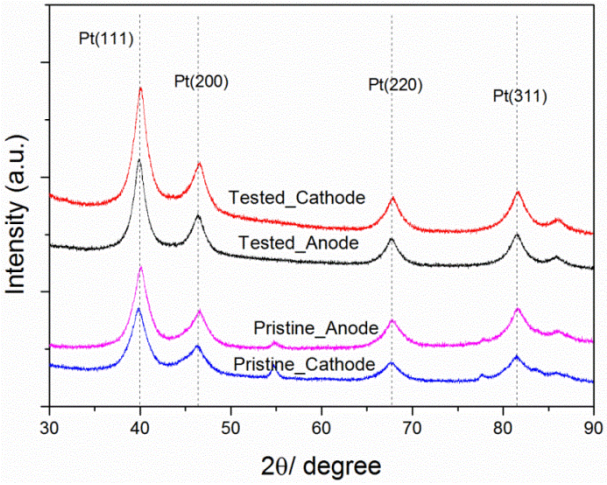

Fig. 4.36 – The XRD patterns of Pt particles from anode and cathode of a pristine MEA and a tested MEA

It can be concluded from the post-mortem analysis on the tested MEA that both the catalyst layer in anode and cathode experienced degradation after the H_2 starvation degradation test. In cathode side the increase in the platinum particle size resulted in the decrease in the ECSA. While in anode side the significant loss in the platinum catalyst was the main reason for the degradation, although the increase in the platinum size was also observed.

4.5. SUMMARY

In summary, the degradation of the HT-PEM fuel cell under several stressed operating conditions, including start/stop cycling, the presence of methanol and CO in the anode stream and H_2 starvation, is investigated and discussed. By thoroughly analysis of the change in cell performance during degradation tests and the characterization of the fuel cell, the degradation mechanisms under these operating conditions are revealed. The results and discussion presented in this section help to

improve the design and the operating strategy of the HT-PEM fuel cell system to achieve the better cell performance and durability.

CHAPTER 5. CONCLUSION

In this final section, the conclusions obtained from all the experiments conducted in this project are presented. By showing all the main scientific contributions of this project in Section 5.1, this chapter tries to give the readers a better understanding how the HT-PEM fuel cells degrade under harsh operating conditions. The limitations of this work are also presented in Section 5.2, showing the future work which can be conducted for further investigation of the degradation in the HT-PEM fuel cells.

5.1. CONCLUSIONS

In this project the experimental works performed on the H_3PO_4/PBI HT-PEM fuel cells are reported to investigate the cell performance and degradation under stressed operating conditions, including start/stop cycling, methanol poisoning, CO poisoning and H_2 starvation. The HT-PEM fuel cells employed in this project are based on the Dapozol G77 MEAs from Danish Power System. All the experiments are conducted on a fuel cell test station from GreenLight Innovation. In Section 5.1.1 – 5.1.3, the conclusions obtained from all the experiments are presented. In Section 5.1.4, a brief summary about the work is given.

5.1.1. LONG-TERM DEGRADATION TEST WITH THE PRESENCE OF METHANOL

The proper procedure and duration of break-in are vital for the HT-PEM fuel cell to reach a better performance. With the presence of methanol in the anode stream, the performance decay rate is increased to a large extend. During the start/stop test, there is a significant decrease in cell performance which could be caused by improper procedure of the startup and shutdown. From the polarization curves and impedance spectra measured during the test, some degradation mechanisms can be revealed. The start/stop operation increases the ohmic resistance and mass transfer resistance of the fuel cell, which can be attributed to the corrosion of carbon support and the PA leaching caused by improper procedure of the startup and shutdown. The presence of methanol causes the increase in charge transfer resistance and mass transfer resistance, which is the reason for the degradation with the presence of methanol.

5.1.2. CO POISONING ON THE HT-PEM FUEL CELL

The CO concentration in the anode stream in the range of 1%vol and 3%vol can cause obvious cell performance decay to the Dapozol HT-PEM MEA under the operating temperature of 150 ^oC. The cell performance degradation caused by CO

poisoning is reversible. When the anode stream is humidified, the CO poisoning can be alleviated. With higher water content, the CO can be oxidized via water gas shift reaction, resulting in the decrease in CO coverage on the catalyst surface and higher cell performance. The CO_2 alone with concentration of 20%vol in the anode stream does not influence the cell performance significantly. However the addition of 20% vol CO_2 can deteriorate the poisoning effect caused by 1%vol CO, which is attributed to the significantly increased charge transfer resistance. The cell performance loss caused by 1%vol CO and 20%vol CO_2 can be also be alleviated by higher water content.

5.1.3. H_2 STARVATION

The H_2 starvation can influence the cell performance and the current density distribution of the HT-PEM fuel cell. Under the H_2 starvation conditions, the cell polarity can be reversed. The current density distribution becomes very uneven at the same time, with high current density values in upstream regions and low current density values in downstream regions. The carbon corrosion and the water electrolysis reaction occur in the anode under severe H_2 starvation conditions which can be confirmed by the existence of CO_2 and O_2 in the anode exhaust. The H_2 starvation degree (H_2 stoichiometry) and the current load affect the cell behavior under H_2 starvation conditions. With lower H_2 stoichiometry and higher current load, the cell reversal becomes more severe, and the current density distribution becomes more uneven. Higher CO_2 and O_2 concentrations suggest that the damage caused by H_2 starvation is more severe under lower H_2 stoichiometry and higher current load conditions.

The decreasing cell performance during the H_2 starvation degradation test confirms that the H_2 starvation can cause severe damage to the HT-PEM fuel cell. The degradation in cell performance is related to the cell reversal under H_2 starvation condition. More severe cell reversal at the end of the degradation test brings about higher performance decay rate. The carbon corrosion in the anode is the main consequence of the cell reversal caused by H_2 starvation and the main reason for the cell performance degradation. The OCV of the fuel cell is not affected by the H_2 starvation degradation test, indicating the H_2 starvation does not cause degradation in the membrane. From the post-mortem analysis such as SEM and XRD, the degradation in anode catalyst layer can be observed. The carbon corrosion results in the massive loss in platinum in anode and the increase in platinum particle size.

5.1.4. FINAL REMARKS

In this project, the degradation of the H_3PO_4/PBI HT-PEM fuel cell caused by impurities in anode stream and H_2 starvation is investigated. The results from this project reveal that both the impurities in anode stream and H_2 starvation cause severe degradation in cell performance of the HT-PEM fuel cell.

The results from the experiments about CO poisoning quantify the cell performance degradation caused by CO poisoning under different operating conditions. The data from these experiments can help to improve the operating strategy of the HT-PEM fuel cell and the fuel cell system, to minimize the influence the CO poisoning on the cell performance and degradation. Based on the fast performance decay under H_2 starvation condition, the H_2 starvation should be avoided during the operation of the HT-PEM fuel cell, even for a short period.

5.2. FUTURE WORK

The degradation mechanisms of the HT-PEM fuel cell under harsh operating conditions have been investigated, as a good start point for the further investigation in mitigating the degradation under these operating conditions and improving the operation strategy of the HT-PEM fuel cell to achieve better durability. This project cannot cover all the aspects of the degradation of the HT-PEM fuel cell, and some underlying degradation mechanisms are not explained by direct evidence. In the future, further investigation is needed to extend the scope of this project.

In the degradation test described in Section 4.1, the duration of the test conducted on each fuel cell is limited to about 300 hours because of high performance decay rate with the presence of methanol in the anode stream. However, the unstable cell performance with the presence of methanol, which may be caused by frequent sudden increase in methanol flow rate, also contributes to the high cell performance decay rate. In the future work, the methanol feeding system should be improved to achieve a more stable methanol flow rate, for eliminating influence of fluctuated cell voltage on the HT-PEM fuel cell degradation.

The break-in performed on all the fuel cells in this project is conducted using the same procedure. Different break-in procedures can be performed to investigate the effect of break-in procedure to the lifetime of the HT-PEM fuel cell in the future. Moreover, the redistribution of PA in the MEA is thought to be the reason for the enhanced cell performance during the break-in. The migration of PA during break-in and the following degradation period of the HT-PEM fuel cell are worth investigating, to understand the role of PA distribution in the performance of the HT-PEM fuel cell.

Lastly but not least importantly, all the tests conducted in this project are performed on a single cell setup. The operating conditions in a single cell are not exactly the same as in a fuel cell stack. To investigate the degradation of the fuel cell under the realistic operating conditions, the degradation test on a fuel cell stack should be performed in the future. Moreover, the degradation test can also be extended to the system level.

BIBLIOGRAPHY

[1] BP Energy Outlook 2035. http://wwwbpcom/content/dam/bp/pdf/Energy-economics/energy-outlook-2015/Energy_Outlook_2035_bookletpdf. 2015.
[2] IPCC. In climate change 2014: Climate change mitigation. Contribution of working group III to the fifth assessment report of the Intergovernment Panel on Climate Change. 2014;pages 1-33.
[3] The Danish Government, The Ministry of Climate, Energy and Building. The Danish Climate Policy Plan towards a Low Carbon Society. 2013.
[4] Lucia U. Overview on fuel cells. Renewable and Sustainable Energy Reviews. 2014;30:164-9.
[5] Yang C, Srinivasan S, Bocarsly AB, Tulyani S, Benziger JB. A comparison of physical properties and fuel cell performance of Nafion and zirconium phosphate/Nafion composite membranes. Journal of Membrane Science. 2004;237:145-61.
[6] Li H, Tang Y, Wang Z, Shi Z, Wu S, Song D, et al. A review of water flooding issues in the proton exchange membrane fuel cell. Journal of Power Sources. 2008;178:103-17.
[7] Tangirala AK. PEM Fuel Cells: Overview.
[8] McNicol B, Rand D, Williams K. Fuel cells for road transportation purposes—yes or no? Journal of Power Sources. 2001;100:47-59.
[9] http://automobiles.honda.com/fcx-clarity/. Honda FCX Clarity
[10] http://www.toyota.com/mirai/fcv.html. Toyota Mirai – The Turning Point.
[11] http://www.mbusa.com/mercedes/benz/green/electric_car. B-Class F-CELL Electric Car.
[12] http://www.chevrolet.com/equinox-fuel-efficient-suv.html. Equinox: Fuel-Efficient SUV.
[13] http://worldwide.hyundai.com/WW/Showroom/Eco/ix35-Fuel-Cell/PIP/index.html. Hyundai ix35 Fuel Cell.
[14] Marbán G, Valdés-Solís T. Towards the hydrogen economy? International Journal of Hydrogen Energy. 2007;32:1625-37.
[15] Kai T, Uemura Y, Takanashi H, Tsutsui T, Takahashi T, Matsumoto Y, et al. A demonstration project of the hydrogen station located on Yakushima Island—Operation and analysis of the station. International Journal of Hydrogen Energy. 2007;32:3519-25.
[16] http://www.fta.dot.gov/14617_15670.html. National Fuel Cell Bus Program Projects.
[17] http://www.global-hydrogen-bus-platform.com/. Clean Urban Transport for Europe.
[18] Hwang J, Wang D, Shih N, Lai D, Chen Co-K. Development of fuel-cell-powered electric bicycle. Journal of Power Sources. 2004;133:223-8.
[19] Hwang JJ. Review on development and demonstration of hydrogen fuel cell scooters. Renewable and Sustainable Energy Reviews. 2012;16:3803-15.

[20] Keränen T, Karimäki H, Viitakangas J, Vallet J, Ihonen J, Hyötylä P, et al. Development of integrated fuel cell hybrid power source for electric forklift. Journal of Power Sources. 2011;196:9058-68.
[21] Wang C, Mao Z, Bao F, Li X, Xie X. Development and performance of 5kw proton exchange membrane fuel cell stationary power system. International Journal of Hydrogen Energy. 2005;30:1031-4.
[22] Feitelberg AS, Stathopoulos J, Qi Z, Smith C, Elter JF. Reliability of Plug Power GenSys™ fuel cell systems. Journal of Power Sources. 2005;147:203-7.
[23] Plug Power wins award to operate GenSys units in NY homes. Fuel Cells Bulletin. 2009;2009:6.
[24] Ballard. PEM fuel cell product portfolio. 2009.
[25] Wang Y, Chen KS, Mishler J, Cho SC, Adroher XC. A review of polymer electrolyte membrane fuel cells: technology, applications, and needs on fundamental research. Applied Energy. 2011;88:981-1007.
[26] Dyer CK. Fuel cells for portable applications. Journal of Power Sources. 2002;106:31-4.
[27] Chen D, Li W, Peng H. An experimental study and model validation of a membrane humidifier for PEM fuel cell humidification control. Journal of Power Sources. 2008;180:461-7.
[28] Baschuk J, Li X. Modelling CO poisoning and O2 bleeding in a PEM fuel cell anode. International Journal of Energy Research. 2003;27:1095-116.
[29] Yu X, Zhou B, Sobiesiak A. Water and thermal management for Ballard PEM fuel cell stack. Journal of Power Sources. 2005;147:184-95.
[30] Li Q, He R, Jensen J, Bjerrum N. PBI‐Based Polymer Membranes for High Temperature Fuel Cells‐Preparation, Characterization and Fuel Cell Demonstration. Fuel Cells. 2004;4:147-59.
[31] Li Q, Rudbeck HC, Chromik A, Jensen JO, Pan C, Steenberg T, et al. Properties, degradation and high temperature fuel cell test of different types of PBI and PBI blend membranes. Journal of Membrane Science. 2010;347:260-70.
[32] Lobato J, Canizares P, Rodrigo MA, Linares JJ, Manjavacas G. Synthesis and characterisation of poly [2, 2-(m-phenylene)-5, 5-bibenzimidazole] as polymer electrolyte membrane for high temperature PEMFCs. Journal of Membrane Science. 2006;280:351-62.
[33] Zhang J, Xie Z, Zhang J, Tang Y, Song C, Navessin T, et al. High temperature PEM fuel cells. Journal of Power Sources. 2006;160:872-91.
[34] Shao Y, Yin G, Wang Z, Gao Y. Proton exchange membrane fuel cell from low temperature to high temperature: material challenges. Journal of Power Sources. 2007;167:235-42.
[35] Chandan A, Hattenberger M, El-Kharouf A, Du S, Dhir A, Self V, et al. High temperature (HT) polymer electrolyte membrane fuel cells (PEMFC)–A review. Journal of Power Sources. 2013;231:264-78.
[36] Wainright J, Wang JT, Weng D, Savinell R, Litt M. Acid‐Doped Polybenzimidazoles: A New Polymer Electrolyte. Journal of The Electrochemical Society. 1995;142:L121-L3.

[37] Li Q, Jensen JO, Savinell RF, Bjerrum NJ. High temperature proton exchange membranes based on polybenzimidazoles for fuel cells. Progress in Polymer Science. 2009;34:449-77.
[38] Jensen JO, Li Q, Pan C, Vestbø AP, Mortensen K, Petersen HN, et al. High temperature PEMFC and the possible utilization of the excess heat for fuel processing. International Journal of Hydrogen Energy. 2007;32:1567-71.
[39] Gao X, Chen M, Andreasen SJ, Kær SK. Potential usage of thermoelectric devices in a high-temperature polymer electrolyte membrane (PEM) fuel cell system: two case studies. Journal of electronic materials. 2012;41:1838-44.
[40] Das SK, Reis A, Berry KJ. Experimental evaluation of CO poisoning on the performance of a high temperature proton exchange membrane fuel cell. Journal of Power Sources. 2009;193:691-8.
[41] Holladay JD, Wainright JS, Jones EO, Gano SR. Power generation using a mesoscale fuel cell integrated with a microscale fuel processor. Journal of Power Sources. 2004;130:111-8.
[42] Poirier M, Sapundzhiev C. Catalytic decomposition of natural gas to hydrogen for fuel cell applications. International Journal of Hydrogen Energy. 1997;22:429-33.
[43] Pan C, He R, Li Q, Jensen JO, Bjerrum NJ, Hjulmand HA, et al. Integration of high temperature PEM fuel cells with a methanol reformer. Journal of Power Sources. 2005;145:392-8.
[44] Andreasen SJ, Kær SK, Sahlin S. Control and experimental characterization of a methanol reformer for a 350 W high temperature polymer electrolyte membrane fuel cell system. International Journal of Hydrogen Energy. 2013;38:1676-84.
[45] Karstedt J, Ogrzewalla J, Severin C, Pischinger S. Development and design of experiments optimization of a high temperature proton exchange membrane fuel cell auxiliary power unit with onboard fuel processor. Journal of Power Sources. 2011;196:9998-10009.
[46] Authayanun S, Mamlouk M, Scott K, Arpornwichanop A. Comparison of high-temperature and low-temperature polymer electrolyte membrane fuel cell systems with glycerol reforming process for stationary applications. Applied Energy. 2013;109:192-201.
[47] Clarke SH, Dicks AL, Pointon K, Smith TA, Swann A. Catalytic aspects of the steam reforming of hydrocarbons in internal reforming fuel cells. Catalysis Today. 1997;38:411-23.
[48] Avgouropoulos G, Paxinou A, Neophytides S. In situ hydrogen utilization in an internal reforming methanol fuel cell. International Journal of Hydrogen Energy. 2014;39:18103-8.
[49] Najafi B, Haghighat Mamaghani A, Rinaldi F, Casalegno A. Long-term performance analysis of an HT-PEM fuel cell based micro-CHP system: Operational strategies. Applied Energy. 2015;147:582-92.
[50] Arsalis A, Kær SK, Nielsen MP. Modeling and optimization of a heat-pump-assisted high temperature proton exchange membrane fuel cell micro-combined-

heat-and-power system for residential applications. Applied Energy. 2015;147:569-81.
[51] Andreasen SJ, Ashworth L, Sahlin S, Becker Jensen H-C, Kær SK. Test of hybrid power system for electrical vehicles using a lithium-ion battery pack and a reformed methanol fuel cell range extender. International Journal of Hydrogen Energy. 2014;39:1856-63.
[52] Su H, Pasupathi S, Bladergroen B, Linkov V, Pollet BG. Optimization of gas diffusion electrode for polybenzimidazole-based high temperature proton exchange membrane fuel cell: Evaluation of polymer binders in catalyst layer. International Journal of Hydrogen Energy. 2013;38:11370-8.
[53] Glipa X, Bonnet B, Mula B, Jones DJ, Rozière J. Investigation of the conduction properties of phosphoric and sulfuric acid doped polybenzimidazole. Journal of Materials Chemistry. 1999;9:3045-9.
[54] Bouchet R, Siebert E. Proton conduction in acid doped polybenzimidazole. Solid State Ionics. 1999;118:287-99.
[55] Litt M, Ameri R, Wang Y, Savinell R, Wainwright J. Polybenzimidazoles/phosphoric acid solid polymer electrolytes: mechanical and electrical properties. MRS Proceedings: Cambridge Univ Press; 1998. p. 313.
[56] Mamlouk M, Scott K. The effect of electrode parameters on performance of a phosphoric acid-doped PBI membrane fuel cell. International Journal of Hydrogen Energy. 2010;35:784-93.
[57] DOE. Fuel Cell Technologies Office Multi-Year Research, Development and Demonstration Plan. http://www1eereenergygov/hydrogenandfuelcells/mypp/.
[58] Tang H, Peikang S, Jiang SP, Wang F, Pan M. A degradation study of Nafion proton exchange membrane of PEM fuel cells. Journal of Power Sources. 2007;170:85-92.
[59] Laconti A, Liu H, Mittelsteadt C, McDonald R. Polymer electrolyte membrane degradation mechanisms in fuel cells-findings over the past 30 years and comparison with electrolyzers. ECS Transactions. 2006;1:199-219.
[60] Curtin DE, Lousenberg RD, Henry TJ, Tangeman PC, Tisack ME. Advanced materials for improved PEMFC performance and life. Journal of Power Sources. 2004;131:41-8.
[61] Li Q, Pan C, Jensen JO, Noyé P, Bjerrum NJ. Cross-linked polybenzimidazole membranes for fuel cells. Chemistry of materials. 2007;19:350-2.
[62] Liao J, Li Q, Rudbeck H, Jensen JO, Chromik A, Bjerrum N, et al. Oxidative degradation of polybenzimidazole membranes as electrolytes for high temperature proton exchange membrane fuel cells. Fuel Cells. 2011;11:745-55.
[63] Liao J, Yang J, Li Q, Cleemann LN, Jensen JO, Bjerrum NJ, et al. Oxidative degradation of acid doped polybenzimidazole membranes and fuel cell durability in the presence of ferrous ions. Journal of Power Sources. 2013;238:516-22.
[64] Chang Z, Pu H, Wan D, Jin M, Pan H. Effects of adjacent groups of benzimidazole on antioxidation of polybenzimidazoles. Polymer Degradation and Stability. 2010;95:2648-53.

[65] Pu H, Tang L. Chemical oxidation stability and anhydrous proton conductivity of polyimides/phosphoric acid/imidazole blends. Polymer international. 2007;56:121-5.
[66] Kerres J. Blended and cross‐linked ionomer membranes for application in membrane fuel cells. Fuel Cells. 2005;5:230-47.
[67] Samms S, Wasmus S, Savinell R. Thermal stability of proton conducting acid doped polybenzimidazole in simulated fuel cell environments. Journal of The Electrochemical Society. 1996;143:1225-32.
[68] Orfanidi A, Daletou M, Sygellou L, Neophytides S. The role of phosphoric acid in the anodic electrocatalytic layer in high temperature PEM fuel cells. Journal of applied electrochemistry. 2013;43:1101-16.
[69] Modestov AD, Tarasevich MR, Filimonov VY, Zagudaeva NM. Degradation of high temperature MEA with PBI-H_3PO_4 membrane in a life test. Electrochimica Acta. 2009;54:7121-7.
[70] Wang J-T, Savinell R, Wainright J, Litt M, Yu H. A H_2O_2 fuel cell using acid doped polybenzimidazole as polymer electrolyte. Electrochimica Acta. 1996;41:193-7.
[71] Borup R, Meyers J, Pivovar B, Kim YS, Mukundan R, Garland N, et al. Scientific aspects of polymer electrolyte fuel cell durability and degradation. Chemical reviews. 2007;107:3904-51.
[72] Watanabe M, Tsurumi K, Mizukami T, Nakamura T, Stonehart P. Activity and Stability of Ordered and Disordered Co‐Pt Alloys for Phosphoric Acid Fuel Cells. Journal of The Electrochemical Society. 1994;141:2659-68.
[73] Berejnov V, Martin Z, West M, Kundu S, Bessarabov D, Stumper J, et al. Probing platinum degradation in polymer electrolyte membrane fuel cells by synchrotron X-ray microscopy. Physical Chemistry Chemical Physics. 2012;14:4835-43.
[74] Ferreira P, Shao-Horn Y, Morgan D, Makharia R, Kocha S, Gasteiger H. Instability of Pt/C electrocatalysts in proton exchange membrane fuel cells a mechanistic investigation. Journal of The Electrochemical Society. 2005;152:A2256-A71.
[75] Hu J, Zhang H, Zhai Y, Liu G, Yi B. 500 h Continuous aging life test on PBI/H_3PO_4 high-temperature PEMFC. International Journal of Hydrogen Energy. 2006;31:1855-62.
[76] Galbiati S, Baricci A, Casalegno A, Marchesi R. Degradation in phosphoric acid doped polymer fuel cells: A 6000 h parametric investigation. International Journal of Hydrogen Energy. 2013;38:6469-80.
[77] Zhai Y, Zhang H, Liu G, Hu J, Yi B. Degradation Study on MEA in H_3PO_4/PBI High-Temperature PEMFC Life Test. Journal of The Electrochemical Society. 2007;154:B72-B6.
[78] Wannek C, Kohnen B, Oetjen HF, Lippert H, Mergel J. Durability of ABPBI-based MEAs for High Temperature PEMFCs at Different Operating Conditions. Fuel Cells. 2008;8:87-95.

[79] Marrony M, Barrera R, Quenet S, Ginocchio S, Montelatici L, Aslanides A. Durability study and lifetime prediction of baseline proton exchange membrane fuel cell under severe operating conditions. Journal of Power Sources. 2008;182:469-75.
[80] Krishnan L, Snelson T, Puffer R, Walczyk D. Durability studies of PBI-based membrane electrode assemblies for high temperature PEMFCs. Automation Science and Engineering (CASE), 2010 IEEE Conference on: IEEE; 2010. p. 21-6.
[81] Suzuki A, Oono Y, Williams MC, Miura R, Inaba K, Hatakeyama N, et al. Evaluation for sintering of electrocatalysts and its effect on voltage drops in high-temperature proton exchange membrane fuel cells (HT-PEMFC). International Journal of Hydrogen Energy. 2012;37:18272-89.
[82] Oono Y, Fukuda T, Sounai A, Hori M. Influence of operating temperature on cell performance and endurance of high temperature proton exchange membrane fuel cells. Journal of Power Sources. 2010;195:1007-14.
[83] Lobato J, Cañizares P, Rodrigo MA, Linares JJ. PBI-based polymer electrolyte membranes fuel cells: Temperature effects on cell performance and catalyst stability. Electrochimica Acta. 2007;52:3910-20.
[84] Zhai Y, Zhang H, Xing D, Shao Z-G. The stability of Pt/C catalyst in H_3PO_4/PBI PEMFC during high temperature life test. Journal of Power Sources. 2007;164:126-33.
[85] Oono Y, Sounai A, Hori M. Long-term cell degradation mechanism in high-temperature proton exchange membrane fuel cells. Journal of Power Sources. 2012;210:366-73.
[86] Moçotéguy P, Ludwig B, Scholta J, Nedellec Y, Jones DJ, Rozière J. Long-Term Testing in Dynamic Mode of HT-PEMFC H_3PO_4/PBI Celtec-P Based Membrane Electrode Assemblies for Micro-CHP Applications. Fuel Cells. 2010;10:299-311.
[87] Kannan A, Kabza A, Scholta J. Long term testing of start–stop cycles on high temperature PEM fuel cell stack. Journal of Power Sources. 2015;277:312-6.
[88] Kim J, Kim M, Lee B-G, Sohn Y-J. Durability of high temperature polymer electrolyte membrane fuel cells in daily based start/stop operation mode using reformed gas. International Journal of Hydrogen Energy. 2015.
[89] Schmidt TJ, Baurmeister J. Properties of high-temperature PEFC Celtec®-P 1000 MEAs in start/stop operation mode. Journal of Power Sources. 2008;176:428-34.
[90] Borup RL, Davey JR, Garzon FH, Wood DL, Inbody MA. PEM fuel cell electrocatalyst durability measurements. Journal of Power Sources. 2006;163:76-81.
[91] Lobato J, Canizares P, Rodrigo MA, Linares JJ. PBI-based polymer electrolyte membranes fuel cells: Temperature effects on cell performance and catalyst stability. Electrochimica Acta. 2007;52:3910-20.
[92] More K, Borup R, Reeves K. Identifying contributing degradation phenomena in PEM fuel cell membrane electride assemblies via electron microscopy. ECS Transactions. 2006;3:717-33.

[93] Pozio A, De Francesco M, Cemmi A, Cardellini F, Giorgi L. Comparison of high surface Pt/C catalysts by cyclic voltammetry. Journal of Power Sources. 2002;105:13-9.
[94] Qi Z, Buelte S. Effect of open circuit voltage on performance and degradation of high temperature PBI–H 3 PO 4 fuel cells. Journal of Power Sources. 2006;161:1126-32.
[95] Yu Y, Li H, Wang H, Yuan X-Z, Wang G, Pan M. A review on performance degradation of proton exchange membrane fuel cells during startup and shutdown processes: causes, consequences, and mitigation strategies. Journal of Power Sources. 2012;205:10-23.
[96] Cho Y-H, Lim JW, Kang YS, Cho Y-H, Kim O-H, Kwon N-H, et al. The dependence of performance degradation of membrane electrode assembly on platinum loading in polymer electrolyte membrane fuel cell. International Journal of Hydrogen Energy. 2012;37:2490-7.
[97] Maass S, Finsterwalder F, Frank G, Hartmann R, Merten C. Carbon support oxidation in PEM fuel cell cathodes. Journal of Power Sources. 2008;176:444-51.
[98] Reiser CA, Bregoli L, Patterson TW, Jung SY, Yang JD, Perry ML, et al. A reverse-current decay mechanism for fuel cells. Electrochemical and Solid-State Letters. 2005;8:A273-A6.
[99] Lim KH, Oh H-S, Jang S-E, Ko Y-J, Kim H-J, Kim H. Effect of operating conditions on carbon corrosion in polymer electrolyte membrane fuel cells. Journal of Power Sources. 2009;193:575-9.
[100] Cleemann LN, Buazar F, Li Q, Jensen JO, Pan C, Steenberg T, et al. Catalyst degradation in high temperature proton exchange membrane fuel cells based on acid doped polybenzimidazole membranes. Fuel Cells. 2013;13:822-31.
[101] Yuka Oono AS, Michio Hori. Influence of the phosphoric acid-doping level in a polybenzimidazole membrane on the cell performance of high-temperature proton exchange membrane fuel cells. Journal of Power Sources. 2009;189:949.
[102] C. Wannek BK, H. F. Oetjen, et al. Durability of ABPBI-based MEAs for high temperature PEMFCs at different operating conditions. Fuel Cells. 2008;8:95.
[103] S. Yu LX, B. C. Benicewicz. Durability studies of PBI-based high temperature PEMFCs. Fuel Cells. 2008;8:176.
[104] Lin H, Hsieh Y, Chiu C, Yu T, Chen L. Durability and stability test of proton exchange membrane fuel cells prepared from polybenzimidazole/poly (tetrafluoro ethylene) composite membrane. Journal of Power Sources. 2009;193:170-4.
[105] Yuka Oono TF, Atsuo Sounai, Michio Hori. Influence of operating temperature on cell performance and endurance of high temperature proton exchange membrane fuel cells. Journal of Power Sources. 2010;195:1014.
[106] Christoph Hartnig TJS. On a new degradation mode for high-temperature polymer electrolyte fuel cells How bipolar plate degradation affects cell performance. Electrochimica Acta. 2011;56:4242.
[107] Kyungjung Kwon JOP, Duck Young Yoo, Jung S. Yi. Phosphoric acid distribution in the membrane electrode assembly of high temperature proton exchange membrane fuel cells. Electrochimica Acta. 2009;54:6575.

[108] Mack F, Heissler S, Laukenmann R, Zeis R. Phosphoric acid distribution and its impact on the performance of polybenzimidazole membranes. Journal of Power Sources. 2014;270:627-33.
[109] Maier W, Arlt T, Wannek C, Manke I, Riesemeier H, Krüger P, et al. In-situ synchrotron X-ray radiography on high temperature polymer electrolyte fuel cells. Electrochemistry Communications. 2010;12:1436-8.
[110] Reimer U, Schumacher B, Lehnert W. Accelerated Degradation of High-Temperature Polymer Electrolyte Fuel Cells: Discussion and Empirical Modeling. Journal of The Electrochemical Society. 2015;162:F153-F64.
[111] Ishigami Y, Takada K, Yano H, Inukai J, Uchida M, Nagumo Y, et al. Corrosion of carbon supports at cathode during hydrogen/air replacement at anode studied by visualization of oxygen partial pressures in a PEFC—Start-up/shut-down simulation. Journal of Power Sources. 2011;196:3003-8.
[112] Yuta Ishigami KT, Hiroshi Yano, et al. Corrosion of carbon supports at cathode during hydrogen/air replacement at anode studied by visualization of oxygen partial pressures in a PEFC—Start-up/shut-down simulation. Journal of Power Sources. 2011;196:3008.
[113] Kim JH, Cho EA, Jang JH, Kim HJ, Lim TH, Oh IH, et al. Effects of Cathode Inlet Relative Humidity on PEMFC Durability during Startup–Shutdown Cycling: I. Electrochemical Study. Journal of The Electrochemical Society. 2010;157:B104-B12.
[114] Jo YY, Cho E, Kim JH, Lim T-H, Oh I-H, Kim S-K, et al. Degradation of polymer electrolyte membrane fuel cells repetitively exposed to reverse current condition under different temperature. Journal of Power Sources. 2011;196:9906-15.
[115] Kim JH, Cho EA, Jang JH, Kim HJ, Lim T-H, Oh I-H, et al. Development of a durable PEMFC startup process by applying a dummy load I. Electrochemical study. Journal of The Electrochemical Society. 2009;156:B955-B61.
[116] Takagi Y, Takakuwa, Y. Effect of shutoff sequence of hydrogen and air on performance degradation in PEFC. ECS Transactions. 2006;3:855.
[117] Yi Yu GW, Zhengkai Tu, Zhigang Zhan, Mu Pan. Effect of gas shutoff sequences on the degradation of proton exchange membrane fuel cells with dummy load during startup and shutdown cycles. Electrochimica Acta. 2012;71:193.
[118] Yi Yu ZT, Haining Zhang, Zhigang Zhan, Mu Pan. Comparison of degradation behaviors for open-ended and closed proton exchange membrane fuel cells during startup and shutdown cycles. Journal of Power Sources. 2011;196:5083.
[119] Hartnig C, Schmidt TJ. Simulated start–stop as a rapid aging tool for polymer electrolyte fuel cell electrodes. Journal of Power Sources. 2011;196:5564-72.
[120] Wu J, Yuan X-Z, Martin JJ, Wang H, Yang D, Qiao J, et al. Proton exchange membrane fuel cell degradation under close to open-circuit conditions: part I: in situ diagnosis. Journal of Power Sources. 2010;195:1171-6.

[121] Teranishi K, Kawata K, Tsushima S, Hirai S. Degradation mechanism of PEMFC under open circuit operation. Electrochemical and Solid-State Letters. 2006;9:A475-A7.
[122] Jiménez S, Soler J, Valenzuela RX, Daza L. Assessment of the performance of a PEMFC in the presence of CO. Journal of Power Sources. 2005;151:69-73.
[123] Krishnan P, Park J-S, Kim C-S. Performance of a poly(2,5-benzimidazole) membrane based high temperature PEM fuel cell in the presence of carbon monoxide. Journal of Power Sources. 2006;159:817-23.
[124] Li Q, He R, Gao J-A, Jensen JO, Bjerrum NJ. The CO poisoning effect in PEMFCs operational at temperatures up to 200 ^{o}C. Journal of The Electrochemical Society. 2003;150:A1599-A605.
[125] Kwon K, Yoo DY, Park JO. Experimental factors that influence carbon monoxide tolerance of high-temperature proton-exchange membrane fuel cells. Journal of Power Sources. 2008;185:202-6.
[126] Chen C-Y, Lai W-H, Chen Y-K, Su S-S. Characteristic studies of a PBI/H_3PO_4 high temperature membrane PEMFC under simulated reformate gases. International Journal of Hydrogen Energy. 2014;39:13757-62.
[127] Boaventura M, Sander H, Friedrich K, Mendes A. The influence of CO on the current density distribution of high temperature polymer electrolyte membrane fuel cells. Electrochimica Acta. 2011;56:9467-75.
[128] Engl T, Käse J, Gubler L, Schmidt TJ. On the Positive Effect of CO during Start/Stop in High-Temperature Polymer Electrolyte Fuel Cells. ECS Electrochemistry Letters. 2014;3:F47-F9.
[129] Engl T, Gubler L, Schmidt TJ. Think Different! Carbon Corrosion Mitigation Strategy in High Temperature PEFC: A Rapid Aging Study. Journal of The Electrochemical Society. 2015;162:F291-F7.
[130] Bergmann A, Gerteisen D, Kurz T. Modelling of CO poisoning and its dynamics in HTPEM fuel cells. Fuel Cells. 2010;10:278-87.
[131] Jiao K, Alaefour IE, Li X. Three-dimensional non-isothermal modeling of carbon monoxide poisoning in high temperature proton exchange membrane fuel cells with phosphoric acid doped polybenzimidazole membranes. Fuel. 2011;90:568-82.
[132] Jiao K, Zhou Y, Du Q, Yin Y, Yu S, Li X. Numerical simulations of carbon monoxide poisoning in high temperature proton exchange membrane fuel cells with various flow channel designs. Applied Energy. 2013;104:21-41.
[133] Oh K, Jeong G, Cho E, Kim W, Ju H. A CO poisoning model for high-temperature proton exchange membrane fuel cells comprising phosphoric acid-doped polybenzimidazole membranes. International Journal of Hydrogen Energy. 2014;39:21915-26.
[134] Rasheed RKA, Chan SH. Transient carbon monoxide poisoning kinetics during warm-up period of a high-temperature PEMFC–Physical model and parametric study. Applied Energy. 2015;140:44-51.
[135] Lopes PP, Freitas KS, Ticianelli EA. CO tolerance of PEMFC anodes: mechanisms and electrode designs. Electrocatalysis. 2010;1:200-12.

[136] Modestov AD, Tarasevich MR, Filimonov VY, Davydova ES. CO tolerance and CO oxidation at Pt and Pt–Ru anode catalysts in fuel cell with polybenzimidazole–H_3PO_4 membrane. Electrochimica Acta. 2010;55:6073-80.
[137] Ehteshami SMM, Chan SH. A review of electrocatalysts with enhanced CO tolerance and stability for polymer electrolyte membarane fuel cells. Electrochimica Acta. 2013;93:334-45.
[138] Divisek J, Oetjen HF, Peinecke V, Schmidt VM, Stimming U. Components for PEM fuel cell systems using hydrogen and CO containing fuels. Electrochimica Acta. 1998;43:3811-5.
[139] Gu T, Lee W-K, Van Zee J. Quantifying the 'reverse water gas shift'reaction inside a PEM fuel cell. Applied Catalysis B: Environmental. 2005;56:43-50.
[140] Simon Araya S, Juhl Andreasen S, Venstrup Nielsen H, Knudsen Kær S. Investigating the effects of methanol-water vapor mixture on a PBI-based high temperature PEM fuel cell. International Journal of Hydrogen Energy. 2012;37:18231-42.
[141] Araya SS, Grigoras IF, Zhou F, Andreasen SJ, Kær SK. Performance and endurance of a high temperature PEM fuel cell operated on methanol reformate. International Journal of Hydrogen Energy. 2014;39:18343-50.
[142] Sethuraman VA, Weidner JW. Analysis of sulfur poisoning on a PEM fuel cell electrode. Electrochimica Acta. 2010;55:5683-94.
[143] Schmidt TJ, Baurmeister J. Durability and reliability in high-temperature reformed hydrogen PEFCs. ECS Transactions. 2006;3:861-9.
[144] Yi Yu X-ZY, Hui Li, Elton Gu, Haijiang Wang, Guangjin Wang, Mu Pan. Current mapping of a proton exchange membrane fuel cell with a segmented current collector during the gas starvation and shutdown processes. International Journal of Hydrogen Energy. 2012;37:15300.
[145] Guangsheng Zhang SS, Liejin Guo, Hongtan Liu. Dynamic characteristics of local current densities and temperatures in proton exchange membrane fuel cells during reactant starvations. International Journal of Hydrogen Energy. 2012;37:1892.
[146] Yousfi-Steiner N, Moçotéguy P, Candusso D, Hissel D. A review on polymer electrolyte membrane fuel cell catalyst degradation and starvation issues: Causes, consequences and diagnostic for mitigation. Journal of Power Sources. 2009;194:130-45.
[147] Liang D, Dou M, Hou M, Shen Q, Shao Z, Yi B. Behavior of a unit proton exchange membrane fuel cell in a stack under fuel starvation. Journal of Power Sources. 2011;196:5595-8.
[148] Liang D, Shen Q, Hou M, Shao Z, Yi B. Study of the cell reversal process of large area proton exchange membrane fuel cells under fuel starvation. Journal of Power Sources. 2009;194:847-53.
[149] Zhang G, Shen S, Guo L, Liu H. Dynamic characteristics of local current densities and temperatures in proton exchange membrane fuel cells during reactant starvations. International Journal of Hydrogen Energy. 2012;37:1884-92.

[150] Taniguchi A, Akita T, Yasuda K, Miyazaki Y. Analysis of degradation in PEMFC caused by cell reversal during air starvation. International Journal of Hydrogen Energy. 2008;33:2323-9.
[151] Pérez LC, Brandão L, Sousa JM, Mendes A. Segmented polymer electrolyte membrane fuel cells—A review. Renewable and Sustainable Energy Reviews. 2011;15:169-85.
[152] Neyerlin KC, Gasteiger HA, Mittelsteadt CK, Jorne J, Gu W. Effect of Relative Humidity on Oxygen Reduction Kinetics in a PEMFC. Journal of The Electrochemical Society. 2005;152:A1073-A80.
[153] Yuan X, Wang H, Colin Sun J, Zhang J. AC impedance technique in PEM fuel cell diagnosis—A review. International Journal of Hydrogen Energy. 2007;32:4365-80.
[154] Hu J, Zhang H, Gang L. Diffusion–convection/electrochemical model studies on polybenzimidazole (PBI) fuel cell based on AC impedance technique. Energy Conversion and Management. 2008;49:1019-27.
[155] Springer T, Zawodzinski T, Wilson M, Gottesfeld S. Characterization of polymer electrolyte fuel cells using AC impedance spectroscopy. Journal of The Electrochemical Society. 1996;143:587-99.
[156] Koponen U, Kumpulainen H, Bergelin M, Keskinen J, Peltonen T, Valkiainen M, et al. Characterization of Pt-based catalyst materials by voltammetric techniques. Journal of Power Sources. 2003;118:325-33.
[157] Roth C, Martz N, Fuess H. An X-ray diffraction and transmission electron microscopy study of Pt—Ru fuel cell catalysts before and after operation. Journal of applied electrochemistry. 2004;34:345-8.
[158] Boaventura M, Mendes A. Activation procedures characterization of MEA based on phosphoric acid doped PBI membranes. International Journal of Hydrogen Energy. 2010;35:11649-60.
[159] Galbiati S, Baricci A, Casalegno A, Carcassola G, Marchesi R. On the activation of polybenzimidazole-based membrane electrode assemblies doped with phosphoric acid. International Journal of Hydrogen Energy. 2012;37:14475-81.
[160] Andreasen SJ, Vang JR, Kær SK. High temperature PEM fuel cell performance characterisation with CO and CO_2 using electrochemical impedance spectroscopy. International Journal of Hydrogen Energy. 2011;36:9815-30.
[161] Kim J-R, Yi JS, Song T-W. Investigation of degradation mechanisms of a high-temperature polymer-electrolyte-membrane fuel cell stack by electrochemical impedance spectroscopy. Journal of Power Sources. 2012;220:54-64.
[162] Mamlouk M, Scott K. Analysis of high temperature polymer electrolyte membrane fuel cell electrodes using electrochemical impedance spectroscopy. Electrochimica Acta. 2011;56:5493-512.
[163] Jespersen JL, Schaltz E, Kær SK. Electrochemical characterization of a polybenzimidazole-based high temperature proton exchange membrane unit cell. Journal of Power Sources. 2009;191:289-96.

[164] Lawrence MG. The relationship between relative humidity and the dewpoint temperature in moist air: A simple conversion and applications. Bulletin of the American Meteorological Society. 2005;86:225-33.
[165] Engl T, Waltar KE, Gubler L, Schmidt TJ. Second Cycle Is Dead: Advanced Electrode Diagnostics for High-Temperature Polymer Electrolyte Fuel Cells. Journal of The Electrochemical Society. 2014;161:F500-F5.
[166] Modestov AD, Tarasevich MR, Leykin AY. CO electrooxidation study on Pt and Pt–Ru in H_3PO_4 using MEA with PBI–H_3PO_4 membrane. Journal of Power Sources. 2011;196:2994-3002.
[167] Smith R, Loganathan M, Shantha MS. A review of the water gas shift reaction kinetics. International Journal of Chemical Reactor Engineering. 2010;8.
[168] Cheng X, Shi Z, Glass N, Zhang L, Zhang J, Song D, et al. A review of PEM hydrogen fuel cell contamination: Impacts, mechanisms, and mitigation. Journal of Power Sources. 2007;165:739-56.
[169] Springer T, Rockward T, Zawodzinski T, Gottesfeld S. Model for Polymer Electrolyte Fuel Cell Operation on Reformate Feed: Effects of CO, H_2 Dilution, and High Fuel Utilization. Journal of The Electrochemical Society. 2001;148:A11-A23.
[170] Taniguchi A, Akita T, Yasuda K, Miyazaki Y. Analysis of electrocatalyst degradation in PEMFC caused by cell reversal during fuel starvation. Journal of Power Sources. 2004;130:42-9.
[171] Larminie J, Dicks A, McDonald MS. Fuel cell systems explained: Wiley New York; 2003.
[172] Kang J, Jung DW, Park S, Lee J-H, Ko J, Kim J. Accelerated test analysis of reversal potential caused by fuel starvation during PEMFCs operation. International Journal of Hydrogen Energy. 2010;35:3727-35.
[173] Zhang J, Tang Y, Song C, Zhang J, Wang H. PEM fuel cell open circuit voltage (OCV) in the temperature range of 23 °C to 120 °C. Journal of Power Sources. 2006;163:532-7.